BEILSTEIN JOURNAL OF ORGANIC CHEMISTRY

Organophosphorus chemistry: from model to application

Edited by György Keglevich

Generated on 06 November 2026, 14:44

Imprint

Beilstein Journal of Organic Chemistry
www.bjoc.org
ISSN 1860-5397
Email: journals-support@beilstein-institut.de

The *Beilstein Journal of Organic Chemistry* is published by the Beilstein-Institut zur Förderung der Chemischen Wissenschaften.

Beilstein-Institut zur Förderung der Chemischen Wissenschaften
Trakehner Straße 7–9
60487 Frankfurt am Main
Germany
www.beilstein-institut.de

The copyright to this document as a whole, which is published in the *Beilstein Journal of Organic Chemistry*, is held by the Beilstein-Institut zur Förderung der Chemischen Wissenschaften. The copyright to the individual articles in this document is held by the respective authors, subject to a Creative Commons Attribution license.

BEILSTEIN JOURNAL OF ORGANIC CHEMISTRY

Organophosphorus chemistry: from model to application

György Keglevich

Editorial

Open Access

Address:
Department of Organic Chemistry and Technology, Budapest University of Technology and Economics, 1521 Budapest, Hungary

Email:
György Keglevich - gkeglevich@mail.bme.hu

Keywords:
organophosphorus chemistry

Beilstein J. Org. Chem. **2023,** *19,* 89–90.
https://doi.org/10.3762/bjoc.19.8

Received: 11 January 2023
Accepted: 20 January 2023
Published: 25 January 2023

This article is part of the thematic issue "Organophosphorus chemistry: from model to application".

Guest Editor: G. Keglevich

© 2023 Keglevich; licensee Beilstein-Institut.
License and terms: see end of document.

The thematic issue “Organophosphorus chemistry: from model to application” shows a number of “hot” topics of the discipline under discussion.

Cross-coupling reactions are also of importance in organophosphorus chemistry. Taddei and co-workers applied an alternative method to the classical Hirao reaction [1]. They utilized the Ni-catalyzed double Michaelis–Arbuzov reaction of bis(bromoaryl) species and related N-heterocycles to prepare the respective bisphosphonate derivatives that were transformed to the corresponding diphosphonic acids.

The Pudovik addition is still an evergreen reaction as it leads to α-hydroxyphosphonates that are versatile intermediates in organophosphorus chemistry. Yang et al. elaborated a Lewis acid-catalyzed one-pot synthesis of phosphinates and phosphonates staring from pyridinecarboxaldehydes and diarylphosphine oxides [2]. This protocol is the analogy of the Pudovik reaction, followed by the phospha-Brook rearrangement applied mainly for the synthesis of phosphoric ester derivatives.

In another study, the synthesis of bis(chlorophenyl)acetylenes that were useful for the preparation of 1,2,3-tris(chlorophenyl)cyclopropenylium bromides was accomplished [3]. The latter species were converted to tributyl(1,2,3-tris(chlorophenyl)cyclopropenyl)phosphonium bromides, affording 3,4,5-tris(chlorophenyl)-1,2-diphosphacyclopentadienides upon reaction with polyphosphides. These ligands were converted to the corresponding ferrocene complexes. This synthesis was elaborated by Zagidullin and his team.

The two remaining articles also indicate the importance of the P-heterocyclic discipline in organophosphorus chemistry.

A series of P-stereogenic chiral thiophosphorus acids, such as a fused 1-hydroxytetrahydrophosphinine 1-sulfide, an oxaphosphinine sulfide analogue, and an azaphosphinine sulfide analogue were synthesized my Montchamp and Winters as potential organocatalysts [4]. The newly prepared thiophosphorus acids were not efficient in the asymmetric transfer hydrogenation of 2-phenylquinoline. However, they may find application in other model reactions. These days, stereoselective syntheses incorporating “green" chemical considerations are of utmost importance in medicinal chemistry and beyond.

Quantum chemical calculations are a great support for organic chemists when exploring structures, reactivities, and mechanisms. In this thematic issue, the Diels–Alder cycloaddition of

2-phosphaindolizine, 1-aza-2-phosphaindolizine, 3-aza-2-phosphaindolizine, and 1,3-diaza-2-phosphaindolizine derivatives, with butadiene has been calculated by Bansal and co-workers using DFT [5]. Therein, the dienophilic reactivity of the N=P and P=C units of the heterocycles was in accordance with the experimental observations.

Additionally, a novel triferrocenyl trithiophosphite was synthesized and studied by single-crystal X-ray diffraction by Khrizanforov et al., and the preferred conformations were substantiated by DFT calculations [6].

Finally, Hersh and Chan presented a method to improve the accuracy of ^{31}P NMR chemical shift calculations by use of scaling methods [7].

György Keglevich

Budapest, January 2023

ORCID® iDs

György Keglevich - https://orcid.org/0000-0002-5366-472X

References

1. Shearan, S. J. I.; Andreoli, E.; Taddei, M. *Beilstein J. Org. Chem.* **2022,** *18,* 1518–1523. doi:10.3762/bjoc.18.160
2. Yang, J.; Qian, D.-W.; Yang, S.-D. *Beilstein J. Org. Chem.* **2022,** *18,* 1188–1194. doi:10.3762/bjoc.18.123
3. Zagidullin, A. A.; Akhmatkhanova, F. F.; Khrizanforov, M. N.; Fayzullin, R. R.; Gerasimova, T. P.; Bezkishko, I. A.; Miluykov, V. A. *Beilstein J. Org. Chem.* **2022,** *18,* 1338–1345. doi:10.3762/bjoc.18.139
4. Winters, K. R.; Montchamp, J.-L. *Beilstein J. Org. Chem.* **2022,** *18,* 1471–1478. doi:10.3762/bjoc.18.154
5. Beig, N.; Peswani, A.; Bansal, R. K. *Beilstein J. Org. Chem.* **2022,** *18,* 1217–1224. doi:10.3762/bjoc.18.127
6. Shekurov, R. P.; Khrizanforov, M. N.; Bezkishko, I. A.; Gerasimova, T. P.; Zagidullin, A. A.; Islamov, D. R.; Miluykov, V. A. *Beilstein J. Org. Chem.* **2022,** *18,* 1499–1504. doi:10.3762/bjoc.18.157
7. Hersh, W. H.; Chan, T.-Y. *Beilstein J. Org. Chem.* **2023,** *19,* 36–56. doi:10.3762/bjoc.19.4

License and Terms

This is an open access article licensed under the terms of the Beilstein-Institut Open Access License Agreement (https://www.beilstein-journals.org/bjoc/terms), which is identical to the Creative Commons Attribution 4.0 International License (https://creativecommons.org/licenses/by/4.0). The reuse of material under this license requires that the author(s), source and license are credited. Third-party material in this article could be subject to other licenses (typically indicated in the credit line), and in this case, users are required to obtain permission from the license holder to reuse the material.

The definitive version of this article is the electronic one which can be found at:
https://doi.org/10.3762/bjoc.19.8

BEILSTEIN JOURNAL OF ORGANIC CHEMISTRY

Lewis acid-catalyzed Pudovik reaction–phospha-Brook rearrangement sequence to access phosphoric esters

Jin Yang[1], Dang-Wei Qian[1] and Shang-Dong Yang[*1,2]

Letter

Open Access

Address:
[1]State Key Laboratory of Applied Organic Chemistry, Lanzhou University, Lanzhou 730000, P. R. China and [2]State Key Laboratory for Oxo Synthesis and Selective Oxidation, Lanzhou Institute of Chemical Physics, Lanzhou 730000, P. R. China

Email:
Shang-Dong Yang[*] - yangshd@lzu.edu.cn

* Corresponding author

Keywords:
Lewis acid; phospha-Brook rearrangement; phosphoric esters; Pudovik reaction

Beilstein J. Org. Chem. **2022,** *18,* 1188–1194.
https://doi.org/10.3762/bjoc.18.123

Received: 01 July 2022
Accepted: 16 August 2022
Published: 09 September 2022

This article is part of the thematic issue "Organophosphorus chemistry: from model to application".

Guest Editor: G. Keglevich

© 2022 Yang et al.; licensee Beilstein-Institut.
License and terms: see end of document.

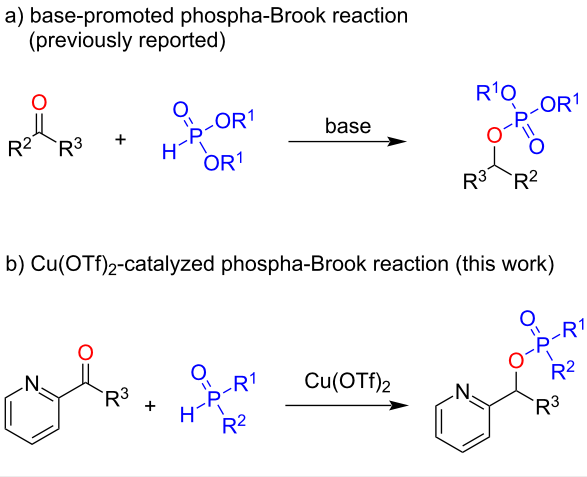
Abstract

Herein, we report a Lewis acid-catalyzed Pudovik reaction–phospha-Brook rearrangement sequence between diarylphosphonates or -phosphinates and α-pyridinealdehydes to access valuable phosphoric ester compounds. This transformation provides an extended substrate scope that is complementary to similar previously reported base-catalyzed transformations.

Introduction

Phosphoric esters are widely used in agrochemistry, biological sciences, clinical treatments, as well as in general organic transformations [1-9]. Therefore, many efficient methods have been developed in the past decades to synthesize different types of phosphoric esters [10-18]. Traditional methods for the construction of P–O bonds in phosphoric esters rely on the phosphorylation of alcohols or phenol with highly air-sensitive and hazardous phosphorus halides, with the assistance of a suitable base [19-24]. As an alternative pathway, the phospha-Brook rearrangement [25-30] represents a green approach to phosphoric esters since it uses α-hydroxyphosphonates, which can be easily prepared by Pudovik reaction (addition of an unsaturated carbonyl compound to a labile P–H bond), to undergo an efficient intramolecular rearrangement, producing phosphoric esters [31-42]. For example, in 2005, Kaïm and co-workers have accomplished the synthesis of phosphoric esters through a 1,8-diazabicyclo[5.4.0]undec-7-ene (DBU)-catalyzed Pudovik reaction–phospha-Brook rearrangement sequence [43]. A decade later, Chakravarty and colleagues reported the efficient synthesis of organic phosphates from ketones and aldehydes using *n*-BuLi as catalyst through a similar transformation under solvent-free conditions [44]. Recently, Zhang's group disclosed a cesium carbonate-catalyzed Pudovik reaction–phospha-Brook rearrangement sequence and extended the phosphorus source from phosphate to phosphonate [45]. Despite of these important advancements, all of the above transformations were carried out under basic conditions, and thus impose barriers for substrates that bear base-sensitive functional groups. More importantly, heteroatom-containing ketones and aldehydes have been proven to be challenging substrates for all of these existing

systems [46-49]. Thus, searching for an alternative catalytic system, for example, a mild Lewis acid-catalyzed system, to achieve a wide applicability and provide a substrate scope complementary to previously reported base-catalyzed reactions, is a highly desirable task. However, such a process is recognized as challenging since there is no single report on such a sequence under Lewis acid catalysis. Herein, we report the synthesis of phosphoric esters by a Lewis acid $Cu(OTf)_2$-catalyzed one-pot Pudovik reaction–phospha-Brook rearrangement sequence between pyridinyl-substituted aldehyde or pyridone with diarylphosphonates and -phosphinates (Scheme 1b). The present method is simple and efficient, providing an extended substrate scope that is complementary to classical similar base-prompted reactions.



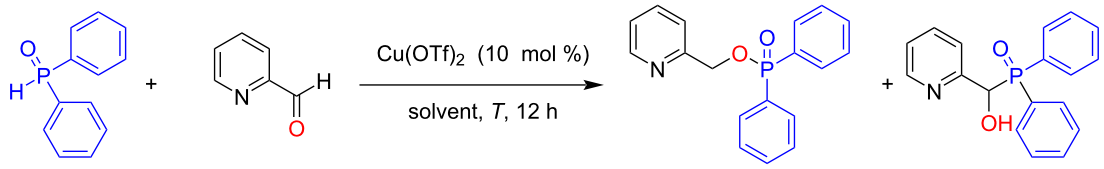
Scheme 1: Different strategies for phospha-Brook reactions.

Results and Discussion

We used diphenylphosphine oxide (**1a**) and 2-pyridinecarboxaldehyde (**2a**) as the standard substrates to test the suitable conditions for the O-phosphination product **3aa**. Delightfully, in the presence of 10 mol % $Cu(OTf)_2$ in toluene at 100 °C, the desired product **3aa** was obtained in 62% yield, and no Pudovik adduct **4aa** was detected (Table 1, entry 1). Inspired by this result, we conducted a careful screening of the other reaction factors to improve the reaction outcome. The screening of solvents was then carried out (Table 1, entries 1−5), and THF was found to be the optimal solvent. The temperature also played a pivotal role in the formation of **3aa**, with traces of, or no desired **3aa** being obtained at a temperature lower than 80 °C, but **4aa** was produced in a high yield (Table 1, entries 7−9). When the reaction was performed at 120 °C, the yield of **3aa** was slightly lower than that at 100 °C.

With the high-yielding reaction conditions established (Table 1, entry 5), we examined a series of reactions of symmetric and asymmetric secondary phosphine oxides with 2-pyridinecarboxaldehyde (**2a**), which produced the corresponding O-phosphination products (Scheme 2). Diarylphosphine oxide substrates with either electron-withdrawing or electron-donating groups tethered to the phenyl ring were well tolerated, and the phosphi-

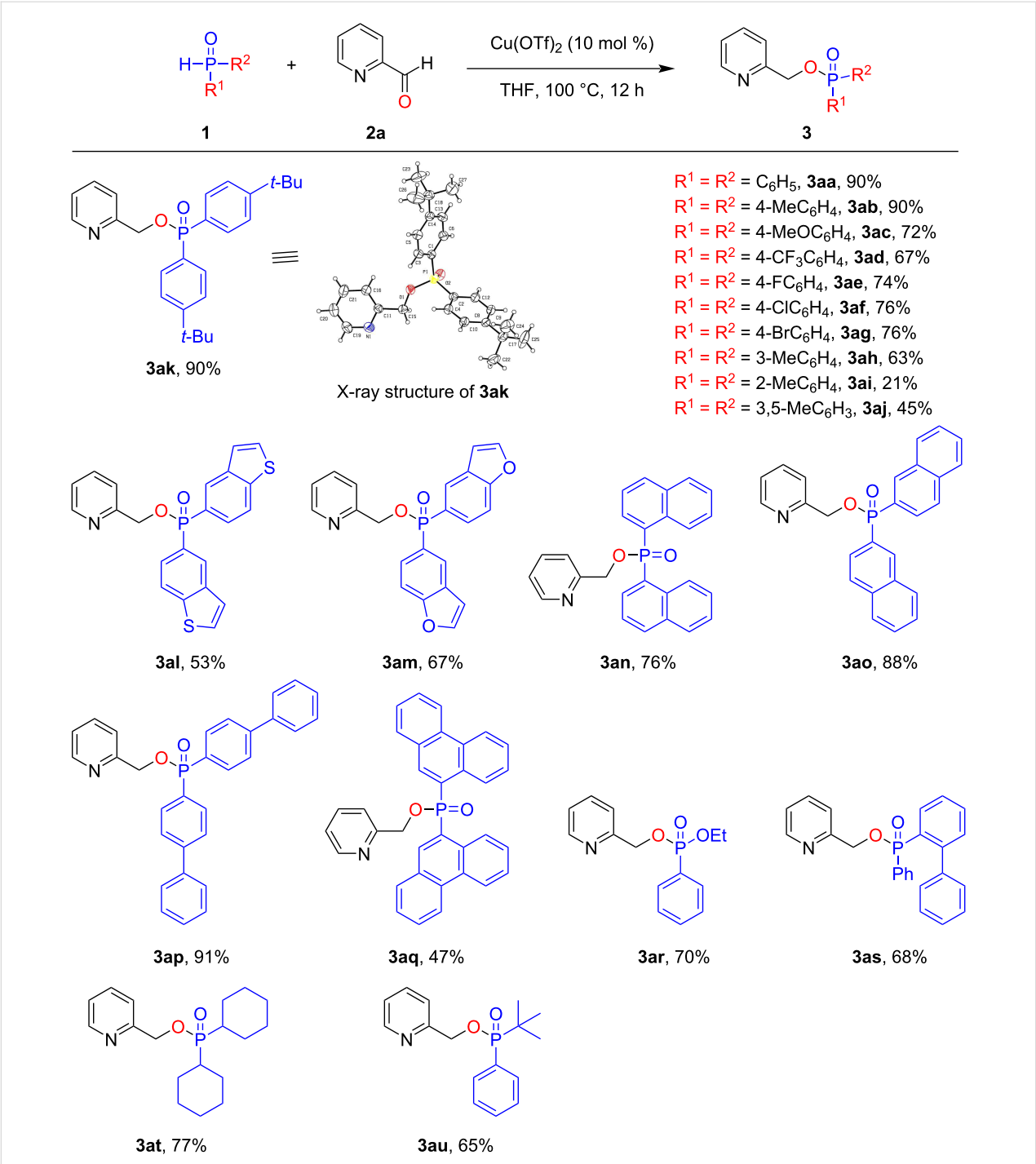
Table 1: Reaction optimization.[a]



1a **2a** **3aa** **4aa**

entry	solvent	*T* (°C)	**3aa** (%)[b]	**4aa** (%)[b]
1	toluene	100	62	n. d.
2	MeCN	100	53	n. d.
3	DCM	100	53	n. d.
4	AcOEt	100	61	n. d.
5	THF	100	90	n. d.
6	THF	80	23	66
7	THF	60	traces	83
8	THF	40	n. d.	72
9	THF	25	n. d.	56
10	THF	120	74	n. d.

[a]Reaction conditions: diphenylphosphine oxide (**1a**, 0.2 mmol), 2-pyridinecarboxaldehyde (**2a**, 0.3 mmol), $Cu(OTf)_2$ (10 mol %), solvent (2 mL), under Ar at 100 °C for 12 h. [b]Isolated yield.



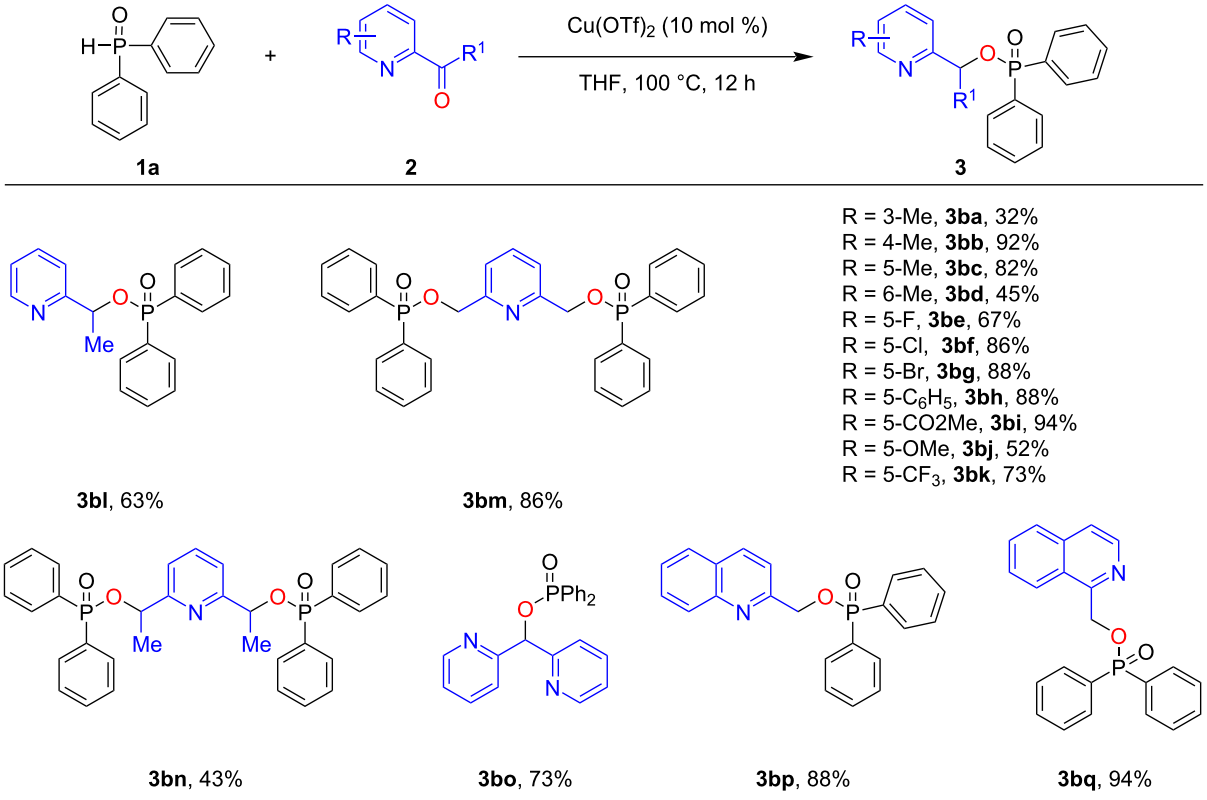
Scheme 2: Scope of **1** (secondary phosphine oxides and phosphonate). Reaction conditions: **1** (0.2 mmol), 2-pyridinecarboxaldehyde (**2a**, 0.3 mmol), $Cu(OTf)_2$ (10 mol %), THF (2 mL), under Ar at 100 °C for 12 h. The isolated yield is given.

nate products **3ab**–**ah** were obtained in moderate to good yield. The steric hindrance effect had a significant influence on the outcome of the reaction. For the phosphine oxide substrate **1i** bearing an *ortho*-methyl-substituted phenyl group, the desired product **3ai** was obtained in 21% yield, while the *meta*-methyl-substituted derivative **1h** was converted into the corresponding product **3ah** in 63% yield. In addition, the configuration of **3ak** was determined by an X-ray crystallographic analysis (CCDC 2177793). To our delight, phosphorus sources containing a heterocycle, such as a benzothiophene (in **1l**) or a benzofuran unit (in **1m**), could smoothly be transformed into the desired products **3al** and **3am**, respectively, in moderate yield. Phosphi-

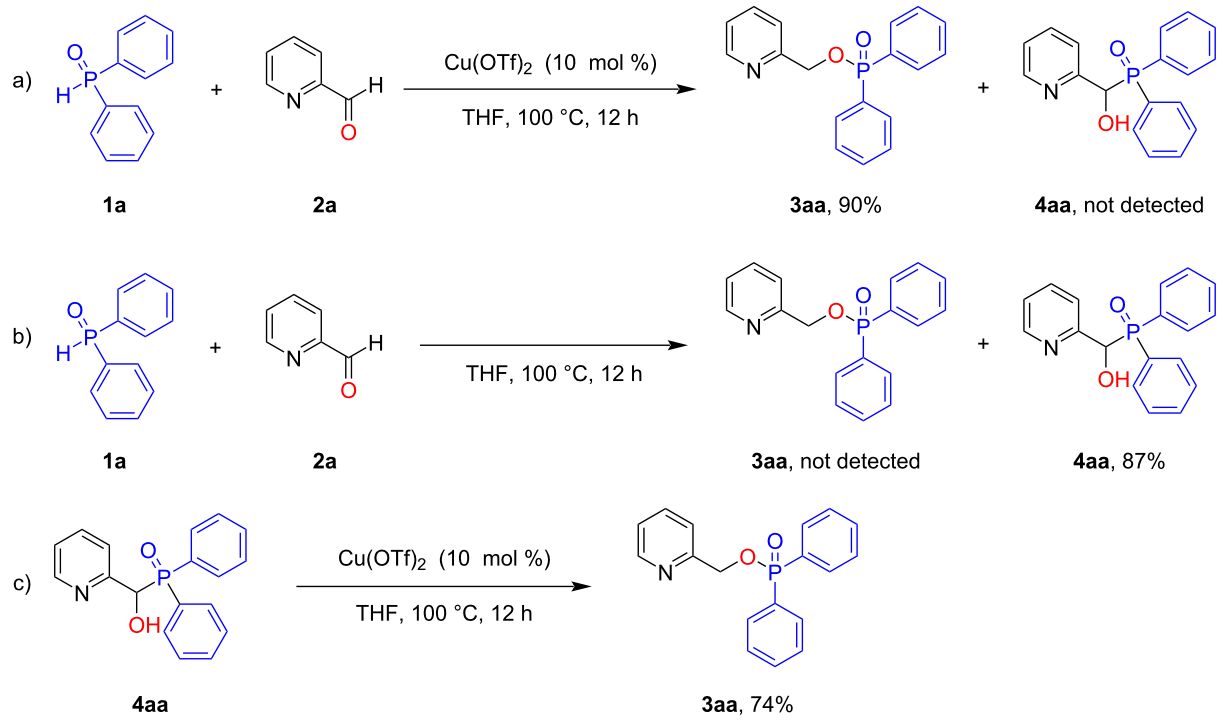
nates **3an** and **3ao** could both be prepared under this Pudovik reaction–phospha-Brook rearrangement sequence in moderate to good yield. When the phenyl groups of the diarylphosphine oxide **1a** were formally replaced by biphenyl units in **1p**, **3ap** was produced in 91% yield under the standard conditions. However, in the presence of bulky anthracene groups in **1q**, only a 47% yield of **3aq** was obtained. The applicability of the reaction system was further demonstrated with various unsymmetrically substituted phosphine oxides under the standard conditions. When the aryl group in the diarylphosphine oxide substrate was replaced by one or two alkyl groups or an ethoxy group, the transformation could also be achieved in moderate to good yield (see **3ar**–**au**).

Next, we studied the scope with respect to the α-pyridinecarboxaldehyde by using **1a** as the reaction partner (Scheme 3). Firstly, we investigated the effect of steric hindrance on the pyridine ring of the α-pyridinealdehyde. Under standard conditions, a methyl group was introduced at either the 3-, 4-, or 5-position of the α-pyridinealdehyde, and the desired products **3ba**–**bc** were obtained in 32%, 92%, and 82%, respectively, indicating that the reaction is sensitive to steric effects. We then investigated the electronic effects of the α-pyridinealdehyde on the reaction outcome. However, no clear trend regarding electronic effects could be observed since α-pyridinealdehydes bearing either an electron-donating group (e.g., Me, MeO, Ph) or electron-withdrawing group (e.g., F, Cl, Br, CF_3, CO_2Me) in position 5 were all well tolerated, and the desired products were generally obtained in moderate to good yield. Delightfully, in addition to aldehydes, a ketone was also applicable under standard conditions, albeit affording the product in a comparably lower yield, probably due to the lower reactivity and steric hindrance of the substrate (see **3bl**). Moreover, pyridine bearing two formaldehyde or ketone groups could also be transformed into the desired diphosphination products **3bm** and **3bn** in moderate to good yield. The generality of the system was further showcased by tolerating quinoline and isoquinoline groups, and the desired products **3bp** and **3bq** were afforded in a high yield.

Additional experiments were conducted in order to clarify the reaction mechanism. Under standard conditions, only pyridin-2-ylmethyl diphenylphosphinate (**3aa**) was produced, and the Pudovik adduct (hydroxy(pyridin-2-yl)methyl)diphenylphos-



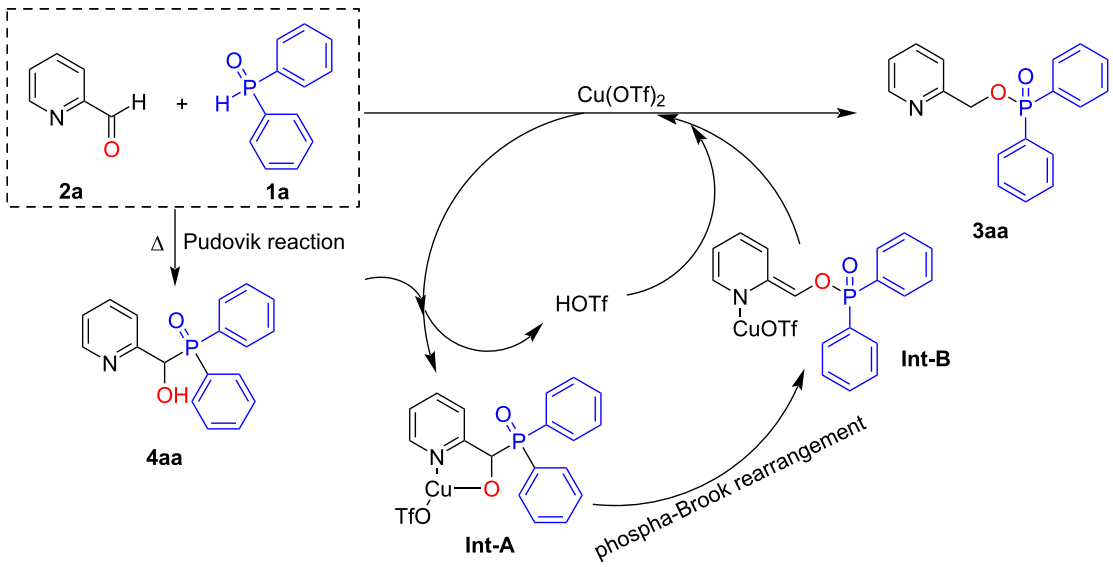
Scheme 3: Scope of **2** (α-pyridinealdehydes and α-pyridones). Reaction conditions: diphenylphosphine oxide (**1a**, 0.2 mmol), **2** (0.3 mmol), $Cu(OTf)_2$ (10 mol %), THF (2 mL), under Ar at 100 °C for 12 h. The isolated yield is given.



Scheme 4: Control experiments.

phine oxide (**4aa**) was not detected (Scheme 4a). The control experiment showed that in the absence of $Cu(OTf)_2$ catalyst, the reaction produced **4aa** as the sole product in 87% yield (Scheme 4b). When **4aa** was used as the substrate to carry out the phospha-Brook rearrangement under the standard conditions, phosphinate **3aa** was afforded in 74% yield (Scheme 4c). Taken together all of the above results, we concluded that **4aa** is the intermediate of this transformation and that $Cu(OTf)_2$ promotes the phospha-Brook rearrangement occurring in the reaction.

Based on the above results and literature reports, the proposed mechanism is shown in Scheme 5. First, diphenylphosphine oxide (**1a**) and 2-pyridinecarboxaldehyde (**2a**) undergo the



Scheme 5: Proposed mechanism.

Pudovik reaction to produce the intermediate adduct **4aa**. Then, $Cu(OTf)_2$ coordinates with **4aa** to form the intermediate **Int-A**, which goes through the phospha-Brook rearrangement process to form **Int-B**. Finally, **Int-B** is transformed into the product **3aa** and releases $Cu(OTf)_2$ to close the catalytic cycle.

Conclusion

In conclusion, a Lewis acid-catalyzed Pudovik reaction–phospha-Brook rearrangement sequence between diarylphosphonates or -phosphinates and α-pyridinealdehydes was developed. This approach provides an efficient approach towards phosphoric esters and provides a scope complementary to previous similar base-catalyzed transformation.

Supporting Information

Supporting Information File 1

Experimental details and characterization data (^{1}H, ^{13}C, and ^{31}P NMR as well as chromatograms) of products.
[https://www.beilstein-journals.org/bjoc/content/supplementary/1860-5397-18-123-S1.pdf]

Funding

We are grateful to the NSFC (No. 22171119), Gansu Province Science and Technology Plan Project (No. 21YF5WA114 and No. 21ZD4WA021) for financial support.

References

1. Williams, N. H.; Wyman, P. *Chem. Commun.* **2001,** 1268–1269. doi:10.1039/b103317b
2. Westheimer, F. H. *Science* **1987,** *235,* 1173–1178. doi:10.1126/science.2434996
3. Protti, S.; Fagnoni, M. *Chem. Commun.* **2008,** 3611–3621. doi:10.1039/b801888j
4. Zhu, J.; Fu, H.; Jiang, Y.; Zhao, Y. *Synlett* **2005,** 1927–1929. doi:10.1055/s-2005-871582
5. Szymańska, A.; Szymczak, M.; Boryski, J.; Stawiński, J.; Kraszewski, A.; Collu, G.; Sanna, G.; Giliberti, G.; Loddo, R.; Colla, P. L. *Bioorg. Med. Chem.* **2006,** *14,* 1924–1934. doi:10.1016/j.bmc.2005.10.048
6. Li, W.; Gong, X.; Fan, X.; Yin, S.; Su, D.; Zhang, X.; Yuan, L. *Chin. Chem. Lett.* **2019,** *30,* 1775–1790. doi:10.1016/j.cclet.2019.07.056
7. Kategaonkar, A. H.; Pokalwar, R. U.; Sonar, S. S.; Gawali, V. U.; Shingate, B. B.; Shingare, M. S. *Eur. J. Med. Chem.* **2010,** *45,* 1128–1132. doi:10.1016/j.ejmech.2009.12.013
8. Molt, O.; Rübeling, D.; Schrader, T. *J. Am. Chem. Soc.* **2003,** *125,* 12086–12087. doi:10.1021/ja035212l
9. Köhn, M.; Breinbauer, R. *Angew. Chem., Int. Ed.* **2004,** *43,* 3106–3116. doi:10.1002/anie.200401744
10. Wang, S.-P.; Tong, Y.-F.; Wang, D.-M.; Wang, N.; Yan, Z.; Huang, P.; Wu, S. *Chin. Chem. Lett.* **2014,** *25,* 1044–1046. doi:10.1016/j.cclet.2014.05.042
11. Fañanás-Mastral, M.; Feringa, B. L. *J. Am. Chem. Soc.* **2014,** *136,* 9894–9897. doi:10.1021/ja505281v
12. Dhineshkumar, J.; Prabhu, K. R. *Org. Lett.* **2013,** *15,* 6062–6065. doi:10.1021/ol402956b
13. Xiong, B.; Wang, G.; Zhou, C.; Liu, Y.; Zhang, P.; Tang, K. *J. Org. Chem.* **2018,** *83,* 993–999. doi:10.1021/acs.joc.7b02422
14. Xiong, B.; Hu, C.; Li, H.; Zhou, C.; Zhang, P.; Liu, Y.; Tang, K. *Tetrahedron Lett.* **2017,** *58,* 2482–2486. doi:10.1016/j.tetlet.2017.05.036
15. Ou, Y.; Huang, Y.; He, Z.; Yu, G.; Huo, Y.; Li, X.; Gao, Y.; Chen, Q. *Chem. Commun.* **2020,** *56,* 1357–1360. doi:10.1039/c9cc09407e
16. Niu, Y.; Yang, S.-D. *Chem. Synth.* **2021,** *1,* 12. doi:10.20517/cs.2021.14
17. Liu, J.; Xiao, H.-Z.; Fu, Q.; Yu, D.-G. *Chem. Synth.* **2021,** *1,* 9. doi:10.20517/cs.2021.07
18. Cai, B.-G.; Xuan, J.; Xiao, W.-J. *Sci. Bull.* **2019,** *64,* 337–350. doi:10.1016/j.scib.2019.02.002
19. Pisarek, S.; Bednarski, H.; Gryko, D. *Synlett* **2012,** *23,* 2667–2671. doi:10.1055/s-0032-1317344
20. Xiong, B.; Zhou, Y.; Zhao, C.; Goto, M.; Yin, S.-F.; Han, L.-B. *Tetrahedron* **2013,** *69,* 9373–9380. doi:10.1016/j.tet.2013.09.001
21. Cao, S.; Guo, Y.; Wang, J.; Qi, L.; Gao, P.; Zhao, H.; Zhao, Y. *Tetrahedron Lett.* **2012,** *53,* 6302–6305. doi:10.1016/j.tetlet.2012.09.056
22. Nowlan, C.; Li, Y.; Hermann, J. C.; Evans, T.; Carpenter, J.; Ghanem, E.; Shoichet, B. K.; Raushel, F. M. *J. Am. Chem. Soc.* **2006,** *128,* 15892–15902. doi:10.1021/ja0658618
23. Georgiev, E. M.; Kaneti, J.; Troev, K.; Roundhill, D. M. *J. Am. Chem. Soc.* **1993,** *115,* 10964–10973. doi:10.1021/ja00076a063
24. Pudovik, A. N.; Konovalova, I. V. *Synthesis* **1979,** 81–96. doi:10.1055/s-1979-28566
25. Rádai, Z.; Szabó, R.; Szigetvári, Á.; Kiss, N. Z.; Mucsi, Z.; Keglevich, G. *Curr. Org. Chem.* **2020,** *24,* 465–471. doi:10.2174/1385272824666200226114306
26. Kuroboshi, M.; Ishihara, T.; Ando, T. *J. Fluorine Chem.* **1988,** *39,* 293–298. doi:10.1016/s0022-1139(00)82785-2
27. Kondoh, A.; Ozawa, R.; Aoki, T.; Terada, M. *Org. Biomol. Chem.* **2017,** *15,* 7277–7281. doi:10.1039/c7ob02059g
28. Kondoh, A.; Terada, M. *Org. Biomol. Chem.* **2016,** *14,* 4704–4711. doi:10.1039/c6ob00739b
29. Demir, A. S.; Eymur, S. *J. Org. Chem.* **2007,** *72,* 8527–8530. doi:10.1021/jo070913c
30. Hayashi, M.; Nakamura, S. *Angew. Chem., Int. Ed.* **2011,** *50,* 2249–2252. doi:10.1002/anie.201007568
31. Wu, Q.; Zhou, J.; Yao, Z.; Xu, F.; Shen, Q. *J. Org. Chem.* **2010,** *75,* 7498–7501. doi:10.1021/jo101743e
32. Abell, J. P.; Yamamoto, H. *J. Am. Chem. Soc.* **2008,** *130,* 10521–10523. doi:10.1021/ja803859p
33. Wang, J.; Li, J.; Wei, Y.; Yang, J.; Huo, C. *Org. Chem. Front.* **2018,** *5,* 3534–3537. doi:10.1039/c8qo01049h
34. Barozzino Consiglio, G.; Queval, P.; Harrison-Marchand, A.; Mordini, A.; Lohier, J.-F.; Delacroix, O.; Gaumont, A.-C.; Gérard, H.; Maddaluno, J.; Oulyadi, H. *J. Am. Chem. Soc.* **2011,** *133,* 6472–6480. doi:10.1021/ja201760c
35. Wynberg, H.; Smaardijk, A. A. *Tetrahedron Lett.* **1983,** *24,* 5899–5900. doi:10.1016/s0040-4039(00)94232-1

36. Smaardijk, A. A.; Noorda, S.; van Bolhuis, F.; Wynberg, H. *Tetrahedron Lett.* **1985,** *26,* 493–496. doi:10.1016/s0040-4039(00)61920-2
37. Akiyama, T.; Morita, H.; Itoh, J.; Fuchibe, K. *Org. Lett.* **2005,** *7,* 2583–2585. doi:10.1021/ol050695e
38. Samanta, S.; Zhao, C.-G. *J. Am. Chem. Soc.* **2006,** *128,* 7442–7443. doi:10.1021/ja062091r
39. Yokomatsu, T.; Yamagishi, T.; Shibuya, S. *Tetrahedron: Asymmetry* **1993,** *4,* 1779–1782. doi:10.1016/s0957-4166(00)80415-2
40. Groaning, M. D.; Rowe, B. J.; Spilling, C. D. *Tetrahedron Lett.* **1998,** *39,* 5485–5488. doi:10.1016/s0040-4039(98)01139-3
41. Wei, X.-H.; Bai, C.-Y.; Wang, A.-J.; Feng, Q.-L.; Zhao, L.-B.; Zhang, P.; Li, Z.-H.; Su, Q.; Wang, Y.-B. *Org. Lett.* **2021,** *23,* 7100–7105. doi:10.1021/acs.orglett.1c02504
42. Wei, X.-H.; Bai, C.-Y.; Zhao, L.-B.; Zhang, P.; Li, Z.-H.; Wang, Y.-B.; Su, Q. *Chin. J. Chem.* **2021,** *39,* 1855–1860. doi:10.1002/cjoc.202100083
43. El Kaïm, L.; Gaultier, L.; Grimaud, L.; Dos Santos, A. *Synlett* **2005,** 2335–2336. doi:10.1055/s-2005-872670
44. Pallikonda, G.; Santosh, R.; Ghosal, S.; Chakravarty, M. *Tetrahedron Lett.* **2015,** *56,* 3796–3798. doi:10.1016/j.tetlet.2015.04.073
45. Qian, Y.; Dai, Q.; Li, Z.; Liu, Y.; Zhang, J. *Org. Lett.* **2020,** *22,* 4742–4748. doi:10.1021/acs.orglett.0c01537
46. Ruveda, M. A.; De Licastro, S. A. *Tetrahedron* **1972,** *28,* 6012–6018. doi:10.1016/0040-4020(72)88135-3
47. Gancarz, R.; Gancarz, I.; Walkowiak, U. *Phosphorus, Sulfur Silicon Relat. Elem.* **1995,** *104,* 45–52. doi:10.1080/10426509508042576
48. Sun, Y.-M.; Xin, N.; Xu, Z.-Y.; Liu, L.-J.; Meng, F.-J.; Zhang, H.; Fu, B.-C.; Liang, Q.-J.; Zheng, H.-X.; Sun, L.-J.; Zhao, C.-Q.; Han, L.-B. *Org. Biomol. Chem.* **2014,** *12,* 9457–9465. doi:10.1039/c4ob01574f
49. Timmler, H.; Kurz, J. *Chem. Ber.* **1971,** *104,* 3740–3749. doi:10.1002/cber.19711041204

License and Terms

This is an open access article licensed under the terms of the Beilstein-Institut Open Access License Agreement (https://www.beilstein-journals.org/bjoc/terms), which is identical to the Creative Commons Attribution 4.0 International License (https://creativecommons.org/licenses/by/4.0). The reuse of material under this license requires that the author(s), source and license are credited. Third-party material in this article could be subject to other licenses (typically indicated in the credit line), and in this case, users are required to obtain permission from the license holder to reuse the material.

The definitive version of this article is the electronic one which can be found at:
https://doi.org/10.3762/bjoc.18.123

BEILSTEIN JOURNAL OF ORGANIC CHEMISTRY

Dienophilic reactivity of 2-phosphaindolizines: a conceptual DFT investigation

Nosheen Beig, Aarti Peswani and Raj Kumar Bansal*

Full Research Paper

Open Access

Address:
Department of Chemistry, The IIS (Deemed to be University), Jaipur 302020, India

Email:
Raj Kumar Bansal* - bansal56@gmail.com

* Corresponding author

Keywords:
dienophilic reactivity; electronic chemical potential; electrophilicity index; Fukui function; global hardness; nucleophilicity index; 2-phosphaindolizines

Beilstein J. Org. Chem. **2022,** *18,* 1217–1224.
https://doi.org/10.3762/bjoc.18.127

Received: 22 June 2022
Accepted: 02 September 2022
Published: 13 September 2022

This article is part of the thematic issue "Organophosphorus chemistry: from model to application".

Guest Editor: G. Keglevich

© 2022 Beig et al.; licensee Beilstein-Institut.
License and terms: see end of document.

Abstract

The >C=P– or –N=P– functionality in 1,3-azaphospholo[1,5-*a*]pyridine, named as 2-phosphaindolizine and its 1- and 3-aza derivatives act as dienophiles and undergo Diels–Alder reactions with 1,3-dienes. However, the dienophilic reactivity is affected by the nature of the substituent groups on the two sides of the σ^2,λ^3-P atom and also by the presence of more nitrogen atom(s) in the five-membered ring. The conceptual density functional theory (DFT) calculations have been used in recent years to predict the reactivity of organic molecules in reactions. We calculated global hardness (η), global softness (S), electronic chemical potential (μ), electrophilicity (ω), and nucleophilicity (*N*) indices of four classes of 2-phosphaindolizines, on the basis of which their observed relative dienophilic reactivities could be rationalized. Besides, the Fukui functions of the carbon/nitrogen and phosphorus atoms of the >C=P– and –N=P– functionalities were also computed which revealed their hard electrophilic character and accorded well with the dienophilic reactivities observed experimentally. Furthermore, energies and symmetries of the lowest unoccupied molecular orbitals (LUMO) of 2-phosphaindolizines were found to be in conformity with their dienophilic reactivities.

Introduction

In 1988, we developed a simple synthetic method for the synthesis of 1,3-azaphospholo[1,5-*a*]pyridine derivative (**1**, R^1 = Me, R^2 = PhCO) from the reaction of 2-ethyl-1-phenacylpyridinium bromide with PCl_3 and Et_3N, which was named as 2-phosphaindolizine perceiving it to result from a formal CH/P exchange at the 2-position of indolizine (**2**) (Figure 1) [1]. Subsequently a good library of these interesting compounds became accessible [1].

The methodology could be extended successfully to the synthesis of 1,3,4-diazaphospholo[1,2-*a*]pyridines, i.e., 1-aza-2-phosphaindolizines **3** [2], 1,2,3-diazaphospholo[1,5-*a*]pyridines, i.e.,

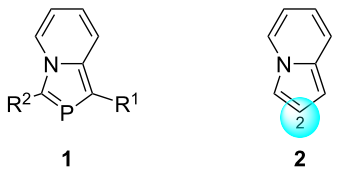


Figure 1: Structures of 2-phosphaindolizine (**1**) and indolizine (**2**).

3-aza-2-phosphaindolizines **4** [3], and 1,2,4,3-triazaphospholo[1,5-*a*]pyridine, i.e., 1,3-diaza-2-phosphaindolizine (**5**, Figure 2) [4]. We succeeded in developing another method involving a 1,5-electrocyclization of the initially formed pyridinium alkoxycarbonyl-dichlorophosphinomethylide followed by 1,2-elimination affording 1,3-bis(alkoxycarbonyl)-2-phosphaindolizines [5].

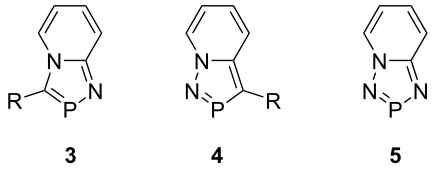


Figure 2: Structures of 1-aza-2-phosphaindolizines **3**, 3-aza-2-phosphaindolizines **4**, and 1,3-diaza-2-phosphaindolizine (**5**).

After having access to a good number of differently substituted derivatives of these four classes of 2-phosphaindolizines, we were motivated to explore their reactivity as they apparently have many active functionalities. In view of the earlier reported results of the Diels–Alders (DA) reaction across the >C=P– functionality in phosphaalkenes [6], phosphaketenes [6], heterophospholes [7], phosphinines [8], and azaphosphinines [9] (a recent review incorporates all these classes [10]), we investigated DA reactions across the >C=P– or –N=P– functionality present in these compounds. During this, we found that these compounds exhibited quite different dienophilic reactivities towards 2,3-dimethyl-1,3-butadiene (DMB). 2-Phosphaindolizines having electron-withdrawing groups (EWG) both at the 1 and 3-positions, namely 1,3-bis(ethoxycarbonyl)-1,3-azaphospholo[1,5-*a*]pyridine (**1**: $R^1 = R^2 =$ COOEt) and its isoquinoline analogue, reacted with DMB and isoprene to give the [2 + 4] cycloadducts, in the latter case, regioselectively [11]. However, 2-phosphaindolizines having an EWG at the 3-position only, namely 3-ethoxycarbonyl-1-methyl-2-phosphaindolizine (**1**: R^1 = Me, R^2 = COOEt) did not undergo the DA reaction with DMB alone or in the presence of sulfur even when refluxing in toluene [12]. The reaction could be accomplished only in the presence of a Lewis acid catalyst, namely ethylaluminum dichloride [13]. Furthermore, when carrying out the reaction of compounds **1** (R^1 = Me, R^2 = COOMe, COOEt, $COOCMe_3$) with DMB in the presence of the catalyst *O*-menthoxyaluminium dichloride, generated in situ, complete diastereoselectivity was observed.

The DA reactions of 1-aza-2-phosphaindolizines **3** with DMB and isoprene occurred at rt, although slowly and were speeded up by the use of sulfur or selenium which oxidized the phosphorus atom of the initially formed product thereby pushing the reaction in the forward direction [14].

The difference in the reactivities of two classes of 2-phosphaindolizines namely the 2-phosphaindolizine substituted by the EWG at 3-position only (**1**, R^1 = Me, $R^2 = CO_2Me$) and substituted by EWGs both at the 1- and 3- positions (**1**, $R^1 = R^2 = CO_2Me$) could be rationalized on the basis of DFT calculations at the B3LYP/6-31G (d,p) level of theory wherein it was revealed that the nitrogen lone-pair is transferred effectively into the azaphospole ring. In compound **1** (R^1 = Me, $R^2 = CO_2Me$) the EWG at the 3-position emphasizes this effect further. As a result, the >C=P– functionality becomes electron-rich and does not undergo a DA reaction with an electron-rich diene such as DMB. However, in the case of compound **1** ($R^1 = R^2 = CO_2Me$), the EWG at the 1-position functions as electron-sink between the nitrogen lone-pair and the >C=P– functionality. As a result, the latter retains its electron-deficient character and undergoes DA reaction with DMB (Figure 3) [15].



Figure 3: Transfer of the nitrogen lone-pair in 2-phosphaindolizines.

The DFT based on the Hohenberg–Kohn theorems and later on the Kohn–Sham approximation made it possible to study the progress of organic reactions with manageable computational costs [16,17]. Parr and co-worker [18] developed "Conceptual DFT", a subfield of DFT which allows to calculate various reactivity descriptors, such as electrochemical potential, electrophilicity and nucleophilicity indices, global hardness, electronegativity, etc.

The concept of hard–soft acid–base (HSAB) was used to explain the reactivity of the organic molecules towards electrophilic and nucleophilic reagents [19]. Thus a quantitative descriptor, the Fukui function was defined as

$$f^{+}(r) = \rho_{N+1}(r) - \rho_{N}(r)$$

for nucleophilic attack and

$$f^{-}(r) = \rho_{N}(r) - \rho_{N+1}(r)$$

for electrophilic attack,

where $\rho_{N+1}(r)$, ρ_N(r), and $\rho_{N-1}(r)$ are the electron densities at a point r in the system with N+1, N, and N−1 electrons, respectively, all with the ground-state geometry of the N-electron system. It was concluded that the regions of a molecule with a large Fukui function are chemically softer than the regions where the Fukui function is small. Thus, by invoking the HSAB principle it becomes possible to predict the behavior of a particular site in the molecule towards hard or soft reagents [19].

Yang and Mortier [20] suggested the use of the gross charge (q_r) at a particular atom r in a molecule obtained from the Mulliken population analysis (MPA) for the calculation of the condensed Fukui function (f(r)) at that atom. The condensed Fukui function using MPA often has negative values and in this context, the use of Hirshfeld population analysis (HPA) based on the Stock-Holder idea was recommended [21,22].

We report herein different conceptual DFT descriptors of four classes of 2-phosphaindolizines and the attempts to compare the dienophilic reactivities of the >C=P– or –N=P– functionality present in these compounds towards 1,3-butadiene.

Results and Discussion

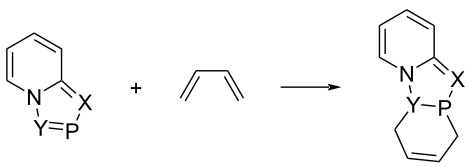
We investigated the following model DA reactions (Table 1) at the DFT (B3LYP/6-31+G (d)) level of theory.

The values of the energies of the frontier molecular orbitals (FMOs) global hardness (η), global softness (S), electronic chemical potential (μ), electrophilicity (ω) and nucleophilicity (N) indices of 2-phosphaindolizines **6** and 1,3-butadiene (**7**) are given in Table 2.

2-Phosphaindolizines and 1,3-butadiene are soft electrophiles and nucleophile, respectively, and in accordance with the HSAB principle, they are expected to react. In the series **6A** of 2-phosphaindolizines, the softness decreases in the order **6Ad** > **6Ab** > **6Ac** > **6Aa**. No representatives of **6Aa** and **6Ab** have been prepared so far. Thus, compound **6Ad** is expected to undergo a DA reaction faster than compound **6Ac** which is in agreement with the reported results; the former reacts with DMB without the aid of a catalyst [11] whereas the latter undergoes DA reaction only in the presence of a catalyst [13]. However, it may be noted that although compounds **6Bb** and **6D** are less soft than **6Ac**, they undergo DA reaction without the aid of a catalyst [14]. As discussed later, this can be rationalized on the basis of the local hardness represented by the Fukui function.

The electronic chemical potential (μ) is another useful descriptor that reveals efficacy of charge transfer from the species of higher chemical potential to a species with lower chemical potential [23]. The reactivities of two substrates A and B with the same reagent C can be compared on the basis of the relative values of ΔμAC and ΔμBC; the greater the value of Δμ is, the faster will be the reaction. In this context, it may be noted that except for compound **6Aa**, i.e., the unsubstituted 2-phosphaindolizine, the electronic chemical potentials of the other 2-phosphaindolizines are smaller than the electronic chemical potential of 1,3-butadiene indicating the possibility of an effective charge transfer from the latter to the former. Furthermore, the gap between the chemical potentials of 2-phosphaindolizines and 1,3-butadiene decreases in the order **6Ad** > **6Ab** > **6Ac**; **6Bb** > **6Ba**; **6Cb** > **6Ca**. This order is similar to the one derived on the basis of global hardness discussed earlier and is also in conformity with the experimental results.

Table 1: Model DA reactions of 2-phosphaindolizines with 1,3-butadiene computed at the B3LYP/6-31+G(d) level of theory.



6 **7** **8**

6	Aa	Ab	Ac	Ad	Ba	Bb	Ca	Cb	D
X	CH	C-CO_2Me	CH	C-CO_2Me	N	N	CH	C-CO_2Me	N
Y	CH	CH	C-CO_2Me	C-CO_2Me	CH	C-CO_2Me	N	N	N

Table 2: Energies of frontier molecular orbitals, global hardness, global softness, electronic chemical potential, electrophilicity, and nucleophilicity indices of 2-phosphaindolizines and 1,3-butadiene.

Compounds **6**	E_{HOMO} (eV)	E_{LUMO} (eV)	Global hardness η (eV)	Global softness S (eV)	Electronic chemical potential μ (eV)	Electrophilicity index ω (eV) × 10^2	Nucleophilicity index[a] N (eV) × 10^2
Aa	–0.211	–0.025[b]	0.079	6.361	–0.132	0.110	–
Ab	–0.222	–0.033[b]	0.076	6.548	–0.146	0.139	–
Ac	–0.221	–0.068	0.077	6.510	–0.144	0.135	–
Ad	–0.230	–0.080	0.075	6.644	–0.155	0.160	–
Ba	–0.232	–0.001[c]	0.084	5.952	–0.148	0.128	–
Bb	–0.242	–0.080	0.081	6.184	–0.161	0.160	–
Ca	–0.231	–0.042[b]	0.085	5.899	–0.146	0.125	–
Cb	–0.240	–0.078	0.081	6.161	–0.159	0.156	–
D	–0.256	–0.052[b]	0.091	5.494	–0.164	0.148	–
7	–0.242	–0.042	0.100	5.000	–0.142	–	0.104

[a]With respect to TCNE = E_{HOMO} = –0.346; [b]LUMO + 1 as LUMO is not of proper symmetry; [c]LUMO + 3 as LUMO is not of proper symmetry.

The electrophilicity (ω) [24] and nucleophilicity (N) [25,26] indices are other useful descriptors that explain relative reactivities of molecules in chemical reactions [27]. The electrophilicity indices of 2-phosphaindolizines also decrease in the same order as observed on the basis of global hardness and electronic chemical potential. Furthermore, the electrophilicity index of compound **6D** (0.148) is close to that of **6Cb** (0.156) and like **6Cb**, it is expected to undergo a DA reaction with 1,3-butadiene without the aid of a catalyst, a fact in conformity with the experimental results.

Concept of local hardness/softness

Fukui function analysis

As discussed earlier, the descriptor Fukui function was developed to determine the hard/soft character of the reactive site in a molecule [19-21]. The Fukui functions at the carbon/nitrogen and phosphorus atoms of the >C=P– or –N=P– functionality of 2-phosphaindolizines calculated from the Mulliken and Hirshfeld charges are given in Table 3.

A close look at the Fukui functions calculated from the Mulliken and Hirshfeld charges reveals that they follow almost a similar pattern; in view of this, our further discussion is based on the Fukui functions calculated from the former. As the P atom is common in the >C=P– and –N=P– functionalities, we concentrated on the relative values of the Fukui functions of the P atom in different 2-phosphamdolizines. The values of the Fukui function of the P atom in the series of different 2-phosphaindolizines decrease in the order: **Ad** > **Ac** > **AB** > **Aa**; **Ba** > **Bb**; **Cb** > **Ca**.

Except the series, **Ba** > **Bb**, this order is similar to those obtained on the basis of the other descriptors discussed earlier. It may be noted that the values of the Fukui function of the P atom in compounds **D** (−0.361) and **Bb** (−0.382) are comparable with that in **Ca** indicating their comparable reactivities towards the DA reaction with 1,3-butadiene, i.e., they are expected to undergo the DA reaction without the aid of a catalyst.

Frontier molecular orbital (FMO) treatment of the DA reaction

The FMOs of a molecule are very important parameters to reveal its reactivity towards a reagent [28]. In the DA reaction of 2-phosphaindolizines with 1,3-butadiene, the HOMO of the latter will interact with the LUMO of the former and the energy gap (ΔE) between the two will give an indication about the reactivity of the 2-phosphaindolizines (Figure 4).

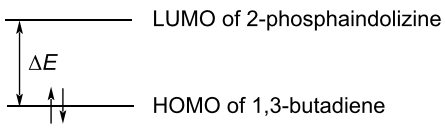


Figure 4: Energy gap (ΔE) between HOMO of 1,3-butadiene and LUMO of 2-phosphaindolizine.

The HOMO of 1,3-butadiene (ψ_2) and the LUMOs of different 2-phosphaindolizines are given in Figure 5. It may be mentioned that for compounds **Aa**, **Ab**, **Ba**, **Ca**, and **D**, the respective LUMOs were not found to be of the appropriate

Table 3: Fukui functions at the Y (C or N) and phosphorus atoms of the >Y=P– functionality of 2-phosphaindolizines (dienophile).

Compounds 6	Fukui function $f^+(r)$ for nucleophilic attack		Fukui function $f^-(r)$ for electrophilic attack	
	Mulliken	Hirshfeld	Mulliken	Hirshfeld
Aa	C –0.086 P –0.276	C –0.162 P –0.186	–	–
Ab	C –0.019 P –0.269	C –0.042 P –0.184	–	–
Ac	C –0.206 P –0.130	C –0.039 P –0.124	–	–
Ad	C –0.154 P –0. 112	C –0.025 P –0.105	–	–
Ba	C –0.057 P –0.296	C –0.048 P –0.222	–	–
Bb	C –0.008 P –0.382	C –0.044 P –0.305	–	–
Ca	N –0.058 P –0.321	N –0.054 P –0.222	–	–
Cb	N –0.042 P –0.298	N –0.049 P –0.217	–	–
D	N(9) –0.047 P(8) –0.361	N(9) –0.052 P(8) –0.278	–	–
7	–	–	C(1) –0.166 C(4) –0.191	C(1) –0.186 C(4) –0.197

symmetry. Instead, LUMO + 1 for **Aa**, **Ab**, **Ca**, and **D** and the LUMO + 3 for **Ba** have the required symmetry.

A closer look at the energies of the LUMOs (or LUMO + 1 for **Aa**, **Ab**, **Ca**, **D** and LUMO + 3 for **Ba**) reveals that they increase in the following order: **Ad** < **Ac** < **Ab** < **Aa**. In view of this, the reactivity of 2-phosphaindolizines towards DA reaction with 1,3-butadiene is expected to change in the order: **Ad** > **Ac** > **Ab** > **Aa**. Similarly, the order of reactivity in the other two classes would be **Bb** > **Bc**; **Cb** > **Ca**. These orders of reactivities are almost similar to those obtained on the basis of other reactivity descriptors discussed earlier.

Conclusion

The reactivity descriptors, namely global hardness/softness, electronic chemical potential, electrophilicity and nucleophilicity indices as well as the Fukui functions computed from the conceptual DFT calculation at the B3LYP/6-31+G (d) level of theory could be used successfully to rationalize the experimentally observed dienophilic reactivites of four classes of 2-phosphaindolizenes. The energies of the LUMOs (or in some cases LUMO + 1 or LUMO + 3) of 2-phosphaindolizines with respect to the energy of the HOMO of 1,3-butadiene were also found in accordance with their relative dienophilic reactivites. Thus, conceptual DFT descriptors can be advantageously used to predict the reactivities of the organophosphorus compounds.

Computational Methods

All calculations were done using the *Gaussian 16* program [29]. We found that almost without exception, hybrid of Becke 3 and LYP correlation functional [30,31] has been used for determining reactivity descriptors [32-35] and the results were found to be independent of the basis sets [33]. In view of this, we carried out all calculations at the B3LYP/6-31+G (d) level of theory. Furthermore, Phukan et al. [32] calculated electrophilicity indices of a number of aziridines in the gas and solvent phases and observed that in both cases, a similar pattern of varying the values is followed. In view of this, we carried out all calculations in the gas phase only. Thus all geometries were optimized in the gas phase at the B3LYP/6-31+G(d) level of theory. Frequency calculations were done at the same level to determine zero-point correction and to characterize energy minimum with no imaginary frequency.

Chemical reactivity descriptors were calculated as follows:

$$\eta = \frac{E_{\mathrm{LUMO}} - E_{\mathrm{HOMO}}}{2}$$

$$\mathrm{S} = \frac{1}{2\eta}$$

$$\mu = \frac{E_{\mathrm{HOMO}} + E_{\mathrm{LUMO}}}{2}$$

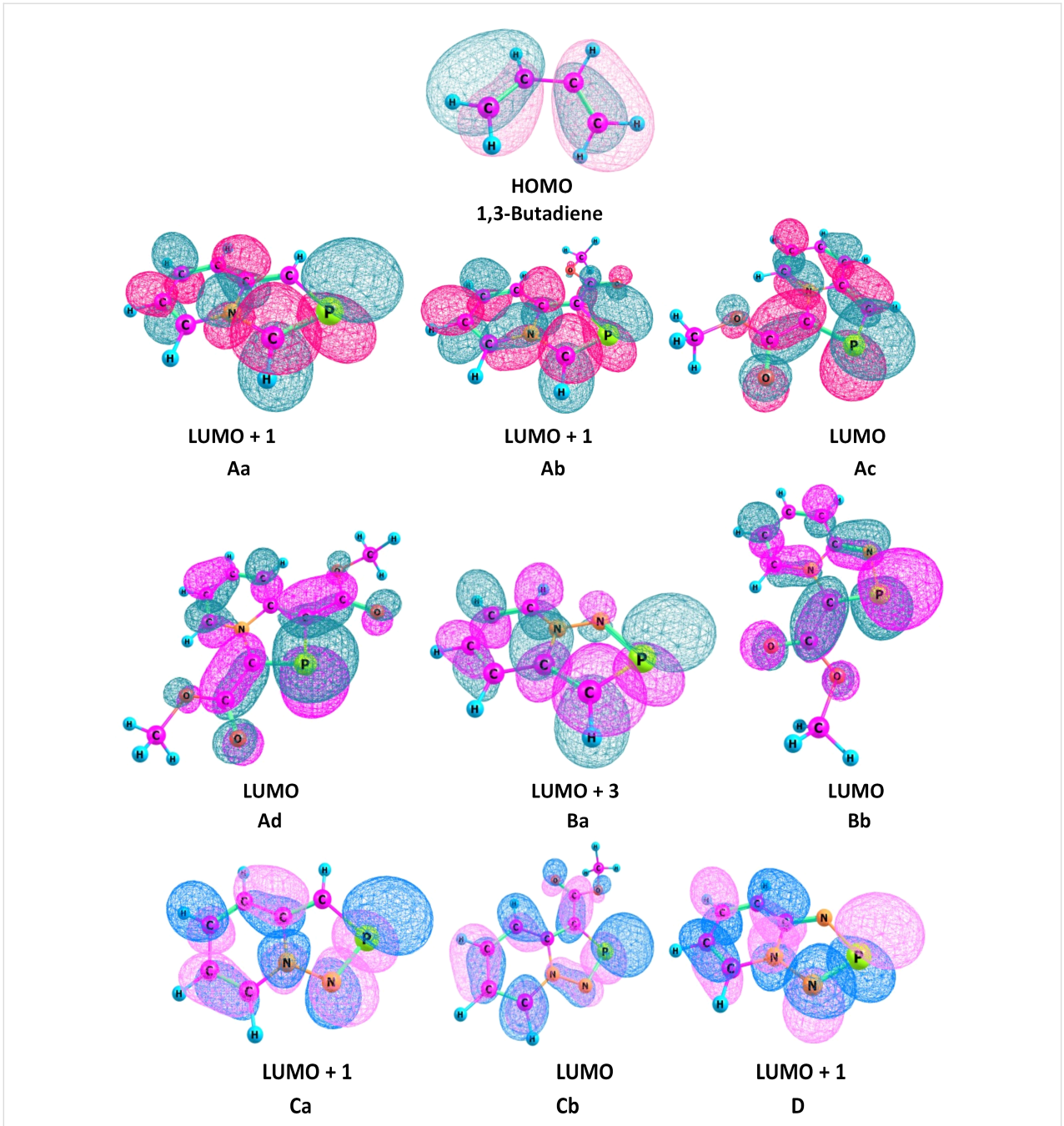


Figure 5: Kohn–Shan HOMO of 1,3-butadiene and LUMOs of 2-phosphaindolizines computed at the B3LYP/6-31+G(d) level of theory.

$$\omega = \frac{\mu^2}{2\eta}$$

$$N = E_{\mathrm{HOMO}}\ (\mathrm{nuclophile}) - E_{\mathrm{HOMO}}\ (\mathrm{TCNE})$$

$$f^{+}(r) = \mathrm{qr}_{(N+1)} - \mathrm{qr}_{(\mathrm{N})}\ [\mathrm{nucleophilic\ attack}]$$

$$f^{-}(r) = \mathrm{qr}_{(N)} - \mathrm{qr}_{(\mathrm{N-1})}\ [\mathrm{electrophilic\ attack}]$$

Supporting Information

Supporting Information File 1

Cartesian coordinates of the geometries optimized (Table S1) at the B3LYP/6-31+G (d) level of theory.
[https://www.beilstein-journals.org/bjoc/content/supplementary/1860-5397-18-127-S1.pdf]

Acknowledgements

The computational facilities provided by the IIS (deemed to be university), Jaipur, India are gratefully acknowledged.

ORCID® iDs

Raj Kumar Bansal - https://orcid.org/0000-0002-8154-9817

Preprint

A non-peer-reviewed version of this article has been previously published as a preprint: https://doi.org/10.3762/bxiv.2022.53.v1

References

1. Bansal, R. K.; Karaghiosoff, K.; Gupta, N.; Schmidpeter, A.; Spindler, C. *Chem. Ber.* **1991,** *124,* 475–480. doi:10.1002/cber.19911240309
2. Karaghiosoff, K.; Bansal, R. K.; Gupta, N. *Z. Naturforsch., B: J. Chem. Sci.* **1992,** *47,* 373–378. doi:10.1515/znb-1992-0312
3. Bansal, R. K.; Pandey, G.; Gupta, R.; Karaghiosoff, K.; Schmidpeter, A. *Synthesis* **1995,** 173–175. doi:10.1055/s-1995-3865
4. Bansal, R. K.; Gandhi, N.; Schmidpeter, A.; Karaghiosoff, K. *Z. Naturforsch., B: J. Chem. Sci.* **1995,** *50,* 558–562. doi:10.1515/znb-1995-0414
5. Bansal, R. K.; Surana, A.; Gupta, N. *Tetrahedron Lett.* **1999,** *40,* 1565–1568. doi:10.1016/s0040-4039(98)02645-8
6. Appel, R. In *Multiple Bonds and Low Coordination in Phosphorus Chemistry;* Regitz, M.; Scherer, O. J., Eds.; Thieme: Stuttgart, Germany, 1990; p 157.
7. Bansal, R. K.; Gupta, N.; Gupta, N. *Heteroat. Chem.* **2004,** *15,* 271–287. doi:10.1002/hc.20002
8. Maerkl, G. In *Multiple Bonds and Low Coordination in Phosphorus Chemistry;* Regitz, M.; Scherer, O. J., Eds.; Thieme: Stuttgart, Germany, 1990; p 220.
9. Maerkl, G.; Kreitmeier, P. Six-membered Rings with Two or More Heteroatoms with at least One Phosphorus Atom. In *Phosphorus–Carbon Heterocyclic Chemistry;* Mathey, F., Ed.; Pergamon Press: Oxford, UK; p 535. doi:10.1016/b978-008043952-5/50014-0
10. Bansal, R. K.; Kumawat, S. K. *Tetrahedron* **2008,** *64,* 10945–10976. doi:10.1016/j.tet.2008.09.037
11. Bansal, R. K.; Jain, V. K.; Gupta, N.; Gupta, N.; Hemrajani, L.; Baweja, M.; Jones, P. G. *Tetrahedron* **2002,** *58,* 1573–1579. doi:10.1016/s0040-4020(02)00004-2
12. Bansal, R. K.; Gupta, N.; Kumawat, S. K.; Dixit, G. *Tetrahedron* **2008,** *64,* 6395–6401. doi:10.1016/j.tet.2008.04.080
13. Jangid, R. K.; Sogani, N.; Gupta, N.; Bansal, R. K.; Hopffgarten, M. v.; Frenking, G. *Beilstein J. Org. Chem.* **2013,** *9,* 392–400. doi:10.3762/bjoc.9.40
14. Bansal, R. K.; Karaghiosoff, K.; Gupta, N.; Gandhi, N.; Kumawat, S. K. *Tetrahedron* **2005,** *61,* 10521–10528. doi:10.1016/j.tet.2005.08.045
15. Bansal, R. K.; Gupta, N.; Dixit, G.; Kumawat, S. K. *J. Phys. Org. Chem.* **2009,** *22,* 125–129. doi:10.1002/poc.1436
16. Hohenberg, P.; Kohn, W. *Phys. Rev.* **1964,** *136,* B864–B871. doi:10.1103/physrev.136.b864
17. Kohn, W.; Sham, L. J. *Phys. Rev.* **1965,** *140,* A1133–A1138. doi:10.1103/physrev.140.a1133
18. Parr, R. G.; Yang, W. *Annu. Rev. Phys. Chem.* **1995,** *46,* 701–728. doi:10.1146/annurev.pc.46.100195.003413
19. Mendez, F.; Gazquez, J. L. *J. Am. Chem. Soc.* **1994,** *116,* 9298–9301. doi:10.1021/ja00099a055
20. Yang, W.; Mortier, W. J. *J. Am. Chem. Soc.* **1986,** *108,* 5708–5711. doi:10.1021/ja00279a008
21. Hirshfeld, F. L. *Theor. Chim. Acta* **1977,** *44,* 129–138. doi:10.1007/bf00549096
22. Oláh, J.; Van Alsenoy, C.; Sannigrahi, A. B. *J. Phys. Chem. A* **2002,** *106,* 3885–3890. doi:10.1021/jp014039h
23. Job, G.; Herrmann, F. *Eur. J. Phys.* **2006,** *27,* 353–371. doi:10.1088/0143-0807/27/2/018
24. Pérez, P.; Domingo, L. R.; Aizman, A.; Contreras, R. The Electrophilicity Index In Organic Chemistry. *Theoretical and Computational Chemistry;* Elsevier: New York, NY, USA, 2007; Vol. 19, pp 139–201. doi:10.1016/s1380-7323(07)80010-0
25. Domingo, L. R.; Chamorro, E.; Pérez, P. *J. Org. Chem.* **2008,** *73,* 4615–4624. doi:10.1021/jo800572a
26. Domingo, L. R.; Pérez, P. *Org. Biomol. Chem.* **2011,** *9,* 7168–7175. doi:10.1039/c1ob05856h
27. Domingo, L. R.; Ríos-Gutiérrez, M.; Pérez, P. *Molecules* **2016,** *21,* 748. doi:10.3390/molecules21060748
28. Fleming, I. *Frontier Orbitals and Organic Chemical Reactions;* John Wiley & Sons: London, UK, 1976. doi:10.1002/prac.19783200525
29. *Gaussian 16,* Revision C.01; Gaussian, Inc.: Wallingford, CT, 2016.
30. Becke, A. D. *J. Chem. Phys.* **1993,** *98,* 5648–5652. doi:10.1063/1.464913
31. Lee, C.; Yang, W.; Parr, R. G. *Phys. Rev. B* **1988,** *37,* 785–789. doi:10.1103/physrevb.37.785
32. Baruah, B.; Deuri, S.; Phukan, P. *Comput. Theor. Chem.* **2014,** *1027,* 197–202. doi:10.1016/j.comptc.2013.11.005
33. Cerda-Monje, A.; Ormazábal-Toledo, R.; Cárdenas, C.; Fuentealba, P.; Contreras, R. *J. Phys. Chem. B* **2014,** *118,* 3696–3701. doi:10.1021/jp5009994
34. Melin, J.; Aparicio, F.; Subramanian, V.; Galván, M.; Chattaraj, P. K. *J. Phys. Chem. A* **2004,** *108,* 2487–2491. doi:10.1021/jp037674r
35. Melin, J.; Ayers, P. W.; Ortiz, J. V. *J. Phys. Chem. A* **2007,** *111,* 10017–10019. doi:10.1021/jp075573d

License and Terms

This is an open access article licensed under the terms of the Beilstein-Institut Open Access License Agreement (https://www.beilstein-journals.org/bjoc/terms), which is identical to the Creative Commons Attribution 4.0 International License (https://creativecommons.org/licenses/by/4.0). The reuse of material under this license requires that the author(s), source and license are credited. Third-party material in this article could be subject to other licenses (typically indicated in the credit line), and in this case, users are required to obtain permission from the license holder to reuse the material.

The definitive version of this article is the electronic one which can be found at:
https://doi.org/10.3762/bjoc.18.127

BEILSTEIN JOURNAL OF ORGANIC CHEMISTRY

Synthesis and electrochemical properties of 3,4,5-tris(chlorophenyl)-1,2-diphosphaferrocenes

Almaz A. Zagidullin*, Farida F. Akhmatkhanova, Mikhail N. Khrizanforov, Robert R. Fayzullin, Tatiana P. Gerasimova, Ilya A. Bezkishko and Vasili A. Miluykov

Full Research Paper

Open Access

Address:
Arbuzov Institute of Organic and Physical Chemistry, FRC Kazan Scientific Center, Russian Academy of Sciences, 8 Arbuzov Street, 420088 Kazan, Russian Federation

Email:
Almaz A. Zagidullin* - almaz_zagidullin@mail.ru

* Corresponding author

Keywords:
cyclopropenyl bromide; electrochemical properties; phosphacyclopentadienide anion; phosphaferrocene; phosphonium salt; phosphorus heterocycle

Beilstein J. Org. Chem. **2022,** *18,* 1338–1345.
https://doi.org/10.3762/bjoc.18.139

Received: 11 July 2022
Accepted: 09 September 2022
Published: 27 September 2022

This article is part of the thematic issue "Organophosphorus chemistry: from model to application".

Guest Editor: G. Keglevich

© 2022 Zagidullin et al.; licensee Beilstein-Institut.
License and terms: see end of document.

Abstract

A novel representative of sodium 3,4,5-triaryl-1,2-diphosphacyclopentadienide containing a chloro substituent in the *meta*-position of the aryl groups was obtained with a high yield based on the reaction of tributyl(1,2,3-triarylcyclopropenyl)phosphonium bromide and sodium polyphosphides. Further reaction of sodium 3,4,5-tris(3-chlorophenyl)-1,2-diphosphacyclopentadienide with $[FeCp(\eta^6\text{-}C_6H_5CH_3)][PF_6]$ complex gives a new 3,4,5-tris(3-chlorophenyl)-1,2-diphosphaferrocene. The electrochemical properties of 3,4,5-tris(3-chlorophenyl)-1,2-diphosphaferrocene were studied and compared to 3,4,5-tris(4-chlorophenyl)-1,2-diphosphaferrocene. It was found that the position of the chlorine atom on the aryl fragment has an influence on the reduction potential of 1,2-diphosphaferrocenes, while the oxidation potentials do not change.

Introduction

Among the various heterometallocenes reported to date, phosphaferrocenes are by far the most investigated because of their structural and electronic features [1,2] and remain the objects of growing interest in the fields of coordination chemistry [3-5] and asymmetric catalysis [6,7]. Due to the sp^2-hybridization of the phosphorus atom, phosphaferrocenes are commonly regarded as phosphorus ligands with weaker σ-donor character than classical tertiary phosphines and stronger π-acceptor properties closer to phosphites $P(OR)_3$ [8,9]. Since the P atom in phosphaferrocenes retains an electron lone pair, phosphaferrocenes have been used as P-donor ligands [10-12] as well as nucleophilic catalysts [13,14]. Recently, the pentaphosphaferrocene $Cp^*Fe(\eta^5\text{-}P_5)$ has been used as a mediator in the synthesis of asymmetric phosphines starting from white phosphorus [15]. Moreover, the presence of the lone pair of the P atom opens the route to polynuclear complexes [16-18]

and coordination polymers [19-21] with the mixed σ-/π-coordination mode, which is not typical for classical ferrocene species.

Various effective synthetic approaches were developed for 1-mono- [22-24], 1,2,3-tri- [25-27], 1,2,4-tri- [28-30], and pentaphosphaferrocenes [31-33], whereby the chemistry of these compounds is most investigated and well represented at present time. In contrast, very limited data are available concerning 1,2-diphosphaferrocenes due to the absence of simple and effective synthetic routes [34-36]. Recently, we have reported a convenient synthesis of 3,4,5-triaryl-1,2-diphosphaferrocenes with various substituents at the *para*-positions of aryl groups [37]. Based on this method, herein we report on the complete multistep synthesis of new sodium 3,4,5-tris(3-chlorophenyl)-1,2-diphosphacyclopentadienide and corresponding 1,2-diphosphaferrocene with *meta*-chlorophenyl substituents and the influence of the position of the Cl atom on aryl moiety on the electrochemical properties.

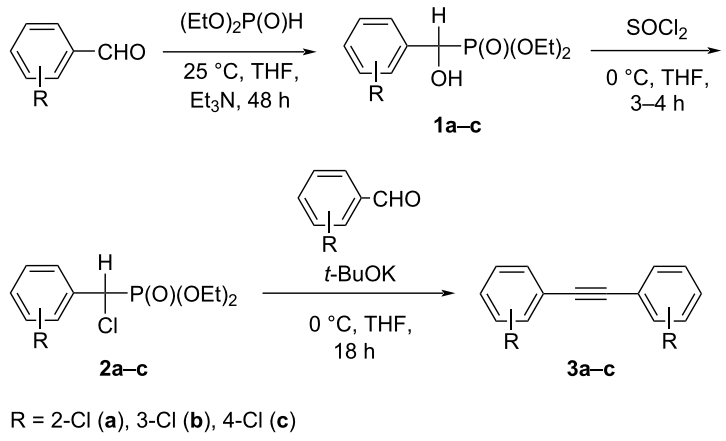
Results and Discussion

Synthesis of tris(chlorophenyl)cyclopropenyl bromides and derivatives

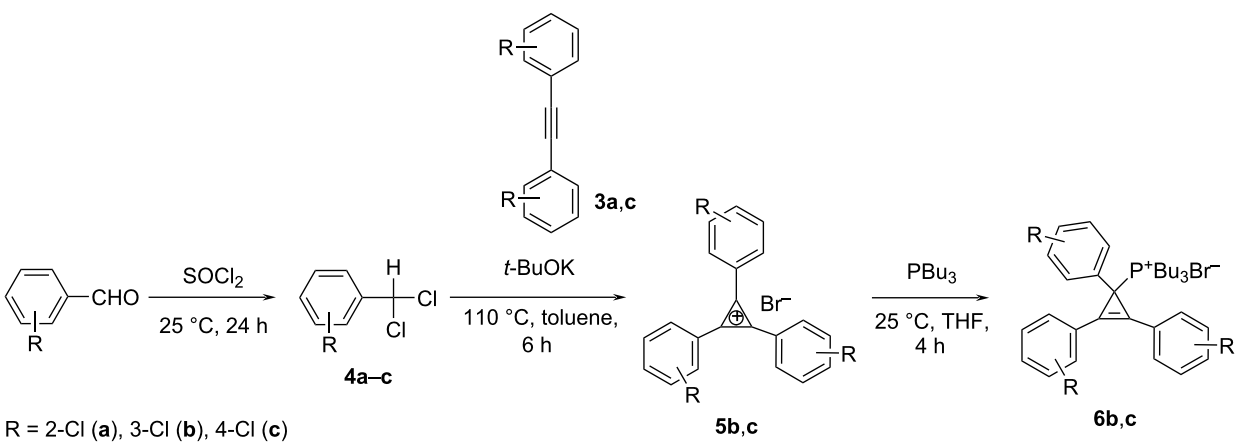
Cyclopropenium (cyclopropenylium) ions have always attracted attention of the synthetic chemists because of the unique combination of stability and reactivity [38-40]. The synthesis of corresponding 1,2,3-cyclopropenium bromides was realized by a classical approach: combination of C_1 and C_2 building blocks, i.e., the addition of a carbene species to a triple bond of diarylacetylene, followed by treatment of the produced cyclopropene with HBr to convert it to the corresponding cyclopropenylium cation. Using this approach, tris(4-chlorophenyl)- and tris(3-chlorophenyl)cyclopropenyl bromides were prepared for the first time. The advantage of this approach is the possibility of synthesis of substituted diarylacetylenes, the corresponding substituted benzal chlorides, and triarylcyclopropenyl bromides from one starting aryl aldehyde.

Diethyl phosphite was allowed to react with appropriately substituted benzaldehydes in THF for 48 hours at 25 °C to afford diethyl (hydroxy(aryl)methyl)phosphonates **1**, which were detected by ^{31}P NMR spectroscopy in THF (21.4 ppm for **1a**, 21.0 ppm for **1b**, and 21.5 ppm for **1c**). Further, reaction mixtures with compounds **1** were treated with $SOCl_2$ for 3–4 h at 0 °C and converted to chloro derivatives **2**. In the next step, compounds **2** and starting substituted benzaldehydes were subsequently treated with 2 equiv of potassium *tert*-butoxide in THF for 18 hours at room temperature to afford substituted diarylacetylenes **3**. Based on this reaction, the desired compounds **3** were prepared from 2-chloro-, 3-chloro-, and 4-chlorophenyl aldehydes, respectively, in 3 steps in 10–53% yield (10% for **3a**, 48% for **3b**, 53% for **3c**, Scheme 1). This method is an alternative way to different transition metal-catalyzed cross-coupling reactions broadly used for the preparation of different diarylacetylenes and, rarely, bis(chlorophenyl)acetylenes.

Next, starting substituted benzaldehydes were treated with an excess of $SOCl_2$ for 24 h at 25 °C. Corresponding substituted benzal chlorides **4** were distilled at reduced pressure to give pure compounds. In a final step, we used the above mentioned approach of combining the C_1 and C_2 building blocks and found that chloroarylcarbenes, generated from the corresponding benzal chlorides **4b**,**c** under the action of potassium *tert*-butoxide, reacted with 1,2-bis(chlorophenyl)ethynes **3b**,**c** to form triarylcyclopropenylium salts **5b**,**c** in 22 and 15% yield (Scheme 2). Unfortunately, it was not possible to synthesize tris(2-chlorophenyl)cyclopropenylium bromide **5a** using this method.



Scheme 1: Synthesis of bis(chlorophenyl)acetylenes **3**.



Scheme 2: Synthesis of 1,2,3-tris(chlorophenyl)cyclopropenylium bromides **5** and tributyl(1,2,3-tris(chlorophenyl)cyclopropenyl)phosphonium bromides **6**.

The structures of **3**–**5** were confirmed by ^{1}H and ^{13}C NMR as well as IR spectroscopic methods and, for **5c**, single-crystal X-ray crystallography (Figure 1a). The ^{13}C NMR signals of the cationic carbon atoms of the three-membered ring appeared at about 145 ppm. Besides, the ^{1}H NMR spectra of **5** were unremarkable and consistent with the suggested formulas.

As a next step, we synthesized a series of tributyl(1,2,3-triarylcyclopropenyl)phosphonium bromides **6** containing a Cl substituent in the *meta*- or *para*-position of each aryl group. This was done by reaction of appropriate 1,2,3-triarylcyclopropenylium bromides **5** with PBu_3 at 25 °C in THF in 34 and 39% yield (Scheme 2). The structures of **6** were confirmed by ^{31}P, ^{1}H, and ^{13}C NMR spectroscopy. The ^{31}P{^{1}H} NMR spectra of phosphonium bromides **6** showed a singlet at about 40 ppm, which is typical for phosphonium salts. The ^{13}C{^{1}H} NMR spectra consisted of a doublet at about 20 ppm, corresponding to the carbon atom C1, which is characteristic for the sp^3-hybridized carbon atom, with a coupling constant of $^{1}J_{CP} \approx 45$ Hz. Additionally, the structure of **6c** in the crystal was confirmed by X-ray crystallography (Figure 1b).

Synthesis, structure, and electrochemical properties of 3,4,5-tris(chlorophenyl)-1,2-diphosphaferrocenes

The obtained phosphonium salts **6** were treated with a mixture of sodium polyphosphides of the type Na_xP_y (obtained in situ from sodium metal and white phosphorus P_4), containing

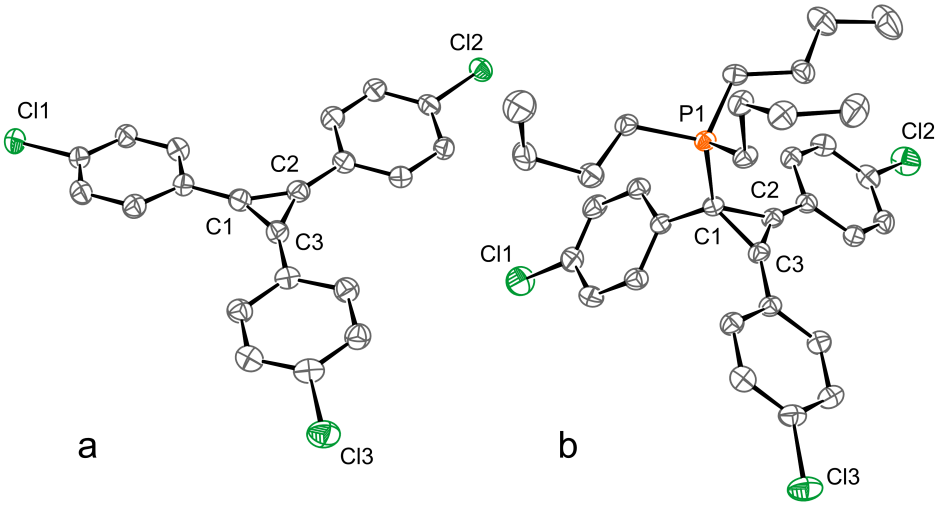


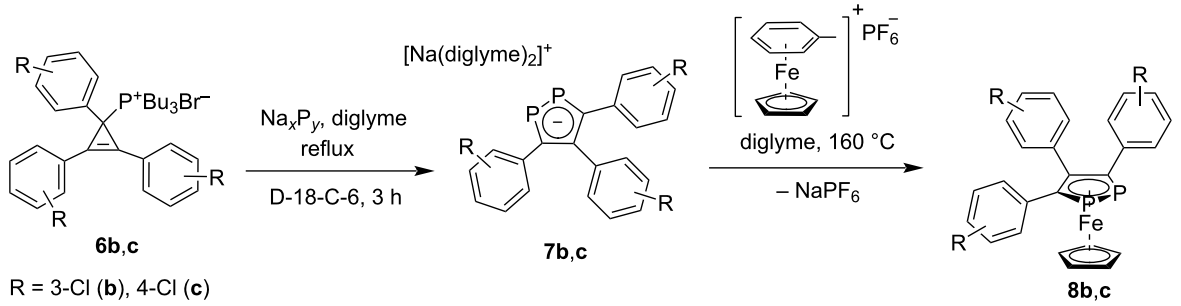
Figure 1: ORTEP representations for cations **5c** (a) and **6c** (b) at the 50% probability level. Bromide anion and co-crystallized solvent molecules are omitted for clarity. For **6c**, only one of two symmetry-independent molecules is shown. Selected interatomic distances (Å): C1–C2 1.387(7), C1–C3 1.372(7), C2–C3 1.380(7) for **5c**; C1–C2 1.521(5), C1–C3 1.521(5), C2–C3 1.298(5), P1–C1 1.837(3) for **6c**. Deposition numbers 2176393 for **5c** and 2176394 for **6c** contain the supplementary crystallographic data for this paper [41].

mainly NaP_5 and Na_3P_7 [42]), resulting in sodium 3,4,5-tris(chlorophenyl)-1,2-diphosphacyclopentadienides **7** in good yields (60 and 63%, Scheme 3). This reaction allowed a selective and controllable conversion of Na_xP_y to the 1,2-diphospholide anion, in which two new C–P bonds could selectively be formed [43,44]. The obtained sodium 3,4,5-triaryl-1,2-diphospholides **7** were isolated in good purity from the reaction mixture by filtration and further washing with a mixture of THF/*n*-hexane. The $^{31}P\{^1H\}$ NMR spectra of **7** showed a singlet at about 200 ppm, which is typical for sodium 1,2-diphospholides ($^{31}P\{^1H\}$ in THF: 201 ppm for **7b** and 198 ppm for **7c**). Further, the $^{13}C\{^1H\}$ NMR spectra of **7** showed two multiplets at about 147 and 160 ppm for the heteroaromatic P_2C_3 ring backbone.

Recently, we have reported a convenient method for the preparation of 1,2-diphosphaferrocenes [37] and 1,2,3-triphosphaferrocenes [25] with various substituents at *para*-positions of aryl groups. Using this approach, sodium bis(diglyme) 3,4,5-tris(3-chlorophenyl)-1,2-diphosphacyclopentadienide (**7b**) was treated in a 1:1 ratio with $[FeCp(\eta^6\text{-}C_6H_5CH_3)][PF_6]$ at 160 °C in diglyme. Evaporation of diglyme at reduced pressure and extraction of the product with toluene, followed by filtration through silica, resulted in 3,4,5-tris(3-chlorophenyl)-1,2-diphosphaferrocene (**8b**) in 68% yield and high purity (Scheme 3).

The structure of 3,4,5-triaryl-1,2-diphosphaferrocene **8b** was confirmed by ^{31}P, ^1H, and ^{13}C NMR spectroscopy. The $^{31}P\{^1H\}$ NMR spectrum of **8b** showed a singlet at about −10 ppm, shifted upfield by about 210 ppm in comparison to the starting 1,2-diphospholide anion **7b**. In the ^1H NMR spectra, characteristic signals of the cyclopentadienyl ring (4.61 ppm) and ClC_6H_4 substituents (6.88–7.42 ppm) were observed. The $^{13}C\{^1H\}$ NMR spectrum of **8b** showed pseudotriplets at about 106 ppm and 117 ppm for the carbon atoms of the P_2C_3 ring and a singlet at about 75 ppm for the cyclopentadienyl ring.

Quantum chemically, two possible conformations of **8b** were considered, **8b-I** and **8b-II** (Figure 2). Similar to a previous



Scheme 3: Synthesis of 3,4,5-tris(chlorophenyl)-1,2-diphosphacyclopentadienides **7** and 3,4,5-tris(chlorophenyl)-1,2-diphosphaferrocenes **8**.

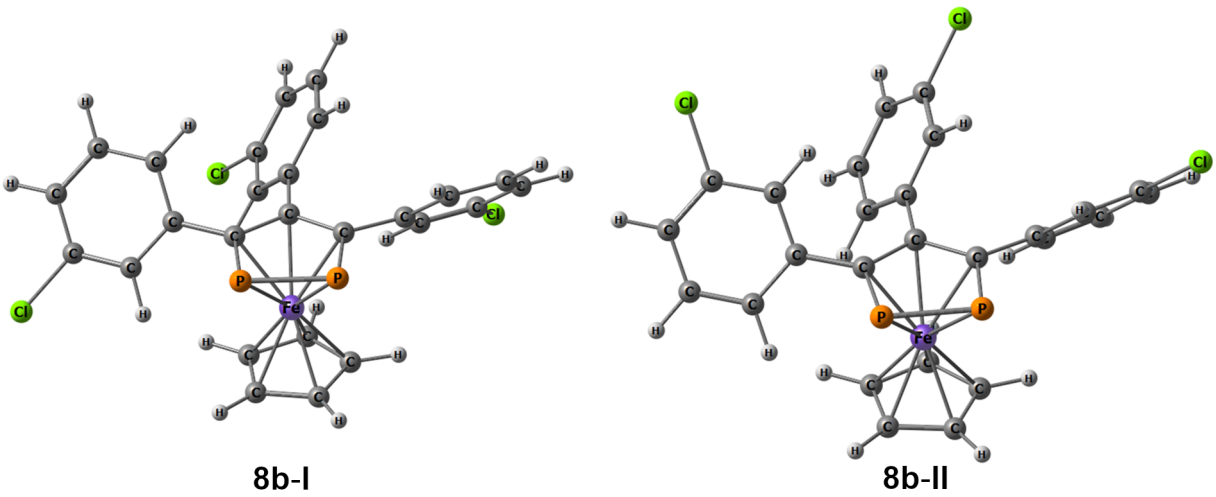


Figure 2: Considered conformations of **8b-I** and **8b-II**.

report on **8c** [37], both **8b-I** and **8b-II** adopted an almost eclipsed conformation during optimization. Computations predicted slightly lower energy (1 kcal·mol^{-1}) for conformation **8b-I**, with Cl oriented towards the Fe atom. According to the computations, **8b-I** is also slightly more advantageous compared to **8c** with the same energy difference.

The experimental UV–vis spectra of **8b** and **8c** in CH_2Cl_2 were similar and contained bands at about 280, 320, and 380 nm. The bands at 280 and 320 nm were more intense in the spectrum of **8c**, which is in full agreement with quantum chemical predictions (Figure 3). According to the computations, **8b-I** and **8b-II** demonstrated almost the same absorption. The bands at about 250 and 280 nm were caused by π–π* transitions. The dominating transition contributing to the lowest-energy absorption (380 nm) was the one corresponding to a transition between HOMO−1 and LUMO+1 (Figure 4). Both orbitals were localized mostly at the P_2C_3–Fe–Cp moiety, and the former was also contributed to by atomic orbitals of the aryl ring in the 4-position. Similar to **8c**, the atomic orbitals of the Cl atoms in **8b** practically did not participate in the frontier orbitals, which explained the similarity of the low-energy range of the experimental spectra.

The electrochemical properties of 1,2-diphosphaferrocene **8b** were studied by cyclic voltammetry and compared to data for **8c** (Table 1 and Figure 5). During oxidation, there were no noticeable differences between **8b** and **8c**. The oxidation potentials of **8b** and **8c** were shifted to the positive region relative to pure ferrocene by 0.48–0.53 V. This, in turn, indicated that the chlorine atoms in the η^5-$P_2C_3R_3$ fragment did not significantly affect the HOMO energy of 1,2-diphosphaferrocenes **8**. The number of phosphorus atoms in cyclopentadiene had a much

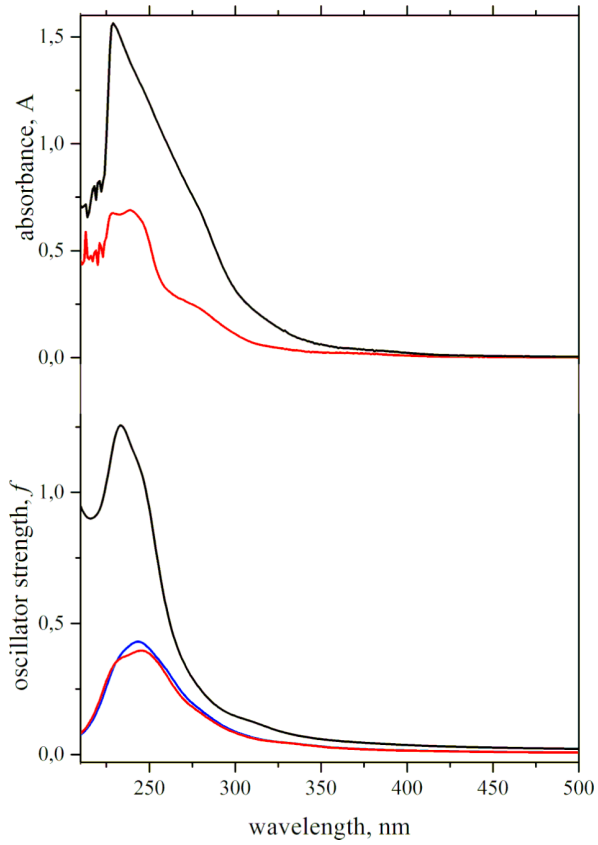


Figure 3: Top: experimental UV–vis spectra of **8c** (black) and **8b** (red). Bottom: broadened calculated UV–vis spectra of **8c** (black), **8b-I** (red), and **8b-II** (blue). Experimental UV–vis spectra of **8c** republished with permission of Royal Society of Chemistry from [37] ("Synthesis, structure and electrochemical properties of 3,4,5-triaryl-1,2-diphosphaferrocenes" by I. A. Bezkishko et al., *Inorg. Chem. Front.*, vol. 9, Issue 11, © 2022); permission conveyed through Copyright Clearance Center, Inc. This content is not subject to CC BY 4.0.

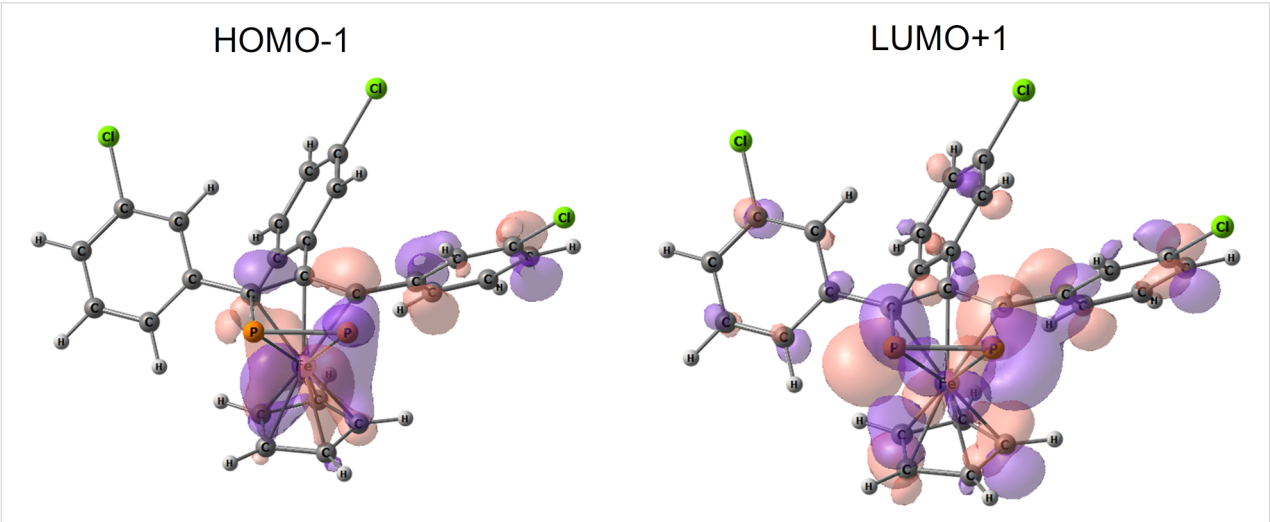


Figure 4: Frontier orbitals of **8b-II** contributing to absorption bands at about 380 nm.

Table 1: Electrochemical data for the redox properties of 3,4,5-triaryl-1,2-diphosphaferrocenes **8b** and **8c**.

compound	E_{ox}^1 (V) vs Ag/AgCl	E_{red}^1 (V)	$^1E_{HOMO}$ (eV)	$^1E_{LUMO}$ (eV)	gap (eV)
ferrocene [48]	0.48	–3.19[a]	–4.79[a]	–1.61[a]	3.18[a]
FeCp(η^5-$P_2C_3R_3$) (R = 3-Cl-C_6H_4, **8b**)	0.96	–2.15	–5.28	–2.2	2.84
FeCp(η^5-$P_2C_3R_3$) (R = 4-Cl-C_6H_4, **8c**) [37]	1.01	–1.83	–5.36	–2.48	2.88
Cp*Fe(η^5-P_5) [45]	1.12[b]	–1.55[b]	–5.47[b]	–2.80[b]	2.57[b]

[a]Conditions: –50 °C, glassy carbon working electrode, Ag/AgCl reference electrode, *c* 0.5 mM, Bu_4NBF_4, DMF, 100 mV·s^{-1}. [b]Conditions: –13 °C, Pt working electrode, Ag/AgCl reference electrode (recalculated from Fc/Fc$^+$), *c* 0.5 mM, Bu_4NPF_6, CH_2Cl_2, 500 mV·s^{-1}.

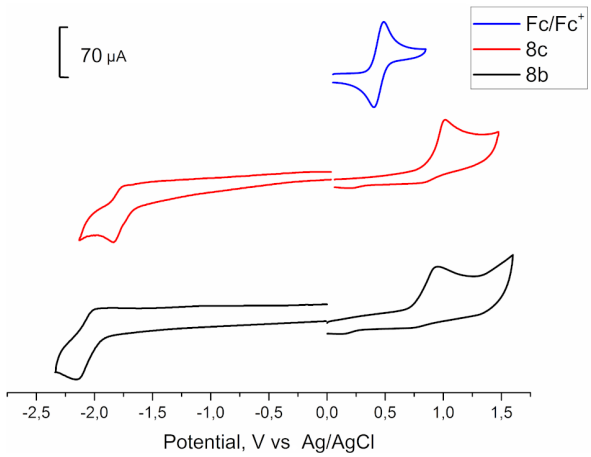


Figure 5: Cyclic voltammograms of 3,4,5-triaryl-1,2-diphosphaferrocenes **8b** and **8c** in CH_3CN on glassy carbon electrode (0.5 mM complex). Potentials vs Ag/AgCl. Scan rate = 100 mV·s^{-1}, room temperature. Cyclic voltammogram of **8c** republished with permission of Royal Society of Chemistry from [37] ("Synthesis, structure and electrochemical properties of 3,4,5-triaryl-1,2-diphosphaferocenes" by I. A. Bezkishko et al., *Inorg. Chem. Front.*, vol. 9, Issue 11, © 2022); permission conveyed through Copyright Clearance Center, Inc. This content is not subject to CC BY 4.0.

greater effect on the shifts of the Fe^{II}/Fe^{III} oxidation potential. As shown earlier, an increase in the number of phosphorus atoms led to the irreversible oxidation of phosphaferrocenes containing an unsubstituted Cp ring. It was shown that Cp*Fe(η^5-P_5) was irreversibly oxidized at a potential of 0.57 V relative to Fc/Fc$^+$, and the presence of even five phosphorus atoms makes an insignificant contribution to the HOMO energy level [45]. The situation changed fundamentally when both rings were replaced with phosphacyclopentadienyl ligands. Related diphosphacyclobutadiene complexes Fe(η^4-$P_2C_2R_2$)$_2$ were oxidized much more cathodically (negative by 1.7–2.0 V) [46,47], which indicated a significant contribution of the phosphacyclopentadienyl ligands to the iron atomic orbitals. Of course the structures of **8** and diphosphacyclobutadiene complexes are not isolobal, but it would be interesting to study electrochemical properties of Fe(η^5-$P_2C_3R_3$)$_2$ complexes in the future.

For reduction, the electrochemical properties changed more noticeable since the contribution to the LUMO came from the cyclopentadiene fragments. For 1,2-diphosphaferrocene **8b**, the reduction potential was positively shifted by 0.32 V as compared to **8c**. It should be noted that an increase of phosphorus atoms' number in phosphaferrocenes leads to a greater positive potential, which in turn leads to the formation of dimers, which was shown for pentaphosphaferrocene Cp*Fe(η^5-P_5) [49] and the corresponding Sm complexes [50].

Conclusion

In summary, a series of bis(chlorophenyl)acetylenes **3**, substituted benzal chlorides **4**, and tris(chlorophenyl)cyclopropenylium bromides **5** were synthesized starting from corresponding chloro-substituted benzaldehydes. We found that the reaction of tributyl(1,2,3-tris(chlorophenyl)cyclopropenyl)phosphonium bromides **6** with sodium polyphosphides can be successfully used for the preparation of sodium 3,4,5-tris(chlorophenyl)-1,2-diphosphacyclopentadienides **7**. A facile synthesis of 3,4,5-tris(3-chlorophenyl)-1,2-diphosphaferrocene (**8b**) from sodium bis(diglyme) 3,4,5-tris(3-chlorophenyl)-1,2-diphosphacyclopentadienide (**7b**) and [FeCp(η^6-$C_6H_5CH_3$)][PF_6] is described. The structure of **8b** was studied using experimental NMR, UV–vis, and electrochemical analyses as well as theoretical studies. The *meta*- and *para*-substitution of the Cl atoms in the aryl fragments did not significantly effect the oxidation potentials of 1,2-diphosphaferrocenes **8**, while the reduction potential of **8b** was shifted by 0.33 V to a more negative region as compared to **8c**.

Supporting Information

Supporting Information File 1

Experimental procedures and characterization data of synthesized compounds.
[https://www.beilstein-journals.org/bjoc/content/supplementary/1860-5397-18-139-S1.pdf]

Acknowledgements

The meausurements have been carried out using the equipment of Distributed Spectral-Analytical Center of Shared Facilities for Study of Structure, Composition and Properties of Substances and Materials of FRC Kazan Scientific Center of RAS.

Funding

This work was supported by the grant of the Russian Science Foundation No. 21-73-10204.

ORCID® iDs

Almaz A. Zagidullin - https://orcid.org/0000-0003-3125-7506
Robert R. Fayzullin - https://orcid.org/0000-0002-3740-9833
Tatiana P. Gerasimova - https://orcid.org/0000-0001-8473-5327
Ilya A. Bezkishko - https://orcid.org/0000-0002-4563-2859
Vasili A. Miluykov - https://orcid.org/0000-0002-8069-457X

Preprint

A non-peer-reviewed version of this article has been previously published as a preprint: https://doi.org/10.3762/bxiv.2022.61.v1

References

1. Le Floch, P. *Coord. Chem. Rev.* **2006,** *250,* 627–681. doi:10.1016/j.ccr.2005.04.032
2. Carmichael, D.; Mathey, F. *Top. Curr. Chem.* **2002,** *220,* 27–51. doi:10.1007/3-540-45731-3_2
3. Bezkishko, I. A.; Zagidullin, A. A.; Milyukov, V. A.; Sinyashin, O. G. *Russ. Chem. Rev.* **2014,** *83,* 555–574. doi:10.1070/rc2014v083n06abeh004442
4. Bai, J.; Virovets, A. V.; Scheer, M. *Science* **2003,** *300,* 781–783. doi:10.1126/science.1081119
5. Peresypkina, E.; Virovets, A.; Scheer, M. *Coord. Chem. Rev.* **2021,** *446,* 213995. doi:10.1016/j.ccr.2021.213995
6. Fu, G. C. *Acc. Chem. Res.* **2006,** *39,* 853–860. doi:10.1021/ar068115g
7. Ogasawara, M.; Watanabe, S.; Nakajima, K.; Takahashi, T. *J. Am. Chem. Soc.* **2010,** *132,* 2136–2137. doi:10.1021/ja910348z
8. Frison, G.; Mathey, F.; Sevin, A. *J. Phys. Chem. A* **2002,** *106,* 5653–5659. doi:10.1021/jp0258816
9. Kostic, N. M.; Fenske, R. F. *Organometallics* **1983,** *2,* 1008–1013. doi:10.1021/om50002a012
10. Willms, H.; Frank, W.; Ganter, C. *Organometallics* **2009,** *28,* 3049–3058. doi:10.1021/om8012025
11. Carmichael, D.; Goldet, G.; Klankermayer, J.; Ricard, L.; Seeboth, N.; Stankevič, M. *Chem. – Eur. J.* **2007,** *13,* 5492–5502. doi:10.1002/chem.200601715
12. Ogasawara, M.; Ito, A.; Yoshida, K.; Hayashi, T. *Organometallics* **2006,** *25,* 2715–2718. doi:10.1021/om060138b
13. Wang, L.-S.; Hollis, T. K. *Org. Lett.* **2003,** *5,* 2543–2545. doi:10.1021/ol034816r
14. Garrett, C. E.; Fu, G. C. *J. Org. Chem.* **1997,** *62,* 4534–4535. doi:10.1021/jo970419g
15. Reichl, S.; Mädl, E.; Riedlberger, F.; Piesch, M.; Balázs, G.; Seidl, M.; Scheer, M. *Nat. Commun.* **2021,** *12,* 5774. doi:10.1038/s41467-021-26002-7
16. Liebscher, M.; Bruhn, C.; Siemeling, U.; Baio, J.; Lu, H.; Weidner, T. *Eur. J. Inorg. Chem.* **2017,** 351–359. doi:10.1002/ejic.201600892
17. Piesch, M.; Dielmann, F.; Reichl, S.; Scheer, M. *Chem. – Eur. J.* **2020,** *26,* 1518–1524. doi:10.1002/chem.201905240
18. Elsayed Moussa, M.; Welsch, S.; Dütsch, L.; Piesch, M.; Reichl, S.; Seidl, M.; Scheer, M. *Molecules* **2019,** *24,* 325. doi:10.3390/molecules24020325
19. Peresypkina, E.; Heindl, C.; Virovets, A.; Brake, H.; Mädl, E.; Scheer, M. *Chem. – Eur. J.* **2018,** *24,* 2503–2508. doi:10.1002/chem.201705883
20. Brake, H.; Peresypkina, E.; Heindl, C.; Virovets, A. V.; Kremer, W.; Scheer, M. *Chem. Sci.* **2019,** *10,* 2940–2944. doi:10.1039/c8sc05471a
21. Schiller, J.; Peresypkina, E.; Virovets, A. V.; Scheer, M. *Angew. Chem., Int. Ed.* **2020,** *59,* 13647–13650. doi:10.1002/anie.202004988
22. Ogasawara, M.; Arae, S.; Watanabe, S.; Subbarayan, V.; Sato, H.; Takahashi, T. *Organometallics* **2013,** *32,* 4997–5000. doi:10.1021/om400496b
23. Escobar, A.; Mathey, F. *Organometallics* **2010,** *29,* 1053–1056. doi:10.1021/om9010164
24. Masaoka, K.; Ohkubo, M.; Taue, H.; Wakioka, M.; Ohki, Y.; Ogasawara, M. *ChemistrySelect* **2022,** *7,* e202104472. doi:10.1002/slct.202104472
25. Petrov, A. V.; Zagidullin, A. A.; Bezkishko, I. A.; Khrizanforov, M. N.; Kholin, K. V.; Gerasimova, T. P.; Ivshin, K. A.; Shekurov, R. P.; Katsyuba, S. A.; Kataeva, O. N.; Budnikova, Y. H.; Miluykov, V. A. *Dalton Trans.* **2020,** *49,* 17252–17262. doi:10.1039/d0dt03281f
26. Scherer, O. J.; Hilt, T.; Wolmershäuser, G. *Angew. Chem., Int. Ed.* **2000,** *39,* 1425–1427. doi:10.1002/(sici)1521-3773(20000417)39:8<1425::aid-anie1425>3.0.co;2-1
27. Deng, S.; Schwarzmaier, C.; Zabel, M.; Nixon, J. F.; Timoshkin, A. Y.; Scheer, M. *Organometallics* **2009,** *28,* 1075–1081. doi:10.1021/om801118k
28. Heindl, C.; Schindler, A.; Bodensteiner, M.; Peresypkina, E. V.; Virovets, A. V.; Scheer, M. *Phosphorus, Sulfur Silicon Relat. Elem.* **2015,** *190,* 397–403. doi:10.1080/10426507.2014.979985
29. Schindler, A.; Zabel, M.; Nixon, J. F.; Scheer, M. *Z. Naturforsch., B: J. Chem. Sci.* **2009,** *64,* 1429–1437. doi:10.1515/znb-2009-11-1225
30. Schindler, A.; Balázs, G.; Zabel, M.; Gröger, C.; Kalbitzer, R.; Scheer, M. *C. R. Chim.* **2010,** *13,* 1241–1248. doi:10.1016/j.crci.2010.05.003
31. Milyukov, V. A.; Hey-Hawkins, E.; Sinyashin, O. G. *Russ. Chem. Bull.* **2007,** *56,* 549–551. doi:10.1007/s11172-007-0089-x
32. Dielmann, F.; Merkle, R.; Heinl, S.; Scheer, M. *Z. Naturforsch., B: J. Chem. Sci.* **2009,** *64,* 3–10. doi:10.1515/znb-2009-0102
33. Heinl, C.; Peresypkina, E.; Balázs, G.; Mädl, E.; Virovets, A. V.; Scheer, M. *Chem. – Eur. J.* **2021,** *27,* 7542–7548. doi:10.1002/chem.202100203
34. Weber, L.; Sommer, O.; Stammler, H.-G.; Neumann, B.; Kölle, U. *Chem. Ber.* **1995,** *128,* 665–671. doi:10.1002/cber.19951280703
35. Weber, L.; Kirchhoff, R.; Boese, R.; Stammler, H.-G.; Neumann, B. *Organometallics* **1993,** *12,* 731–737. doi:10.1021/om00027a024
36. Maigrot, N.; Avarvari, N.; Charrier, C.; Mathey, F. *Angew. Chem., Int. Ed. Engl.* **1995,** *34,* 590–592. doi:10.1002/anie.199505901

37. Bezkishko, I. A.; Zagidullin, A. A.; Khrizanforov, M. N.; Gerasimova, T. P.; Ivshin, K. A.; Kataeva, O. N.; Ganushevich, Y. S.; Miluykov, V. A.; Lönnecke, P.; Hey-Hawkins, E. *Inorg. Chem. Front.* **2022,** *9,* 2608–2616. doi:10.1039/d2qi00446a
38. Komatsu, K.; Kitagawa, T. *Chem. Rev.* **2003,** *103,* 1371–1428. doi:10.1021/cr010011q
39. Lyons, D. J. M.; Crocker, R. D.; Blümel, M.; Nguyen, T. V. *Angew. Chem., Int. Ed.* **2017,** *56,* 1466–1484. doi:10.1002/anie.201605979
40. Ranga, P. K.; Ahmad, F.; Singh, G.; Tyagi, A.; Vijaya Anand, R. *Org. Biomol. Chem.* **2021,** *19,* 9541–9564. doi:10.1039/d1ob01549d
41. These data are provided free of charge by the joint Cambridge Crystallographic Data Centre and Fachinformationszentrum Karlsruhe Access Structures service http://www.ccdc.cam.ac.uk/structures.
42. Zagidullin, A. A.; Petrov, A. V.; Bezkishko, I. A.; Miluykov, V. A. *Russ. Chem. Bull.* **2021,** *70,* 1260–1268. doi:10.1007/s11172-021-3209-0
43. Bezkishko, I. A.; Zagidullin, A. A.; Milyukov, V. A. *Russ. Chem. Bull.* **2020,** *69,* 435–448. doi:10.1007/s11172-020-2782-y
44. Zagidullin, A. A.; Khrizanforov, M. N.; Bezkishko, I. A.; Lönnecke, P.; Hey-Hawkins, E.; Miluykov, V. A. *J. Organomet. Chem.* **2021,** *956,* 122122. doi:10.1016/j.jorganchem.2021.122122
45. Winter, R. F.; Geiger, W. E. *Organometallics* **1999,** *18,* 1827–1833. doi:10.1021/om9809724
46. Wolf, R.; Ehlers, A. W.; Khusniyarov, M. M.; Hartl, F.; de Bruin, B.; Long, G. J.; Grandjean, F.; Schappacher, F. M.; Pöttgen, R.; Slootweg, J. C.; Lutz, M.; Spek, A. L.; Lammertsma, K. *Chem. – Eur. J.* **2010,** *16,* 14322–14334. doi:10.1002/chem.201001913
47. Hierlmeier, G.; Coburger, P.; Scott, D. J.; Maier, T. M.; Pelties, S.; Wolf, R.; Pividori, D. M.; Meyer, K.; Leest, N. P.; Bruin, B. *Chem. – Eur. J.* **2021,** *27,* 14936–14946. doi:10.1002/chem.202102335
48. Khrizanforov, M.; Strekalova, S.; Kholin, K.; Khrizanforova, V.; Grinenko, V.; Gryaznova, T.; Budnikova, Y. *RSC Adv.* **2016,** *6,* 42701–42707. doi:10.1039/c6ra04480h
49. Butovskiy, M. V.; Balázs, G.; Bodensteiner, M.; Peresypkina, E. V.; Virovets, A. V.; Sutter, J.; Scheer, M. *Angew. Chem., Int. Ed.* **2013,** *52,* 2972–2976. doi:10.1002/anie.201209329
50. Li, T.; Gamer, M. T.; Scheer, M.; Konchenko, S. N.; Roesky, P. W. *Chem. Commun.* **2013,** *49,* 2183–2185. doi:10.1039/c3cc38841g

License and Terms

This is an open access article licensed under the terms of the Beilstein-Institut Open Access License Agreement (https://www.beilstein-journals.org/bjoc/terms), which is identical to the Creative Commons Attribution 4.0 International License (https://creativecommons.org/licenses/by/4.0). The reuse of material under this license requires that the author(s), source and license are credited. Third-party material in this article could be subject to other licenses (typically indicated in the credit line), and in this case, users are required to obtain permission from the license holder to reuse the material.

The definitive version of this article is the electronic one which can be found at:
https://doi.org/10.3762/bjoc.18.139

BEILSTEIN JOURNAL OF ORGANIC CHEMISTRY

Design, synthesis, and evaluation of chiral thiophosphorus acids as organocatalysts

Karen R. Winters and Jean-Luc Montchamp*

Full Research Paper

Open Access

Address:
Department of Chemistry and Biochemistry, Texas Christian University, Fort Worth, Texas 76129, United States

Email:
Jean-Luc Montchamp* - j.montchamp@tcu.edu

* Corresponding author

Keywords:
asymmetric; heterocycles; organocatalysis; phosphorus; synthesis

Beilstein J. Org. Chem. **2022,** *18,* 1471–1478.
https://doi.org/10.3762/bjoc.18.154

Received: 06 July 2022
Accepted: 30 September 2022
Published: 17 October 2022

This article is part of the thematic issue "Organophosphorus chemistry: from model to application".

Guest Editor: G. Keglevich

© 2022 Winters and Montchamp; licensee Beilstein-Institut.
License and terms: see end of document.

Abstract

A series of *P*-stereogenic chiral phosphorus acids (CPAs) were synthesized to determine the requirements for efficient asymmetric organocatalysis. In order to eliminate the need for C_2-symmetry in common CPAs, various scaffolds containing C_1-symmetrical thiophosphorus acids were chosen. These new compounds were synthesized and evaluated in the asymmetric transfer hydrogenation of 2-phenylquinoline. Although the efficacy of the thiophosphorus acids was disappointing for this reaction, the work should be useful for developing structural design elements.

Introduction

The importance of asymmetric organocatalysis was demonstrated by the 2021 Nobel Prize in Chemistry awarded to McMillan and List. A subclass of organocatalysts introduced independently by Akiyama and Terada in 2004 [1,2], are the C_2-symmetrical chiral phosphorus acids (CPAs) initially derived from the BINOL scaffold, and later extended to other scaffolds such as VAPOL [3] and SPINOL [4,5] (Figure 1). The great success of these CPAs in asymmetric organocatalysis, is demonstrated by the publication of thousands of articles and reviews [6-17]. In all cases the C_2-symmetry is required because of the prototropic tautomeric equilibrium in the hydroxyphosphoryl (P(=O)OH) moiety which renders the phosphorus atom achiral. Substituents can be introduced on the ring system by ortho-functionalization with R groups on each ring. This functionalization helps introduce steric bulk and a range of electron densities extending the C_2-symmetry of the BINOL, creating a chiral pocket or environment for enantioselective transformations within the proximity of the acidic proton and phosphoryl oxygen. Additionally, the choice of phosphoric acid diesters also provides a bifunctional catalyst containing both an acidic and basic site (Figure 1).

Despite the proven value of the CPAs described in the literature, several disadvantages can be identified [18]. As mentioned

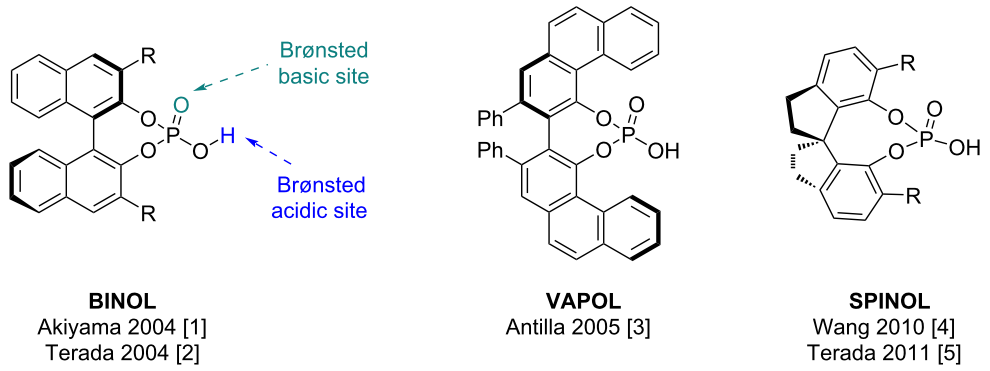
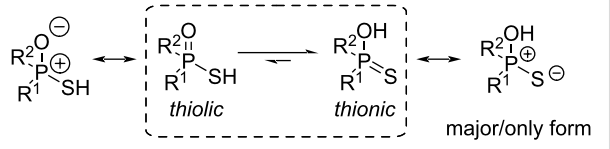


Figure 1: Chiral phosphorus acids (CPAs) derived from BINOL, VAPOL, and SPINOL. R = H, Ph, 4-PhC_6H_4-, 4-β-naphthylphenyl, 9-anthryl, 3,5-dimesitylphenyl, 3,5-diphenylphenyl, 4-MeC_6H_4-, 4-$CF_3C_6H_4$-, 4-*t*-BuC_6H_4-, β-naphthyl, 3,5-*t*-$Bu_2C_6H_3$-, 2,4,6-$Me_3C_6H_2$-, 2,4,6-i$Pr_3C_6H_2$-, Ph_3Si-, etc.

above, C_2-symmetry is required for the catalysts to provide a chiral pocket around the phosphorus. As a result, the CPAs have very high molecular weights (>> 450 g/mol) and require a wasteful duplicative functionalization of the backbone. Moreover, commercially available CPAs are extremely expensive (>> 500,000 $/mol) and immobilizing the CPAs on a solid support is not straightforward [19,20]. In order to avoid this, a significant investment in time must be made to complete the multistep-syntheses that are required [1-4]. Additionally, whereas either enantiomer of BINOL is relatively inexpensive (109 $/mol), it is not the case with SPINOL (17,000 $/mol), and VAPOL is not commercially available. Although one could synthesize these precursors as well, this multistep synthesis is time-consuming and costly. For example, the resolution of racemic SPINOL uses 2.4 equivalents of menthyl chloroformate [21] which itself costs 1,000 $/mol. Furthermore, the R group often needs to be optimized to obtain good enantioselectivities and there does not seem to be a universally successful CPA at this time. Consequently, the availability of each CPA enantiomer requires significant synthetic efforts from the diphenol precursor.

In order to address these issues, we became interested in exploring C_1-symmetrical CPAs, in which the chirality resides exclusively at the phosphorus atom. For this exploratory work, thiophosphorus acids were chosen due to their appropriate acidity and intrinsic chirality. Thiophosphorus acids undergo a tautomeric equilibrium between the thiolic and the thionic forms [22] (Scheme 1). If the substituents R^1 and R^2 are different, the phosphorus atom is always chiral. Chiral thiophosphorus acids have been obtained by resolution with a chiral amine as early as 1958 [23-27], or from other precursors [28-30].

Having selected chiral thiophosphorus acids for our model study, further design requirements were included (Figure 2) to



Scheme 1: The thiolic/thionic tautomeric equilibrium in thiophosphorus acids.

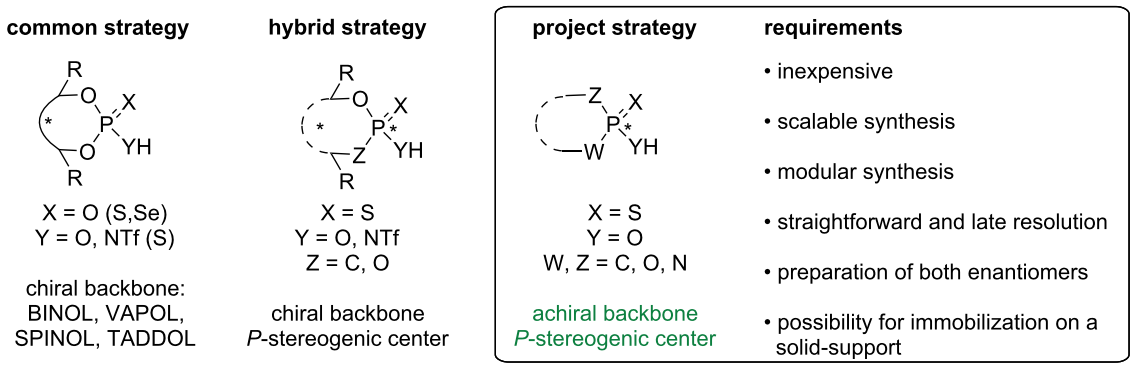


Figure 2: Project strategy and requirements for C_1-symmetrical CPAs.

address some issues listed above for the C_2-symmetrical catalysts. First and foremost, the compounds must be inexpensive to make, which implies that their syntheses should be easily scaled. A modular synthesis is also desirable if some structure optimization is required. The resolution of the phosphorus center should be straightforward and accomplished late-stage, to avoid carrying the chirality through multiple steps and the possible erosion of enantiomeric excesses. Preferably, both enantiomers of the CPA should also be available and immobilization of the CPA on a solid support should be possible. In this paper, we report our progress towards these objectives.

It should be noted that a few examples of a "hybrid strategy" in which both the backbone and the phosphorus atom are chiral have been reported by Guinchard [31] and Murai [32].

Results and Discussion

CPA Design

At the outset, we were interested in probing the geometry and influence of the substituent position in the CPAs (Figure 3). In the BINOL-derived CPA, the R-substituent and the phosphorus atom are separated by three bonds. In the indole-based CPAs **1** and **2**, the distance is reduced to two bonds, whereas in CPA **3** it is three bonds, and in **4** it is just one bond. Both **3** and **4** are based on 9,10-dihydro-9-oxa-10-phosphaphenanthrene-10-oxide (DOPO) [33].

Synthesis

In this section, the syntheses of CPA targets are described. It should be noted that little yield optimization was accomplished since only a small amount of product was needed for the evaluation as an enantioselective catalyst. On the other hand, their successful completions attest to the inexpensive and scalable requirements we had set.

Indole scaffolds

The synthesis of racemic tryptophol CPA **1** is shown in Scheme 2. Commercially available tryptophol (**5**, 225 $/mol) was N-arylated into **6** via copper-catalyzed cross-coupling [34] in excellent yield. Esterification of **6** with monomethyl *H*-phosphonate *tert*-butylamine salt [35] resulted in the mixed *H*-phosphonate ester **7** in excellent yield.

Cyclization using our homolytic aromatic substitution methodology [36] gave *P*-heterocycle **8** in modest yield. Other methods based on silver either gave a complex mixture or unreacted starting material. Phosphonate **8** was converted into the corresponding thiophosphonate **9** in moderate yield using Lawesson's reagent. Cleavage of the methyl ester was easily accomplished in quantitative yield, producing racemic tryptophol CPA **1**. The resolution of compound **1** was not conducted at this point because its synthesis was deemed problematic. While relatively short (5 steps), the overall yield was only 20% due to a low-yielding key step and a problematic thionation step immediately following. Unfortunately, thionation of **8** with an alternative [37] to Lawesson's reagent did not solve the problem. This prompted our search for alternative methodologies for the synthesis of thiophosphorus acids [38], particularly using the Stec reaction [39,40]. This work also led to the synthesis of CPA **3** [38]. Alternatives to the Stec reaction to prepare chiral thiophosphorus acids have been described [41-43]. Once equipped with our new methods [38], the synthesis of indole-derived **2** was undertaken (Scheme 3).

Known 3-allylindole (**10**) [44] was obtained from indole uneventfully. Intermediate **11** was furnished in moderate yield via our palladium-catalyzed hydrophosphinylation [45]. The key heterocyclization of **11** into **12** was accomplished using silver-promoted homolytic aromatic substitution [46], which was superior to our own manganese methodology (43% yield) [36]. Copper-catalyzed arylation [34] of **12** with iodobenzene and 4-nitroiodobenzene gave intermediates **13a** and **13b**, respectively. Next, conversion of ethyl phosphinate **13** into phosphinamide **14** was accomplished uneventfully [38] with inexpensive (*S*)-1-phenylethylamine (15 $/mol) as the chiral element. A single diastereoisomer of phosphinamide **14b** was

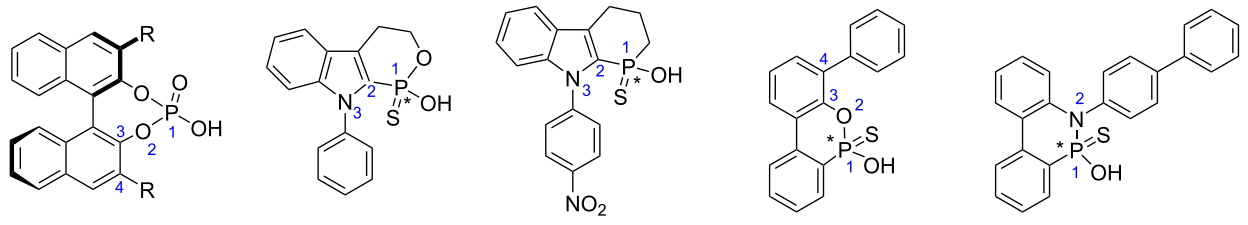
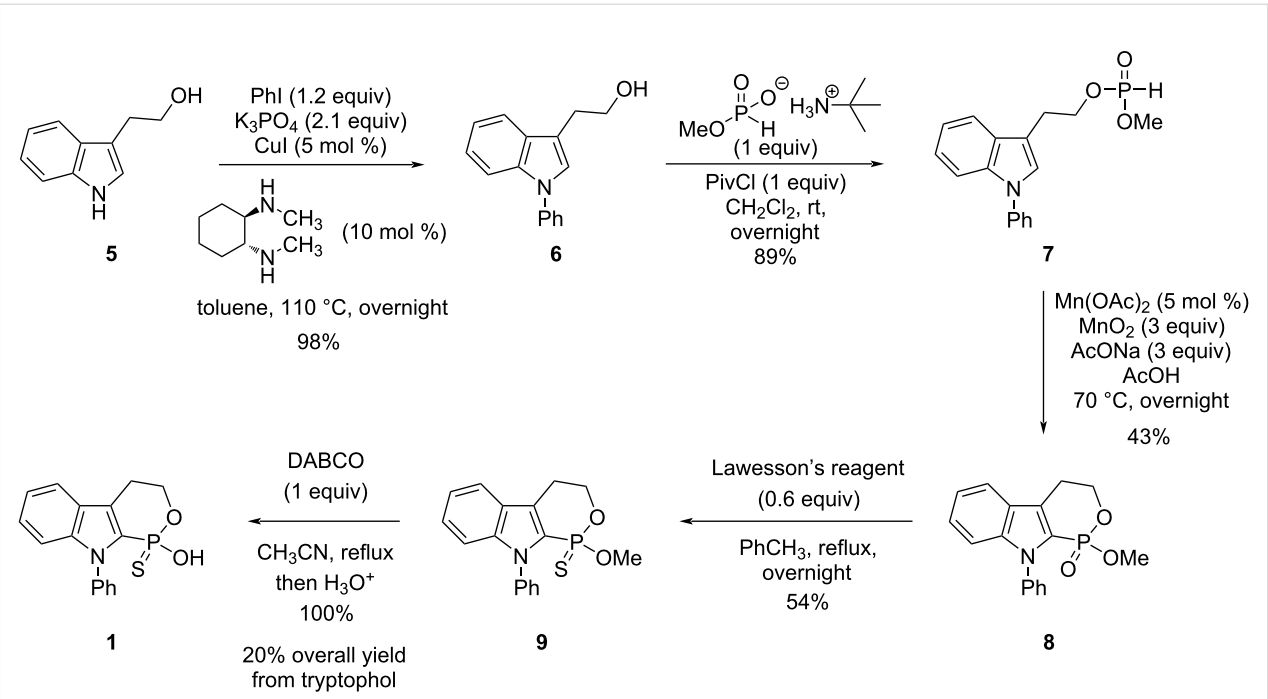
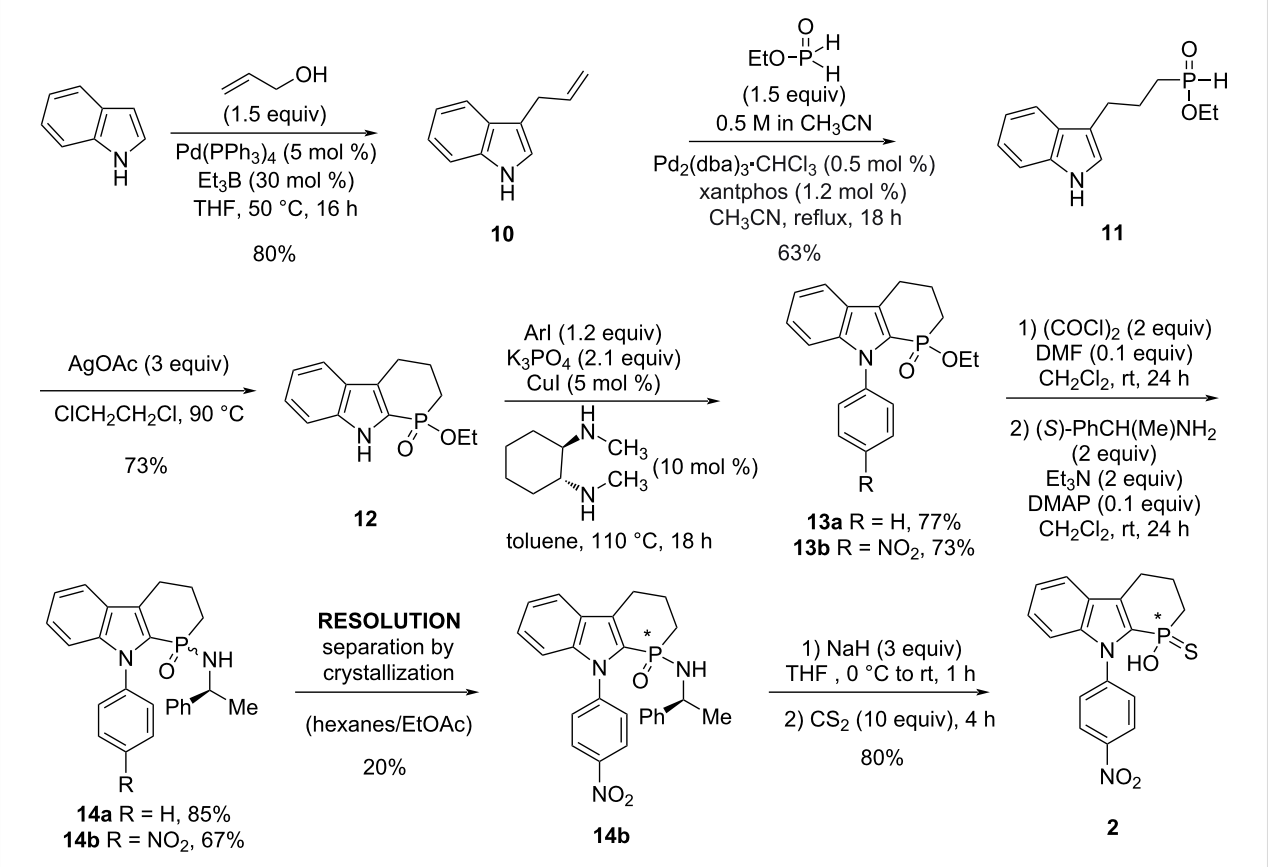


Figure 3: BINOL CPA and C_1-symmetrical CPA targets **1**–**4**.



Scheme 2: Synthesis of tryptophol-derived thiophosphorus acid **1**.



Scheme 3: Synthesis of indole-derived thiophosphorus acid **2**.

easily obtained by crystallization in 20% yield. Subsequent Stec reaction [38-40] gave chiral CPA **2** stereospecifically with retention of configuration [39]. This synthesis accomplishes a few of the requirements that were set inititally (see Figure 2). The chemistry is straightforward and can be scaled easily. The indole N-substituent can be introduced later to make the synthesis more modular, and the resolution is straightforward late in the synthesis. Additionally, the presence of the nitro group in CPA **2** was chosen for two reasons: 1) the possibility to further functionalize at this position through reduction, diazotization, and metal-catalyzed cross-coupling, and 2) immobilization on a solid support via reduction and reaction of the aniline with an electrophile such as polystyrene isocyanate.

DOPO scaffold

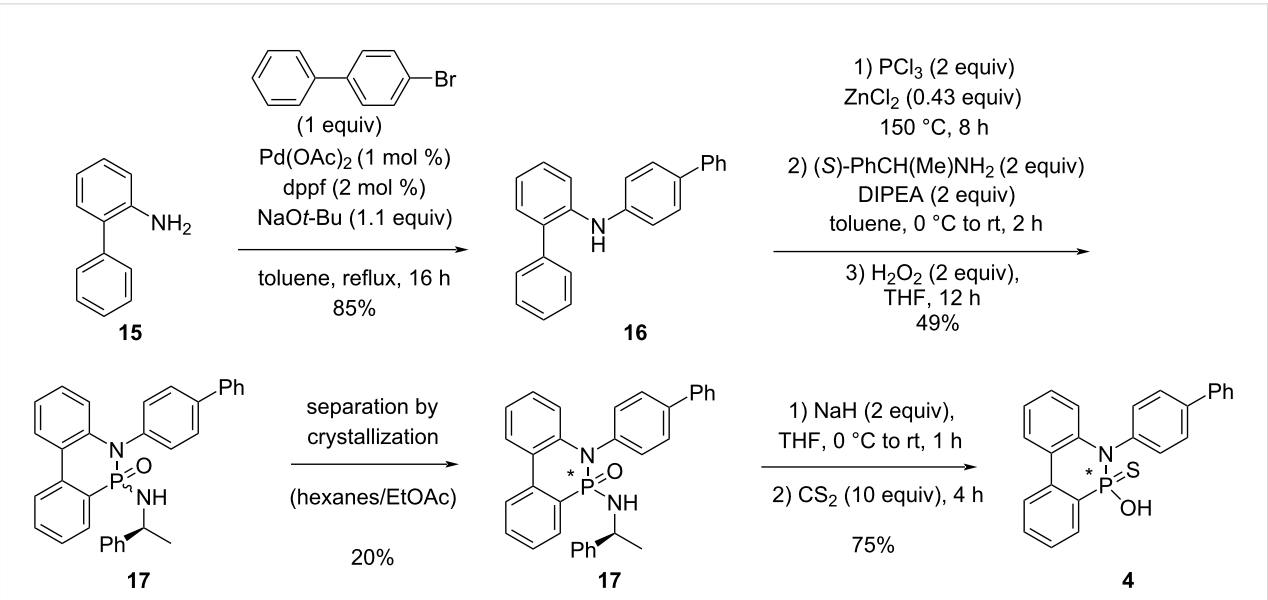
We previously reported the syntheses of both enantiomers of 8-phenyl DOPO **3** [38]. The syntheses proceed in only three steps (including the separation of the (*S*)-1-phenylethylamine-derived phosphonamide diastereoisomers) with S_P-**3** and R_P-**3** obtained in 13% and 9% respectively starting from 2,6-diphenylphenol.

Finally, *N*-biphenyl-DOPO CPA **4** was synthesized in four steps as shown in Scheme 4. Although compound **16** is commercially available, it was synthesized from 2-aminobiphenyl according to the literature [47]. Subsequent reaction with phosphorus trichloride and electrophilic aromatic substitution gave a chlorophosphine intermediate, which was directly reacted with (*S*)-1-phenylethylamine, then hydrogen peroxide. Phosphonamide diastereoisomers **17** were obtained in moderate yield. Crystallization gave a single diastereoisomer in 20% yield. Stec reaction [38-40] finally gave the desired CPA **4**. Although the entire sequence proceeded in only 6% overall yield, it was conducted on a multigram-scale so that more than 0.4 g of **4** was obtained.

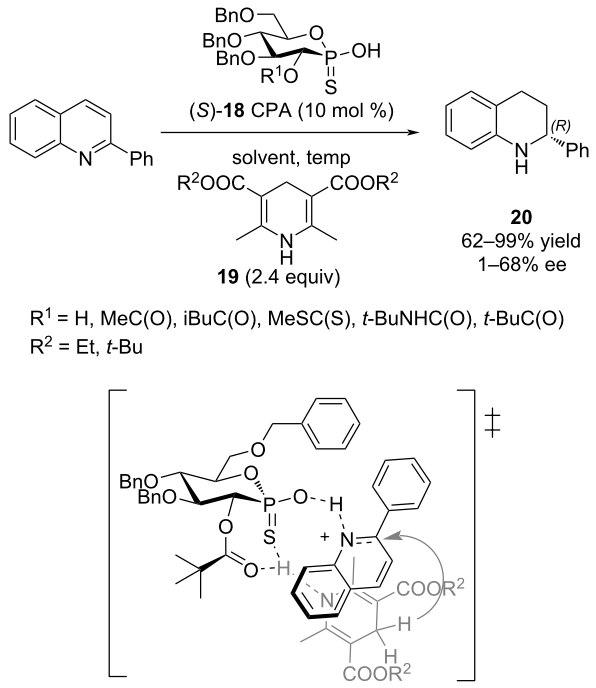
Evaluation of the catalysts

With our various CPAs **2**–**4** in hand, their evaluation in asymmetric organocatalysis was conducted. The reaction could have been chosen from a tremendous number of possibilities [1-17]. We selected the one Guinchard used to evaluate his thioacid hybrid-CPAs (Scheme 5) [31]. The transfer hydrogenation of 2-phenylquinoline with a Hantzsch ester **19** is a test reaction commonly used in asymmetric synthesis. The best performing of Guinchard's thiophostones **18** was the pivalate ester (R^1 = *t*-BuC(O)) with an 86% yield of **20** and a 52% ee (**19** R^2 = Et (2.4 equiv), toluene, 60 °C). Further optimization with the pivalate led to **20** in 82% yield and 68% ee (**19** R^2 = *t*-Bu (2 equiv), cyclopentyl methyl ether, 22 °C).

To account for the best results observed with pivalate **18**, Guinchard and coworkers proposed the transition-state shown in Scheme 5 [31]. Based on the fact that the cis-configuration between the sulfur and the pivalate was absolutely required for enantioselectivity, an interaction between both the sulfur and pivalate carbonyl oxygen with the hydrogen of Hantzsch ester's NH was proposed (Scheme 5). Thus, rather weak interactions might still be important in the assembly of a ternary complex and the enantioselectivity of the reaction.



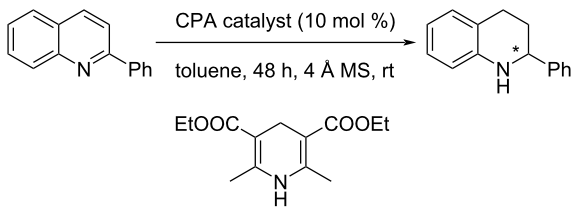
Scheme 4: Synthesis of *N*-biphenyl-DOPO CPA **4**.



Scheme 5: Transfer hydrogenation of 2-phenylquinoline and transition-state proposed by Guinchard and coworkers [28].

The evaluation of the catalysts is shown in Table 1. CPA **4** was completely ineffective at inducing chirality (Table 1, entry 1) and catalyst **2** was not much better (entry 2). Catalyst **3** on the other hand showed a modest induction (entry 3).

Table 1: *P*-stereogenic CPAs in the transfer hydrogenation of quinolines.



Entry	CPA catalyst	Yield (%)	ee (%)[a]
1	**4**	95	2
2	**2**	90	10
3	**3**	95	30

[a]Enantiomeric excess was determined by HPLC with a Chiracel OD-H column (hexane/iPrOH 95:5, 1 min/mL).

Conclusion

Exploratory efforts toward new C1-symmetrical CPAs were described. Four CPAs were synthesized and three evaluated. The syntheses are straightforward, inexpensive, and scalable. Resolution via the separation of diastereoisomeric phosphorus amides could be accomplished easily, either by chromatography over silica gel or crystallization. Subsequent Stec reaction proved to be a reliable method to convert the resolved amide into the chiral thiophosphorus acids.

The CPAs synthesized clearly failed to induce any significant asymmetry. It is interesting to note, however, that the enantiomeric excess increases with an increase in bond length separation between the phosphorus and the R group. From the reaction evaluation we found that dual activation might be required from the catalyst in certain enantioselective reactions. Thus, CPA platforms that reintroduce a dual donor–acceptor role, such as *P*-stereogenic triflamide CPAs $P(O)NHSO_2CF_3$, is currently under investigation since BINOL-derived triflamides have been successful [48,49]. Another possibility would be to look at reactions in which the catalyst would not require a Brønsted basic site. Both directions are currently under investigation and results will be shared in due course.

Supporting Information

Supporting Information File 1

Experimental procedures and copies of spectra.
[https://www.beilstein-journals.org/bjoc/content/supplementary/1860-5397-18-154-S1.pdf]

Funding

J.L.M. acknowledges the TCU Department of Chemistry and Biochemistry and grant 60979 from the TCU Research and Creative Activities Fund, for partial financial support. We also thank the TCU College of Science & Engineering for a SERC grant to K.R.W.

ORCID® iDs

Jean-Luc Montchamp - https://orcid.org/0000-0002-7327-1800

References

1. Akiyama, T.; Itoh, J.; Yokota, K.; Fuchibe, K. *Angew. Chem., Int. Ed.* **2004,** *43,* 1566–1568. doi:10.1002/anie.200353240
2. Uraguchi, D.; Terada, M. *J. Am. Chem. Soc.* **2004,** *126,* 5356–5357. doi:10.1021/ja0491533
3. Rowland, G. B.; Zhang, H.; Rowland, E. B.; Chennamadhavuni, S.; Wang, Y.; Antilla, J. C. *J. Am. Chem. Soc.* **2005,** *127,* 15696–15697. doi:10.1021/ja0533085

4. Xu, F.; Huang, D.; Han, C.; Shen, W.; Lin, X.; Wang, Y. *J. Org. Chem.* **2010,** *75,* 8677–8680. doi:10.1021/jo101640z
5. Terada, M. *Curr. Org. Chem.* **2011,** *15,* 2227–2256. doi:10.2174/138527211796150732
6. Parmar, D.; Sugiono, E.; Raja, S.; Rueping, M. *Chem. Rev.* **2014,** *114,* 9047–9153. doi:10.1021/cr5001496
7. Maji, R.; Mallojjala, S. C.; Wheeler, S. E. *Chem. Soc. Rev.* **2018,** *47,* 1142–1158. doi:10.1039/c6cs00475j
8. Lin, X.; Wang, L.; Han, Z.; Chen, Z. *Chin. J. Chem.* **2021,** *39,* 802–824. doi:10.1002/cjoc.202000446
9. Fang, G.-C.; Cheng, Y.-F.; Yu, Z.-L.; Li, Z.-L.; Liu, X.-Y. *Top. Curr. Chem.* **2019,** *377,* 23. doi:10.1007/s41061-019-0249-0
10. Mitra, R.; Niemeyer, J. *ChemCatChem* **2018,** *10,* 1221–1234. doi:10.1002/cctc.201701698
11. Li, X.; Song, Q. *Chin. Chem. Lett.* **2018,** *29,* 1181–1192. doi:10.1016/j.cclet.2018.01.045
12. Rahman, A.; Lin, X. *Org. Biomol. Chem.* **2018,** *16,* 4753–4777. doi:10.1039/c8ob00900g
13. Lv, F.; Liu, S.; Hu, W. *Asian J. Org. Chem.* **2013,** *2,* 824–836. doi:10.1002/ajoc.201300097
14. Biaggi, C.; Benaglia, M.; Annunziata, R.; Rossi, S. *Chirality* **2010,** *22,* 369–378. doi:10.1002/chir.20754
15. Zamfir, A.; Schenker, S.; Freund, M.; Tsogoeva, S. B. *Org. Biomol. Chem.* **2010,** *8,* 5262–5276. doi:10.1039/c0ob00209g
16. Terada, M. *Bull. Chem. Soc. Jpn.* **2010,** *83,* 101–119. doi:10.1246/bcsj.20090268
17. Terada, M. *Synthesis* **2010,** 1929–1982. doi:10.1055/s-0029-1218801
18. Antenucci, A.; Dughera, S.; Renzi, P. *ChemSusChem* **2021,** *14,* 2785–2853. doi:10.1002/cssc.202100573
19. Rueping, M.; Sugiono, E.; Steck, A.; Theissmann, T. *Adv. Synth. Catal.* **2010,** *352,* 281–287. doi:10.1002/adsc.200900746
20. Clot-Almenara, L.; Rodríguez-Escrich, C.; Osorio-Planes, L.; Pericàs, M. A. *ACS Catal.* **2016,** *6,* 7647–7651. doi:10.1021/acscatal.6b02621
21. Birman, V. B.; Rheingold, A. L.; Lam, K.-C. *Tetrahedron: Asymmetry* **1999,** *10,* 125–131. doi:10.1016/s0957-4166(98)00481-9
22. Kabachnik, M. I.; Mastrukova, T. A.; Shipov, A. E.; Melentyeva, T. A. *Tetrahedron* **1960,** *9,* 10–28. doi:10.1016/0040-4020(60)80048-8
23. Ribeiro, N.; Kobayashi, Y.; Maeda, J.; Saigo, K. *Chirality* **2011,** *23,* 438–448. doi:10.1002/chir.20702
24. Boter, H. L.; Platenburg, D. H. J. M. *Recl. Trav. Chim. Pays-Bas* **1967,** *86,* 399–404. doi:10.1002/recl.19670860408
25. Stamatia, V. *Curr. Org. Chem.* **2011,** *15,* 2469–2480. doi:10.2174/138527211796150642
26. Aaron, H. S.; Shryne, T. M.; Miller, J. I. *J. Am. Chem. Soc.* **1958,** *80,* 107–110. doi:10.1021/ja01534a029
27. Aaron, H. S.; Braun, J.; Shryne, T. M.; Frack, H. F.; Smith, G. E.; Uyeda, R. T.; Miller, J. I. *J. Am. Chem. Soc.* **1960,** *82,* 596–598. doi:10.1021/ja01488a024
28. Michalski, J.; Radziejewski, C.; Skrzypczynski, Z.; Dabkowski, W. *J. Am. Chem. Soc.* **1980,** *102,* 7974–7976. doi:10.1021/ja00547a044
29. Skrzypczynski, Z.; Michalski, J. *J. Org. Chem.* **1988,** *53,* 4549–4551. doi:10.1021/jo00254a024
30. Haynes, R. K.; Au-Yeung, T.-L.; Chan, W.-K.; Lam, W.-L.; Li, Z.-Y.; Yeung, L.-L.; Chan, A. S. C.; Li, P.; Koen, M.; Mitchell, C. R.; Vonwiller, S. C. *Eur. J. Org. Chem.* **2000,** 3205–3216. doi:10.1002/1099-0690(200009)2000:18<3205::aid-ejoc3205>3.0.co;2-d
31. Ferry, A.; Stemper, J.; Marinetti, A.; Voituriez, A.; Guinchard, X. *Eur. J. Org. Chem.* **2014,** 188–193. doi:10.1002/ejoc.201301253
32. Kuwabara, K.; Maekawa, Y.; Minoura, M.; Murai, T. *Org. Lett.* **2018,** *20,* 1375–1379. doi:10.1021/acs.orglett.8b00147
33. Salmeia, K. A.; Gaan, S. *Polym. Degrad. Stab.* **2015,** *113,* 119–134. doi:10.1016/j.polymdegradstab.2014.12.014
34. Antilla, J. C.; Klapars, A.; Buchwald, S. L. *J. Am. Chem. Soc.* **2002,** *124,* 11684–11688. doi:10.1021/ja027433h
35. Bryant, D. E.; Kilner, C.; Kee, T. P. *Inorg. Chim. Acta* **2009,** *362,* 614–616. doi:10.1016/j.ica.2008.04.028
36. Berger, O.; Montchamp, J.-L. *J. Org. Chem.* **2019,** *84,* 9239–9256. doi:10.1021/acs.joc.9b01239
37. Bergman, J.; Pettersson, B.; Hasimbegovic, V.; Svensson, P. H. *J. Org. Chem.* **2011,** *76,* 1546–1553. doi:10.1021/jo101865y
38. Winters, K. R.; Montchamp, J.-L. *J. Org. Chem.* **2020,** *85,* 14545–14558. doi:10.1021/acs.joc.0c01151
39. Wozniak, L. A.; Okruszek, A. *Chem. Soc. Rev.* **2003,** *32,* 158–169. doi:10.1039/b207207f
40. Wadsworth, W. S., Jr.; Emmons, W. D. *J. Am. Chem. Soc.* **1962,** *84,* 1316–1317. doi:10.1021/ja00866a060
41. Xu, Q.; Zhao, C.-Q.; Han, L.-B. *J. Am. Chem. Soc.* **2008,** *130,* 12648–12655. doi:10.1021/ja804412k
42. Berger, O.; Montchamp, J.-L. *Angew. Chem., Int. Ed.* **2013,** *52,* 11377–11380. doi:10.1002/anie.201306628
43. Varga, B.; Szemesi, P.; Nagy, P.; Herbay, R.; Holczbauer, T.; Fogassy, E.; Keglevich, G.; Bagi, P. *J. Org. Chem.* **2021,** *86,* 14493–14507. doi:10.1021/acs.joc.1c01364
44. Kimura, M.; Futamata, M.; Mukai, R.; Tamaru, Y. *J. Am. Chem. Soc.* **2005,** *127,* 4592–4593. doi:10.1021/ja0501161
45. Deprèle, S.; Montchamp, J.-L. *J. Am. Chem. Soc.* **2002,** *124,* 9386–9387. doi:10.1021/ja0261978
46. Wang, H.; Li, X.; Wan, B. *Synthesis* **2012,** *6,* 941–945. doi:10.1055/s-0031-1289700
47. Riedmüller, S.; Kaufhold, O.; Spreitzer, H.; Nachtsheim, B. J. *Eur. J. Org. Chem.* **2014,** 1391–1394. doi:10.1002/ejoc.201400046
48. Nakashima, D.; Yamamoto, H. *J. Am. Chem. Soc.* **2006,** *128,* 9626–9627. doi:10.1021/ja062508t
49. Rueping, M.; Nachtsheim, B. J.; Moreth, S. A.; Bolte, M. *Angew. Chem., Int. Ed.* **2008,** *47,* 593–596. doi:10.1002/anie.200703668

License and Terms

This is an open access article licensed under the terms of the Beilstein-Institut Open Access License Agreement (https://www.beilstein-journals.org/bjoc/terms), which is identical to the Creative Commons Attribution 4.0 International License (https://creativecommons.org/licenses/by/4.0). The reuse of material under this license requires that the author(s), source and license are credited. Third-party material in this article could be subject to other licenses (typically indicated in the credit line), and in this case, users are required to obtain permission from the license holder to reuse the material.

The definitive version of this article is the electronic one which can be found at:
https://doi.org/10.3762/bjoc.18.154

BEILSTEIN JOURNAL OF ORGANIC CHEMISTRY

Comparison of crystal structure and DFT calculations of triferrocenyl trithiophosphite's conformance

Ruslan P. Shekurov[1], Mikhail N. Khrizanforov[*1,2], Ilya A. Bezkishko[1], Tatiana P. Gerasimova[1], Almaz A. Zagidullin[1], Daut R. Islamov[2,3] and Vasili A. Miluykov[1]

Full Research Paper

Open Access

Address:
[1]Arbuzov Institute of Organic and Physical Chemistry, FRC Kazan Scientific Center, Russian Academy of Sciences, [2]Aleksander Butlerov Institute of Chemistry, Kazan Federal University, Kazan, 420008, 1/29 Lobachevskogo str., Russian Federation and [3]Laboratory for Structural Studies of Biomacromolecules, FRC Kazan Scientific Center of RAS, Lobachevskogo Street 2/31, Kazan 420111, Russian Federation

Email:
Mikhail N. Khrizanforov[*] - khrizanforov@gmail.com

* Corresponding author

Keywords:
DFT calculations; multi-ferrocenyl compounds; phosphorus thioesters; trithiophosphite; X-ray

Beilstein J. Org. Chem. **2022,** *18,* 1499–1504.
https://doi.org/10.3762/bjoc.18.157

Received: 17 August 2022
Accepted: 06 October 2022
Published: 25 October 2022

This article is part of the thematic issue "Organophosphorus chemistry: from model to application".

Guest Editor: G. Keglevich

© 2022 Shekurov et al.; licensee Beilstein-Institut.
License and terms: see end of document.

Abstract

A triferrocenyl trithiophosphite was studied by X-ray single-crystal diffraction. Triferrocenyl trithiophosphite has nine axes of internal rotation: three P–S bonds, three C–S bonds and three Fe–cyclopentadienyl axes. Rotation around the P–S bonds results in a totally asymmetric structure with three ferrocenylthio groups exhibiting different orientations towards the phosphorus lone electron pair (LEP). A comparison of DFT calculations and X-ray diffraction data is presented, herein we show which conformations are preferred for a given ligand.

Introduction

The design of novel "stimuli-responsive" molecules is a very attractive area in modern chemistry due to a number of various practical applications of such compounds [1-6]. Multiferrocenes are of particular fundamental interest because of their multistep electrochemical and magnetic properties. Such switchable systems with conjugated organic fragments containing an Fe^{II}/Fe^{III} system were used in organic electronics as molecular switches, optoelectronic materials and in biochemistry as photonic or redox devices [6].

A promising approach is the coordination self-assembly of multiferrocene ensembles from ferrocene-containing ligands and metal ions or clusters. This makes it possible to realize an almost infinite number of multiferrocene compounds and to

select leading compounds for the successful creation of molecular electronic devices. It should be noted that with the exception of tertiary phosphines, a relatively small number of trivalent phosphorus derivatives has been used to construct multiferrocene compounds. The use of ferrocene derivatives containing a phosphorus–sulfur bond is a promising direction, since coordination with a metal atom can occur both at the phosphorus and sulfur atoms [7]. It is important to know the conformational capabilities of such ligands for construction of such complexes [8-11].

However, to date, XRD data on phosphorus derivatives containing a ferrocenyl substituent at the sulfur atom are presented only in oxidized and sulfurized forms. Trithiophosphite has not been studied by X-ray diffraction analysis, although it is of great interest for the construction of complexes with multiferrocene systems. Herein we present for the first time X-ray diffraction data of $(FcS)_3P$ and compare it with DFT calculations to show which conformation are preferred for a given ligand.

Experimental

General

All reactions and manipulations were carried out under dry pure N_2 using standard Schlenk techniques. All solvents were distilled from sodium/benzophenone and stored under nitrogen before use. The NMR spectra were recorded on a Bruker MSL-400 spectrometer (^{1}H 400 MHz, ^{31}P 161.7 MHz, ^{13}C 100.6 MHz). $SiMe_4$ was used as internal reference for ^{1}H NMR chemical shifts, and 85% H_3PO_4 as external reference for ^{31}P NMR. The elemental analyses were carried out at the microanalysis laboratory of the Arbuzov Institute of Organic and Physical Chemistry, Russian Academy of Sciences.

Synthesis

To a suspension of white phosphorus (0.08 g, 0.645 mmol) in acetone (30 mL) were added diferrocenyldisulfide (1.68 g, 3.8 mmol) and 0.2 mL 15 N solution of potassium hydroxide. The reaction mixture was stirred for 12 h at room temperature and then the solvent was evaporated in vacuo. The product was extracted with benzene (3 × 30 mL) and after evaporation of the solvent triferrocenyl trithiophosphite (1.34 g, 76%) was obtained as a yellow powder. Single crystals suitable for X-ray diffraction were obtained by dissolving the compound in a mixture of benzene/hexane 1:1 and storing the solution in a fridge.

Mp 200–203 °C; ^{1}H NMR (400 MHz, C_6D_6, δ) 4.56 (m, 6 H_β), 4.03 (m, 6 H_α), 4.14 (s, 15H); ^{31}P NMR (161.7 MHz, C_6D_6, δ) 126.6; Anal. calcd for $C_{30}H_{27}Fe_3PS_3$ (760.37): C, 52.82; H, 3.99; P, 4.54; S, 14.09; found: C, 52.84; H, 3.96; P, 4.49; S, 14.04.

Single crystal X-ray diffraction

The data set for single crystals of triferrocenyl trithiophosphite was collected on a Rigaku XtaLab Synergy S instrument with a HyPix detector and a PhotonJet microfocus X-ray tube using Cu Kα (1.54184 Å) radiation at 100 K. Images were indexed and integrated using the CrysAlisPro data reduction package. The data were corrected for systematic errors and absorption using the ABSPACK module. The GRAL module was used for analysis of systematic absences and space group determination. Using Olex2 [11], the structure was solved by direct methods with SHELXT [12] and refined by the full-matrix least-squares on F^2 using SHELXL [13]. Non-hydrogen atoms were refined anisotropically. The figures were generated using the Mercury 4.1 program [14].

Crystal data for $C_{30}H_{27}Fe_3PS_3$ (M = 682.21 g/mol): monoclinic, space group $P2_1/c$ (no. 14), a = 7.49490(10) Å, b = 19.8932(3) Å, c = 18.4291(3) Å, β = 99.792(2)°, V = 2707.70(7) Å^3, Z = 4, T = 100.0(5) K, μ(Cu Kα) = 15.586 mm^{-1}, D_{calc} = 1.674 g/cm^3, 17211 reflections measured (6.59° ≤ 2Θ ≤ 153.132°), 5496 unique (R_{int} = 0.0570, R_{sigma} = 0.0467) which were used in all calculations. The final R_1 was 0.0496 (I > 2σ(I)) and wR_2 was 0.1349 (all data). CCDC number 2201898.

DFT calculations

All calculations were performed with the Gaussian 16 suite of programs [15]. The hybrid PBE0 functional [16] and the Ahlrichs' triple-ζ def-TZVP AO basis set [17] were used for optimization of all structures. In all geometry optimizations, the D3 approach [18] was applied to describe the London dispersion interactions as implemented in the Gaussian 16 program.

Results and Discussion

Previous electrochemical studies for triferrocenyl trithiophosphite revealed in their cyclovoltammograms three reversible one-electron peaks corresponding to stepwise oxidation of the three ferrocene moieties. It should be noted that the first oxidation potential is almost identical to free ferrocene [6]. Herein we report the crystal structure of triferrocenyl trithiophosphite.

For triferrocenyl trithiophosphite a *trans-gauche-gauche* configuration with torsion angles of −34°, −40°, and 173°, respectively, has been observed, although a propeller-like *gauche-gauche-gauche* configuration of alkyl(aryl)thio groups has been observed for trithiophosphites even in the solid state [7] or in the gas phase [8-10].

Triferrocenyl trithiophosphite has nine axes of internal rotation: three P–S bonds, three C–S bonds, and three Fe–cyclopentadienyl axes. The rotation around the P–S bonds results in a totally

unsymmetrical structure with three ferrocenylthio groups exhibiting different orientations towards the phosphorus lone electron pair (Figure 1).

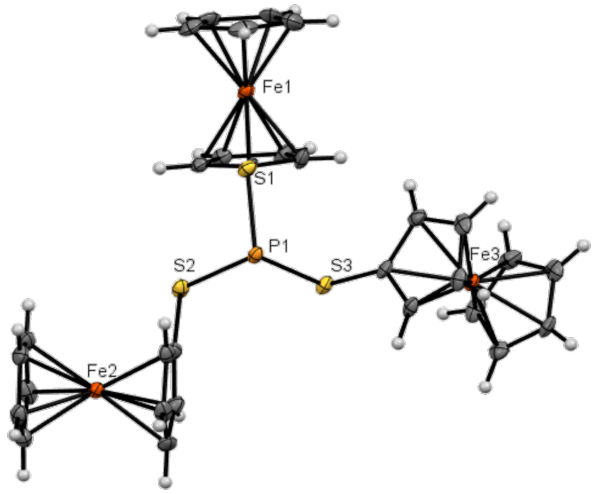


Figure 1: ORTEP representation of triferrocenyl trithiophosphite showing 50% probability thermal ellipsoids.

Several possible conformations of triferrocenyl trithiophosphite have been considered quantum-chemically (Figure 2, Table 1): *trans-trans-trans* (*ttt*), *gauche-trans-trans* (*gtt*), *gauche-gauche-trans* (*ggt*), and *gauche-gauche-gauche* (*ggg*). During optimization the *ggt* conformer adopted a *cis-gauche-trans* conformation with Fc(C)–S–P lone pair dihedral angles of 8°, −60°, and 173°, respectively (Table 1). The lowest energy has been predicted for the *gtt* conformer, nevertheless the energy differences between the *gtt* and *cgt* conformers are negligible (0.23 kcal/mol). Interestingly, the *cgt* conformation has been found previously for tricymantrenyl trithiophosphite [19]. The highest relative energy is predicted for the *ggg* conformer (1.7 kcal/mol). The ferrocene adopts an almost eclipsed confor-

Table 1: Calculated relative energies and dihedral angles Fc(C)–S–P=X (°) (X = LEP, O, S) of four possible conformers of $(FcS)_3P$, $(FcS)_3PO$, and $(FcS)_3PS$.

	$(FcS)_3P$	$(FcS)_3PO$	$(FcS)_3PS$
ttt	0.91	**0**	0.04
	149/151/151	149/149/149	149/149/149
gtt	**0**	0.23	0.20
	−56/175/−161	−56/−173/−135	47/174/135
ggt/*cgt*	0.23	0.52	0.36
	8/−60/173	−62/−47/165	46/45/176
ggg	1.73	0.55	**0**
	−37/−35/−36	−52/−34/−53	42/44/44

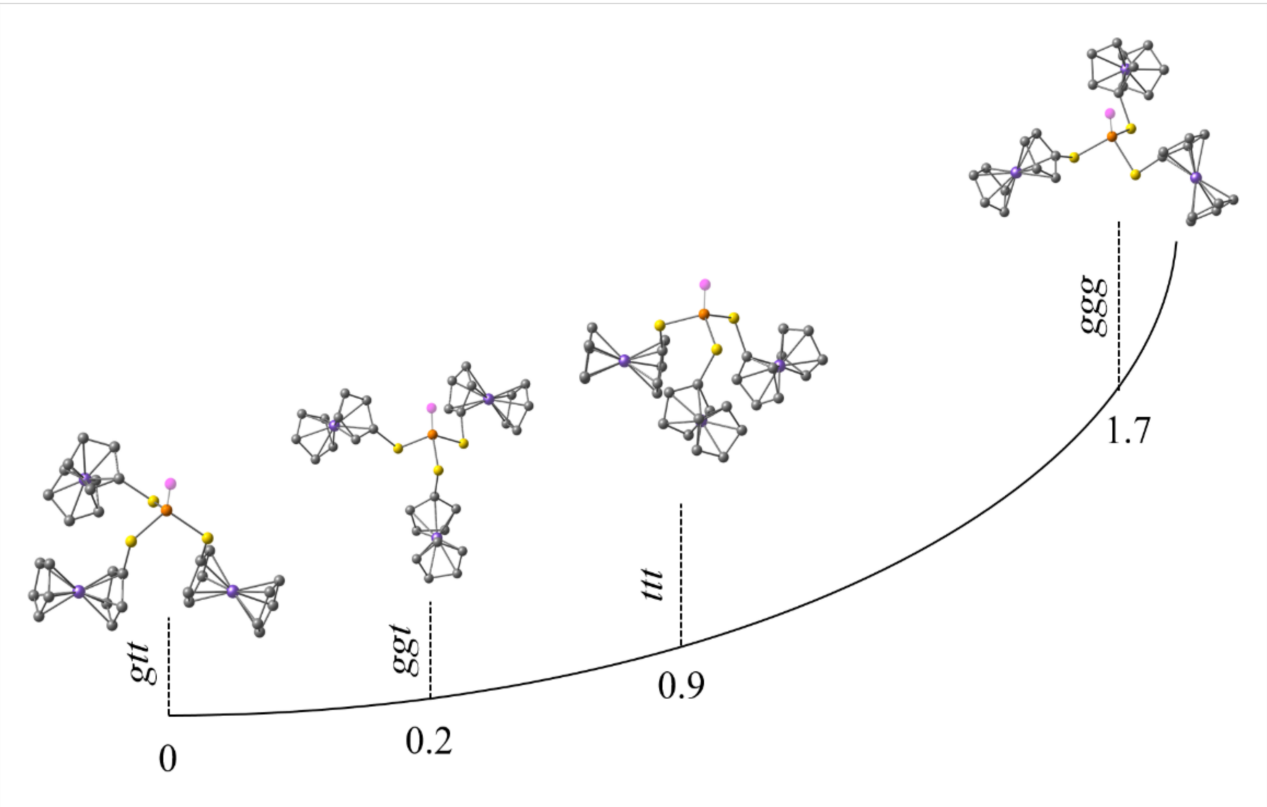


Figure 2: Optimized conformations and relative energies of four possible conformers of triferrocenyl trithiophosphite.

mation in all the models with the dihedral angle between two Cp rings of ≈ 10°. Our previous work indicated that Cp can rotate at room temperature [20]. The Fc(C)–S–P lone pair dihedral angle for the *ttt* conformer is ≈ 150°, and for the *ggg* conformer it is ≈ −35°. For the *gtt*/*cgt* conformers the *trans* S–Fc bonds are almost antiparallel to the phosphorus lone pair (LEP): 175°, −161°/173°. The dihedral angle for the *gauche* S–Fc bond in the *gtt* conformer is −56°, and a close value is predicted for one of the *gauche* S–Fc bonds in the *tgg* conformer (−60°), whereas the second one is almost parallel to LEP (8°).

The energy difference between the considered conformations is quite small, suggesting other factors playing a significant role. The highest energy predicted for the *ggg* conformer is obviously related to the absence of stabilizing intramolecular CH···π (like in the *gtt* and *cgt* cases) or CH···Fe (like in the *ttt* case) interactions between neighboring fragments in the structure. The latter plays an important role from the electrostatic point of view; the NBO analysis predict a negative charge at the Fe ion and positive charges at hydrogen atoms (Figure 3). Thus the crystal structure of $(FcS)_3P$ is defined rather by plural intermolecular interactions than by relative energetics of conformers (Figures S1–S3 in Supporting Information File 1).

Previously, for triferrocenyl trithiophosphate and triferrocenyl tetrathiophosphate with P=O and P=S moieties propeller-like *ggg* conformations have been found by X-ray diffraction analysis. Indeed, computations predict the *ggg* conformer to be the most energetically advantageous for the P=S containing compound, however with very close energies of the *ttt* and the *ggg* conformers (Table 1). For the P=O containing compound the *ttt* conformer is predicted to have the lowest energy. Nevertheless for both P=X compounds computations predict very small energy differences between all four conformers, lower than 0.6 kcal/mol. Thus, one can conclude that in these cases crystal packing influences the conformation. A comparison of the crystal packings for the P_{LEP}, P=O, and P=S containing compounds clearly confirms this conclusion experimentally (Figure 4).

We compared the crystal packings of three similar compounds: $(FcS)_3P$, $(FcS)_3PO$ [19], and $(FcS)_3PS$ [7] (Figure 4). All three compounds form crystals belonging to the monoclinic syngony. In all three cases, the molecules in the crystals form a herringbone motif. In $(FcS)_3P$, C–H···π interactions dominate, while in $(FcS)_3PS$ and $(FcS)_3PO$, in addition to C–H···π interactions, by one C–H···S and two C–H···O interactions, respectively, are observed. It should be noted that $(FcS)_3PO$ crystals contain a solvent molecule that participates in intermolecular interactions. Thus, despite the similarity of the molecular structure of the three compounds and some crystal parameters, the intermolecular interactions differ noticeably from each other.

At the same time one should underline the role of the ferrocene moiety for the crystal structure of the $(FcS)_3P$. The related $(PhS)_3P$ molecule with Ph rings instead of Fc units exist in the propeller-like *gauche-gauche-gauche* configuration [21],

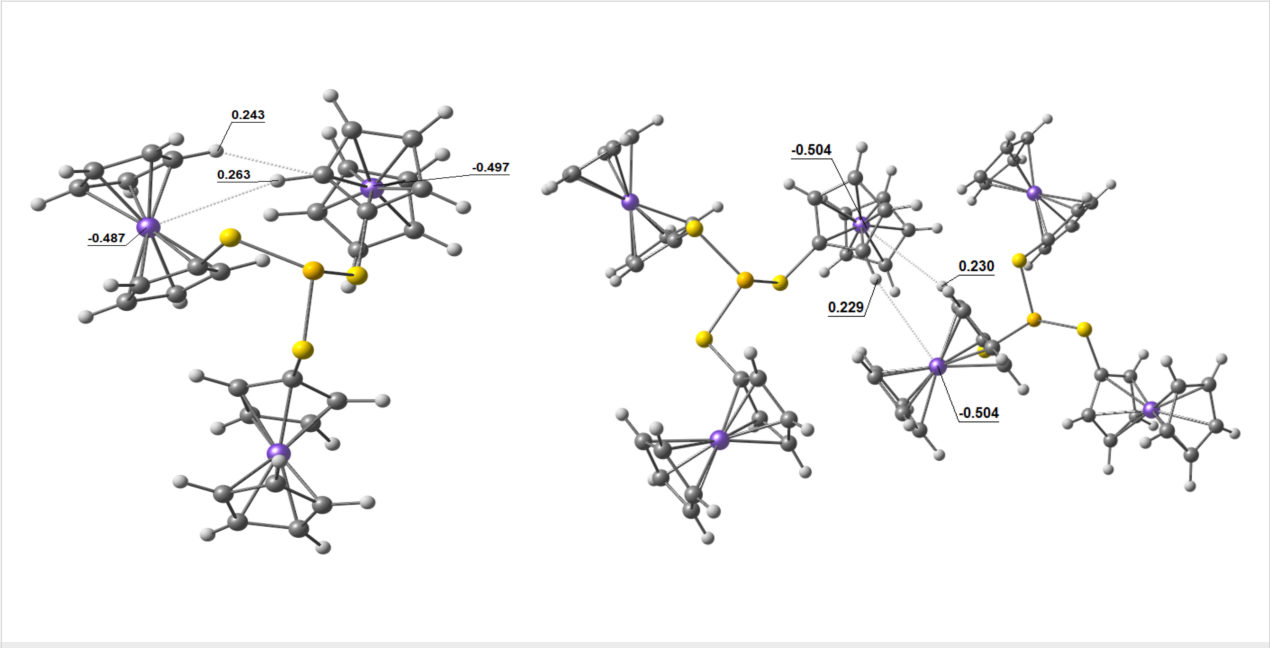


Figure 3: Calculated NBO charges on the Fe ions and hydrogen atoms for the optimized *ttg* conformer (left) and for two neighboring molecules (right) from X-ray analysis data.

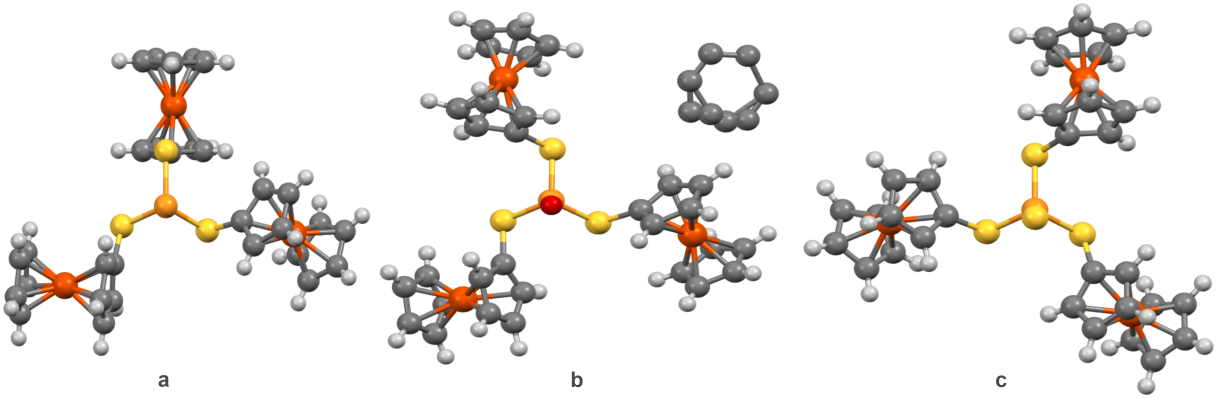


Figure 4: Molecular structures in the solid state of a) $(FcS)_3P$, b) $(FcS)_3PO$ [19], and c) $(FcS)_3PS$ [7] as established by single crystal X-ray diffraction analyses. C atoms – grey, Fe atoms – brown, O atoms – red, P atoms – orange, S atoms – yellow.

forming the C–H···π-bonded dimers (Figures S4 and S5 in Supporting Information File 1). The computations of the relative energies of five possible conformers of $(PhS)_3P$ (*ggg*, *ttt*, *ttg*, *ggt*, *ccg*) predict the lowest energy for the *ccg* conformation (Figure 5). The propeller-like *ggg* conformer found in the solid state has the highest energy. Most obviously the latter is stabilized by intermolecular C–H···π interactions (Figures S4 and S5 in Supporting Information File 1). The bulky Fc moieties do not allow to form such type of dimers.

Conclusion

Triferrocenyl trithiophosphite $(FcS)_3P$ was studied by X-ray single-crystal diffraction for the first time. DFT calculations and X-ray diffraction data were compared, and the preferred conformations were established. Despite the similarity of the molecular structures and some crystal parameters of $(FcS)_3P$, $(FcS)_3PO$, and $(FcS)_3PS$, the intermolecular interactions differ noticeably from each other.

Supporting Information

Supporting Information File 1

Additional figures.
[https://www.beilstein-journals.org/bjoc/content/supplementary/1860-5397-18-157-S1.pdf]

Supporting Information File 2

CIF file for triferrocenyl trithiophosphite.
[https://www.beilstein-journals.org/bjoc/content/supplementary/1860-5397-18-157-S2.cif]

Supporting Information File 3

Check-CIF file for triferrocenyl trithiophosphite.
[https://www.beilstein-journals.org/bjoc/content/supplementary/1860-5397-18-157-S3.htm]

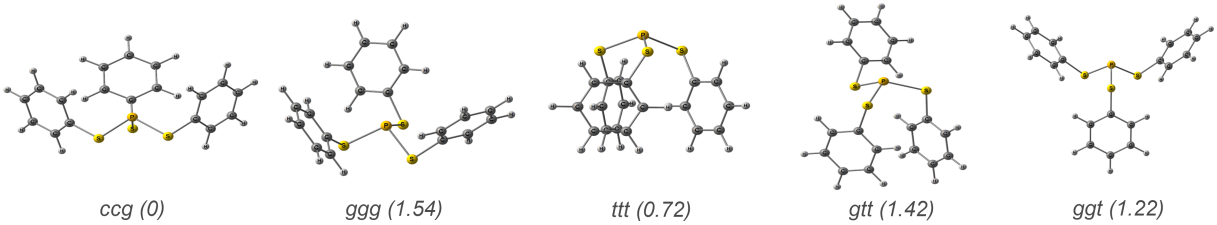


Figure 5: Quantum chemically optimized conformations of the $(PhS)_3P$ molecule and their relative energies (kcal/mol).

Acknowledgements

The measurements have been carried out using the equipment of Distributed Spectral-Analytical Center of Shared Facilities for Study of Structure, Composition and Properties of Substances and Materials of FRC Kazan Scientific Center of RAS.

Funding

This work was supported by the grant of the Russian Science Foundation No. 22-73-10203.

ORCID® iDs

Ruslan P. Shekurov - https://orcid.org/0000-0002-2203-6675
Mikhail N. Khrizanforov - https://orcid.org/0000-0003-4714-4143
Ilya A. Bezkishko - https://orcid.org/0000-0002-4563-2859
Almaz A. Zagidullin - https://orcid.org/0000-0003-3125-7506
Daut R. Islamov - https://orcid.org/0000-0002-5988-1012
Vasili A. Miluykov - https://orcid.org/0000-0002-8069-457X

Preprint

A non-peer-reviewed version of this article has been previously published as a preprint: https://doi.org/10.3762/bxiv.2022.68.v1

References

1. Sakamoto, R.; Murata, M.; Nishihara, H. *Angew. Chem., Int. Ed.* **2006,** *45,* 4793–4795. doi:10.1002/anie.200601067
2. Diallo, A. K.; Absalon, C.; Ruiz, J.; Astruc, D. *J. Am. Chem. Soc.* **2011,** *133,* 629–641. doi:10.1021/ja109380u
3. Kishore, P. V. V. N.; Liao, J.-H.; Hou, H.-N.; Lin, Y.-R.; Liu, C. W. *Inorg. Chem.* **2016,** *55,* 3663–3673. doi:10.1021/acs.inorgchem.6b00201
4. Wang, L.; Chen, L.-J.; Ma, J.-Q.; Wang, C.-H.; Tan, H.; Huang, J.; Xiao, F.; Xu, L. *J. Organomet. Chem.* **2016,** *823,* 1–7. doi:10.1016/j.jorganchem.2016.09.001
5. Straube, A.; Coburger, P.; Michak, M.; Ringenberg, M. R.; Hey-Hawkins, E. *Dalton Trans.* **2020,** *49,* 16667–16682. doi:10.1039/d0dt02743j
6. Donoli, A.; Bisello, A.; Cardena, R.; Prinzivalli, C.; Santi, S. *Organometallics* **2013,** *32,* 1029–1036. doi:10.1021/om301006v
7. Shekurov, R.; Khrizanforov, M.; Gerasimova, T.; Yamaleeva, Z.; Ivshin, K.; Lakomkina, A.; Bezkishko, I.; Kononov, A.; Sinyashin, O.; Budnikova, Y.; Kataeva, O.; Miluykov, V. *Molecules* **2020,** *25,* 939. doi:10.3390/molecules25040939
8. Kursheva, L. I.; Kataeva, O. N.; Krivolapov, D. B.; Gubaidullin, A. T.; Batyeva, E. S.; Sinyashin, O. G. *Heteroat. Chem.* **2008,** *19,* 483–489. doi:10.1002/hc.20459
9. Strasser, C. E.; Cronje, S.; Schmidbaur, H.; Raubenheimer, H. G. *J. Organomet. Chem.* **2006,** *691,* 4788–4796. doi:10.1016/j.jorganchem.2006.07.034
10. Kataeva, O. N.; Krivolapov, D. B.; Gubaidullin, A. T.; Litvinov, I. A.; Kursheva, L. I.; Katsyuba, S. A. *J. Mol. Struct.* **2000,** *554,* 127–140. doi:10.1016/s0022-2860(00)00665-7
11. Dolomanov, O. V.; Bourhis, L. J.; Gildea, R. J.; Howard, J. A. K.; Puschmann, H. *J. Appl. Crystallogr.* **2009,** *42,* 339–341. doi:10.1107/s0021889808042726
12. Sheldrick, G. M. *Acta Crystallogr., Sect. A: Found. Adv.* **2015,** *71,* 3–8. doi:10.1107/s2053273314026370
13. Sheldrick, G. M. *Acta Crystallogr., Sect. A: Found. Crystallogr.* **2008,** *64,* 112–122. doi:10.1107/s0108767307043930
14. Macrae, C. F.; Edgington, P. R.; McCabe, P.; Pidcock, E.; Shields, G. P.; Taylor, R.; Towler, M.; van de Streek, J. *J. Appl. Crystallogr.* **2006,** *39,* 453–457. doi:10.1107/s002188980600731x
15. *Gaussian 16,* Revision B.01; Gaussian, Inc.: Wallingford, CT, 2016.
16. Adamo, C.; Barone, V. *J. Chem. Phys.* **1999,** *110,* 6158–6170. doi:10.1063/1.478522
17. Weigend, F.; Ahlrichs, R. *Phys. Chem. Chem. Phys.* **2005,** *7,* 3297–3305. doi:10.1039/b508541a
18. Grimme, S.; Antony, J.; Ehrlich, S.; Krieg, H. *J. Chem. Phys.* **2010,** *132,* 154104. doi:10.1063/1.3382344
19. Milyukov, V. A.; Zverev, A. V.; Podlesnov, S. M.; Krivolapov, D. B.; Litvinov, I. A.; Gubaidullin, A. T.; Kataeva, O. N.; Ginzburg, A. G.; Sinyashin, O. G. *Eur. J. Inorg. Chem.* **2000,** 225–228. doi:10.1002/(sici)1099-0682(200001)2000:1<225::aid-ejic225>3.0.co;2-u
20. Islamov, D. R.; Shtyrlin, V. G.; Serov, N. Y.; Fedyanin, I. V.; Lyssenko, K. A. *Cryst. Growth Des.* **2017,** *17,* 4703–4709. doi:10.1021/acs.cgd.7b00588
21. Nieger, M.; Niecke, E.; Fischer, U. CSD Communication, 1999; CCDC number 115547. doi:10.5517/cc3w7bj

License and Terms

This is an open access article licensed under the terms of the Beilstein-Institut Open Access License Agreement (https://www.beilstein-journals.org/bjoc/terms), which is identical to the Creative Commons Attribution 4.0 International License (https://creativecommons.org/licenses/by/4.0). The reuse of material under this license requires that the author(s), source and license are credited. Third-party material in this article could be subject to other licenses (typically indicated in the credit line), and in this case, users are required to obtain permission from the license holder to reuse the material.

The definitive version of this article is the electronic one which can be found at:
https://doi.org/10.3762/bjoc.18.157

BEILSTEIN JOURNAL OF ORGANIC CHEMISTRY

An alternative C–P cross-coupling route for the synthesis of novel V-shaped aryldiphosphonic acids

Stephen J. I. Shearan[1], Enrico Andreoli[1] and Marco Taddei[*1,2]

Letter

Open Access

Address:
[1]Energy Safety Research Institute, Swansea University, Fabian Way, Crymlyn Burrows, Skewen, Swansea SA1 8EN, UK and
[2]Dipartimento di Chimica e Chimica Industriale, Università di Pisa, Via Giuseppe Moruzzi, 13, 56124 Pisa, Italy

Email:
Marco Taddei[*] - marco.taddei@unipi.it

* Corresponding author

Keywords:
arylphosphonic acids; cross-coupling reaction; phosphonate esters; transition-metal catalysis

Beilstein J. Org. Chem. **2022,** *18,* 1518–1523.
https://doi.org/10.3762/bjoc.18.160

Received: 04 July 2022
Accepted: 24 October 2022
Published: 07 November 2022

This article is part of the thematic issue "Organophosphorus chemistry: from model to application".

Guest Editor: G. Keglevich

© 2022 Shearan et al.; licensee Beilstein-Institut.
License and terms: see end of document.

Abstract

The synthesis of phosphonate esters is a topic of interest for various fields, including the preparation of phosphonic acids to be employed as organic linkers for the construction of metal phosphonate materials. We report an alternative method that requires no solvent and involves a different order of addition of reactants to perform the transition-metal-catalyzed C–P cross-coupling reaction, often referred to as the Tavs reaction, employing $NiCl_2$ as a pre-catalyst in the phosphonylation of aryl bromide substrates using triisopropyl phosphite. This new method was employed in the synthesis of three novel aryl diphosphonate esters which were subsequently transformed to phosphonic acids through silylation and hydrolysis.

Introduction

Phosphonates and phosphonic acids are a very interesting class of compounds and examples of their use can be found in a number of different areas, including pharmaceuticals [1-6], metal chelation [7-9], anti-corrosion coatings [10-12], fertilizers [13,14], proton conduction [15-17], and catalysis [18], amongst others. Phosphonates can also be employed as organic linkers in combination with metal ions to afford coordination polymers and metal-organic frameworks (MOFs), or more aptly, metal phosphonate frameworks [19,20]. One of the main challenges in the synthesis of metal phosphonates is that the linkers are rarely commercially available and can often be difficult to prepare. Most often, the challenge is, in fact, not the synthesis of the phosphonic acid itself, but that of the phosphonic ester precursor [21].

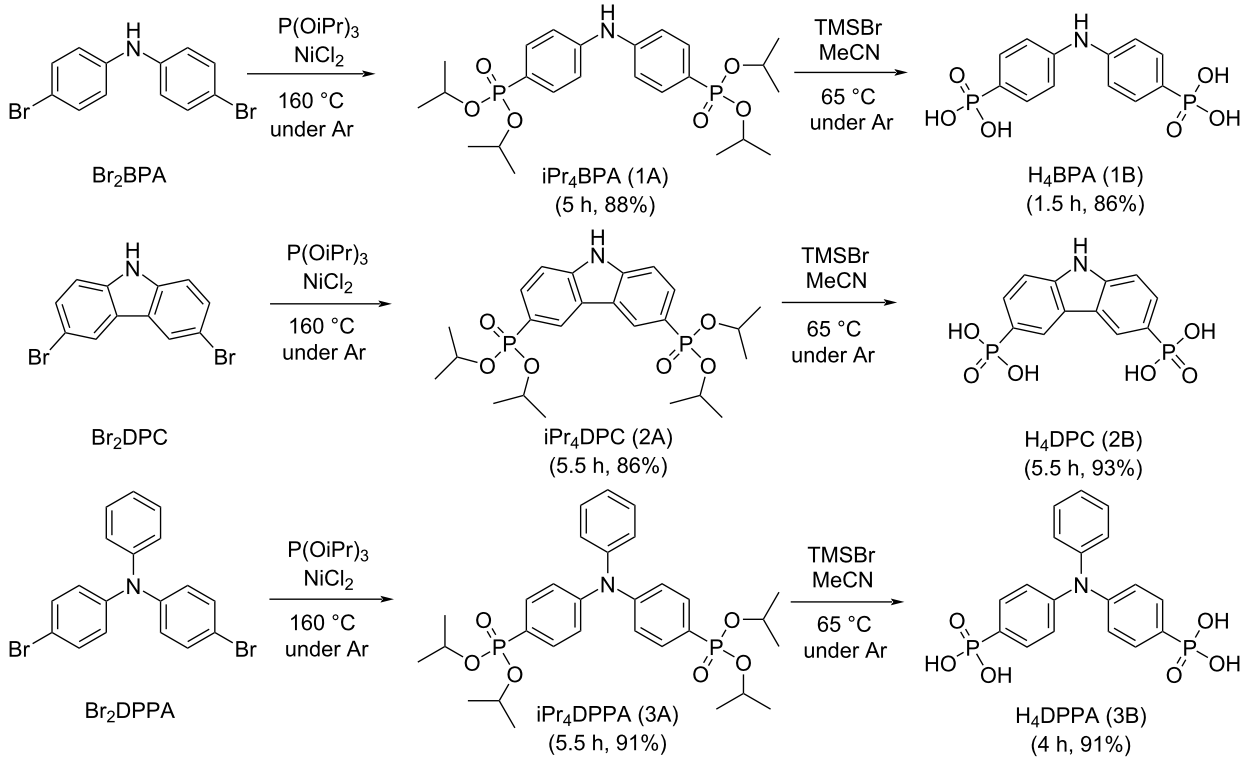
Perhaps the most well-known C–P coupling procedure is the Michaelis–Arbuzov rearrangement involving a reaction between a primary alkyl halide and a trialkyl phosphite, first reported in the late 1890s, the general scheme for which can be seen in Supporting Information File 1, Scheme S1 [22]. It should be noted that this reaction is not suitable for use with aryl halide substrates due to the poor reactivity between aryl halides and trialkyl phosphites [23]. Some of the most studied C–P coupling reactions involving aryl substrates are those em-

ploying catalysts, which are required in order to lower the energy barrier of the reaction and overcome the poor reactivity between aryl halides and trialkyl phosphites [24-26]. These catalytic cross-coupling reactions tend to follow similar pathways to the Michaelis–Arbuzov reaction, with the inclusion of a catalytic intermediate step. A number of suitable catalysts have been identified, ranging from nickel(II) bromide and nickel(II) chloride, to palladium(II) acetate and palladium(II) chloride [23,27,28]. Reactions involving these catalysts are most often carried out at high temperatures, usually in excess of 160 °C, and involve slow dropwise addition of the trialkyl phosphite to the substrate [23]. In the search for milder reaction conditions, a new catalyst, tetrakis(triphenylphosphine)palladium(0), was introduced by Hirao and co-workers, which allowed for the lowering of the reaction temperature to approximately 90 °C [29-31].

In this work, we have developed an alternative experimental protocol to perform the Ni-catalyzed C–P cross-coupling reaction, or Tavs reaction, whose mechanism is shown in Supporting Information File 1, Scheme S2 [32]. Starting from commercially available bromide precursors, we target a series of novel aryldiphosphonic acids sharing the feature of having non-linear – or V-shaped – geometry, intended to be employed as organic linkers for the synthesis of open framework metal phosphonate materials. The proposed protocol does not require a solvent, while featuring reaction times and yields comparable, if not better, to those of most procedures commonly employed in the literature.

Results and Discussion

The goal of this work is the phosphonylation of the commercially available bromo-substituted *N*-aryl precursors bis(4-bromophenyl)amine (Br_2BPA), 3,6-dibromocarbazole (Br_2DPC), and 4-bromo-*N*-(4-bromophenyl)-*N*-phenylaniline (Br_2DPPA) (see Scheme 1). In light of using the resulting phosphonic acids as linkers for the construction of metal phosphonate frameworks, two main considerations were made when selecting these substrates with regards to rigidity and geometry (Figure S1, Supporting Information File 1). In the compounds considered here, rigidity is ensured by the network of sp^2-hybridized carbon atoms, or aromatic rings, and is important to ensure stability in the potential MOF structures derived from the proposed linkers. The geometry of these linkers, termed as V-shaped, was selected to try and move away from the pillared-layered structures that are obtained when using linear diphosphonate linkers, which are often either non-porous or have low porosity and have little to no long-range order. The idea here was that the V-shaped linkers, as well as different substituents attached to nitrogen, could potentially force a non-layered porous structure.



Scheme 1: Scheme showing the transformation of the Br-substrates to phosphonate esters and then to phosphonic acids.

Conventionally, the transition-metal-catalyzed C–P cross-coupling reaction is carried out by placing the aryl halide and the precatalyst into a round-bottomed flask in the presence of a suitable solvent, such as 1,3-diisopropylbenzene or mesitylene, and setting to reflux. The advantage of using such solvents lies in their high boiling point (203 °C and 164 °C, respectively), which allows for reactions to be run at high temperatures, thus enhancing the rate of the reaction. While the reaction mixture is refluxing, the alkyl phosphite is added in several small portions.

The work we present differs from the conventional nickel-catalyzed cross-coupling reaction in two aspects: we use no solvent and we employ a different order of addition of reactants. The absence of solvent presents a few advantages over the original method. First of all, the removal of said solvent by distillation after the completion of the reaction is no longer required and thus there is a simplification of the workup procedure. Second, there is no dilution of the reaction mixture, which lends itself to an increased reaction rate. Contrary to the conventional method, this alternative method starts with the nickel(II) precatalyst and the alkyl phosphite, triisopropyl phosphite in our case, being added to a round-bottomed flask and heated to approximately 160 °C, leading to the formation of the nickel(0) catalyst, more accurately representing the catalytic cycle presented in Scheme S2 (Supporting Information File 1). The solid aryl bromide is then added to the mixture via a powder addition funnel over a 2–4 hour period, depending on the substrate, and is then left to react for an additional 1–3.5 hours to reach complete conversion of the substrate into the respective phosphonic ester. In this way, the dibromide substrate is always the limiting reagent, promoting full conversion to the respective diphosphonic ester and limiting the accumulation of an undesired, partially converted product that would need to be separated during workup.

Figure 1 shows the setup for the reaction, with the solid aryl bromide in grey and the precatalyst/triisopropyl phosphite mixture in red. It is important to note here that the system is kept under a constant flow of either argon or nitrogen, mainly to avoid side reactions with components in the air (humidity, oxygen), but also to prevent the solid in the addition funnel from contacting any vapour and turning soggy before it is added to the round-bottomed flask. As can be seen in Figure 1, this is achieved by flowing the gas through the powder addition funnel via a gas inlet. This also allows for the quick removal (usually complete in less than 30 minutes) of residual triisopropyl phosphite at the end of the reaction by simply increasing the gas flow, thus preventing the equilibrium between the gas and liquid phases and allowing to bypass the further step which would have involved removing these components by vacuum distillation. Although not shown in Figure 1, the addition of a second condenser and collection flask perpendicular, as in a distillation, to the first column also allows for the collection of unreacted phosphite, and byproducts, such as isopropyl bromide. Firstly, this prevents any release of vapours of toxic compounds and facilitates appropriate disposal procedures. Secondly, it is likely that the majority of what remains in the flask at the end is simply unreacted phosphite, which would ideally need to be investigated to assess its recyclability, and lead to a process with greener attributes. In this sense, the phosphite is likely to be the last product coming over via distillation, and should be relatively pure, but further investigation would be required in order to confirm this.

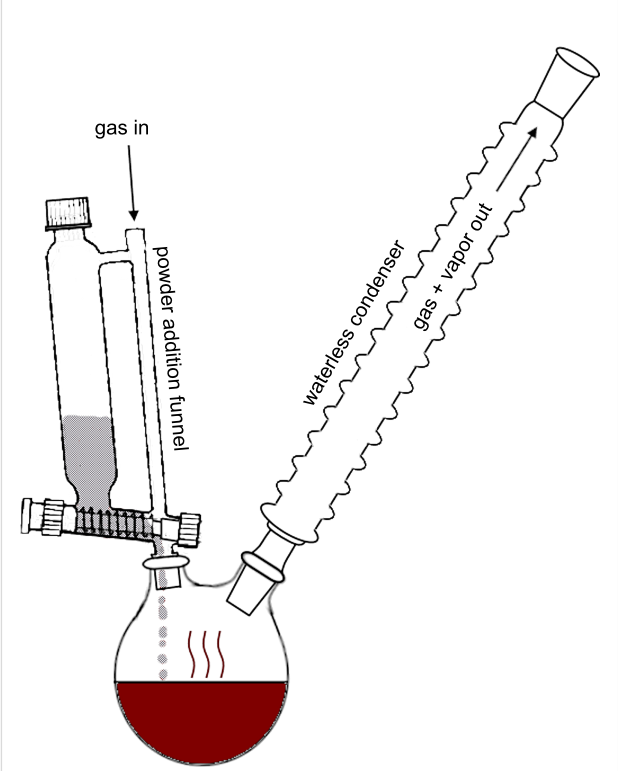


Figure 1: Experimental setup for the improved C–P cross-coupling reaction.

The choice of the phosphite is also important, partially due to the boiling point and the potential for running reactions at higher temperatures, and also the formation of an alkyl halide byproduct. It is the reactivity of this byproduct that determines which phosphite is chosen. In this case, triisopropyl phosphite has been chosen over commonly employed triethyl phosphite, since the latter results in a more reactive alkyl halide (i.e., ethyl bromide), which would react with triethyl phosphite to produce diethyl ethylphosphonate, thus consuming the triethyl phosphite in a competing reaction and introducing undesired side products that would make the workup procedure more labo-

rious. Furthermore, the boiling point of triisopropyl phosphite is 181 °C, versus 156 °C for triethyl phosphite, which allows to run the reaction at higher temperature and reduce the time.

In Table 1, we see a range of different methods based on cross-coupling reactions compared to the method proposed in this work. The first, and one of the most important comparisons, is time. The upper range for our method is in the 5.5 hour mark, whereas most of the literature routes run for at least 6.5 hours. The shorter time for method F is likely due to the fact that it involves a monobromo substrate, with no issues related with the presence of partially converted side products, which are common with polybromo substrates. The shorter time for method H is due to the much higher temperature at which the reaction can be run in a pressure-resistant closed vessel. The relatively short time, in part, can be attributed to the absence of solvent, which we cited previously as an advantage in that we are not diluting the reaction mixture and thus not slowing down the reaction. This in turn explains the high phosphite-to-bromine ratio, which in our case is higher than all the other routes, since the phosphite itself acts as the solvent as well as being a reactant. If this ratio was lower, there would be a considerable drop in the reaction rate towards the end and would likely lead to generally lower yields. This issue could be further minimized upon exploration of recycling the phosphite distillate. It is to be noted that our method, by bypassing the distillation step necessary to remove the solvent in most literature methods, in just 30 minutes on top of the time reported in Table 1 provides a reaction crude that can be then worked up to obtain the desired product. We also manage to use less catalyst than some of the other methods, except for methods F, G, and H. In keeping with the mild conditions, the temperature we use is 160 °C, which is lower than that of the other reactions. Working at 180 °C, close to the boiling point of triisopropyl phosphite, was actually detrimental to the reaction. In these conditions, under a constant stream of inert gas, the phosphite is prone to be swept away, even in the presence of a reflux condenser. Reactions carried out in such conditions afforded a very viscous crude and a low conversion of the starting material, as revealed by TLC.

Table 1: A comparison of literature phosphonate syntheses with the alternative method proposed in this work. The microwave-assisted method made use of a pressure-resistant vessel due to considerable pressure buildup (≈ 10 bar), while the other methods were run under reflux conditions.

	this work	method A [33]	method B [34]	method C [35]	method D [36]
time (h)	4–6	20	20	20	54
scale (g of precursor)	3–5	30	8	10	6.3
temperature (°C)	160	180	180	170	185
P/Br ratio	7	1.5	3	2.1	4.5
mol %/Br (NiX_2)	13% X = Cl	17% X = Br	39% X = Cl	16% X = Br	15% X = Cl
isolated yield (%)	70–90	60	89	61	80
solvent	no solvent	1,3-diisopropyl-benzene	1,3-diisopropyl-benzene	*tert*-butylbenzene	1,3-diisopropyl-benzene
procedure	addition of Br-substrate	addition of phosphite	addition of phosphite	addition of phosphite	addition of phosphite
substrate	dibromo-polyarylamines	1,3,5-tris(4-bromo-phenyl)benzene	2,4,6-tri-(4-bromo-phenyl)-s-triazine	tetra(4-bromo-phenyl)methane	4,4-dibromo-biphenyl
	this work	method E [37]	method F [38]	method G [39]	method H [40]
time (h)	4–6	29.5	6.5	3	0.75
scale (g of precursor)	3–5	19.5	4.5	23	0.543
temperature (°C)	160	180	180	180	225
P/Br ratio	7	1.6	1.5	1.5	5
mol %/Br (NiX_2)	13% X = Cl	6% X = Br	7% X = Br	8% X = Br	5% X = Cl
isolated yield (%)	70–90	78	85	80	82
solvent	no solvent	1,3-diisopropyl-benzene	mesitylene	mesitylene	no solvent
procedure	addition of Br-substrate	addition of phosphite	addition of phosphite	addition of phosphite	one-pot synthesis (microwave assisted)
substrate	dibromo-polyarylamines	1,3-dibromo-benzene	2,5-dibromo-thiophene	methyl 3-bromo-benzoate	1,3,5-tris(4-bromo-phenyl)benzene

Notably, the yield we achieve, which varies between substrates, is generally comparable to those of literature routes. With regards to method H, we note that the scale of this method, originally reported by one of us, was limited to 0.543 g (1 mmol) of substrate. Scale up of this protocol was not attempted, but it might become problematic due to issues with microwave penetration in a medium that contains a strong absorber, such as the Ni catalytic complex. In this work, we have employed either 5.0 g (15.3 mmol), 4.0 g (12.2 mmol) or 3.0 g (7.4 mmol) of substrate.

Once the phosphonate esters had been successfully obtained and characterized by ^{1}H, ^{31}P, ^{13}C NMR and mass spectrometry (see experimental section and Supporting Information File 1), they were then subjected to silylation and subsequent hydrolysis using the method put forward by McKenna et al. (1977), which involves the use of trimethylbromosilane (TMSiBr) in a transesterification of the dialkyl phosphonate to bis(trimethylsilyl) phosphonate, followed by treatment in water or short-chain alcohols to obtain a phosphonic acid, as shown in Supporting Information File 1, Scheme S3 [41,42]. Prior to using this method, the standard hydrolysis under prolonged reflux in 6 M HCl was attempted, though these conditions proved too harsh, and often led to cleavage of the C–P bond. Thus, this popular method was abandoned in favor of using the less harsh method employing TMSiBr, which most often led to achieve overall yields above 70% for the phosphonic acid, based on the initial Br-substrate.

Conclusion

Presented in this article is the synthesis of three novel phosphonate esters and their corresponding phosphonic acids. While the phosphonic acids are indeed the target products, the progress made here is mainly focused on the improvement of the cross-coupling procedure used to obtain the phosphonate esters. Oftentimes, these reactions take up to 24 hours to reach completion, sometimes more, while here we have presented a simple yet effective change that can be made to the order of addition of reactants, which affords a reaction time that is at least five times faster than most literature methods with no considerable effect on the yield or the purity of the product. This has also completely removed the requirement of a solvent, since triisopropyl phosphite acts as the solvent. In making savings for both cost of reagents and in total reaction time, and with no detriment to the yield, it is clear that this method presents an advantage over the literature routes, both in terms of cost and efficient use of time. Referring specifically to the phosphonic acids presented in this work, we have obtained three novel and structurally related linkers for the preparation of metal phosphonates. Each of the linkers was obtained in good yield and with no considerable impurities identified during characterization. This series of linkers will allow to determine the effects of the geometry and of different substituents on the formation of metal phosphonate frameworks.

Supporting Information

Supporting Information File 1

NMR Spectra, MS spectra, and respective discussions.
[https://www.beilstein-journals.org/bjoc/content/supplementary/1860-5397-18-160-S1.pdf]

Acknowledgements

The work presented here was originally part of a Ph.D thesis chapter submitted in April 2022 by S.J.I.S.. Dr. Mariolino Carta (Swansea University) and Dr. Timothy L. Easun (Cardiff University) are acknowledged for the input provided during the viva voce examination.

We thank the National Mass Spectrometry Facility (NMSF), Swansea University Medical School, for their support in obtaining the mass spectrometry data.

Funding

M.T. acknowledges funding from the European Union's Horizon 2020 research and innovation program under the Marie Skłodowska-Curie grant agreement No 663830.

ORCID® iDs

Stephen J. I. Shearan - https://orcid.org/0000-0002-0605-016X
Marco Taddei - https://orcid.org/0000-0003-2805-6375

Preprint

A non-peer-reviewed version of this article has been previously published as a preprint: https://doi.org/10.3762/bxiv.2022.59.v1

References

1. Demadis, K. D.; Paspalaki, M.; Theodorou, J. *Ind. Eng. Chem. Res.* **2011,** *50,* 5873–5876. doi:10.1021/ie102546g
2. Galezowska, J.; Gumienna-Kontecka, E. *Coord. Chem. Rev.* **2012,** *256,* 105–124. doi:10.1016/j.ccr.2011.07.002
3. Pazianas, M.; Abrahamsen, B.; Ferrari, S.; Russell, R. G. *Ther. Clin. Risk Manage.* **2013,** *9,* 395–402. doi:10.2147/tcrm.s52291
4. Lange, R.; ter Heine, R.; Knapp, R. (FF).; de Klerk, J. M. H.; Bloemendal, H. J.; Hendrikse, N. H. *Bone* **2016,** *91,* 159–179. doi:10.1016/j.bone.2016.08.002
5. Papathanasiou, K. E.; Vassaki, M.; Spinthaki, A.; Alatzoglou, F.-E. G.; Tripodianos, E.; Turhanen, P.; Demadis, K. D. *Pure Appl. Chem.* **2019,** *91,* 421–441. doi:10.1515/pac-2018-1012
6. Turhanen, P. A.; Demadis, K. D.; Kafarski, P. *Front. Chem. (Lausanne, Switz.)* **2021,** *9,* 695128. doi:10.3389/fchem.2021.695128

7. Nowack, B.; VanBriesen, J. M. Chelating Agents in the Environment. In *Biogeochemistry of Chelating Agents;* Nowack, B.; VanBriesen, J. M., Eds.; ACS Symp. Ser., Vol. 910; American Chemical Society: Washington, D.C., USA, 2005; pp 1–18. doi:10.1021/bk-2005-0910.ch001
8. Wang, Y.; Stone, A. T. *Environ. Sci. Technol.* **2008,** *42,* 4397–4403. doi:10.1021/es7032668
9. Bhosle, S. M.; Ponrathnam, S.; Tambe, S. S.; Chavan, N. N. *Bull. Mater. Sci.* **2016,** *39,* 1541–1556. doi:10.1007/s12034-016-1295-7
10. Du, T.; Chen, J.; Cao, D. *J. Mater. Sci.* **2001,** *36,* 3903–3907. doi:10.1023/a:1017909919388
11. Touir, R.; Dkhireche, N.; Ebn Touhami, M.; Sfaira, M.; Senhaji, O.; Robin, J. J.; Boutevin, B.; Cherkaoui, M. *Mater. Chem. Phys.* **2010,** *122,* 1–9. doi:10.1016/j.matchemphys.2010.02.063
12. Machado Fernandes, C.; Faro, L. V.; Pina, V. G. S. S.; de Souza, M. C. B. V.; Boechat, F. C. S.; de Souza, M. C.; Briganti, M.; Totti, F.; Ponzio, E. A. *Surf. Interfaces* **2020,** *21,* 100773. doi:10.1016/j.surfin.2020.100773
13. Habash, S.; Al-Banna, L. *J. Nematol.* **2011,** *43,* 95–100.
14. Manghi, M. C.; Masiol, M.; Calzavara, R.; Graziano, P. L.; Peruzzi, E.; Pavoni, B. *Chemosphere* **2021,** *283,* 131187. doi:10.1016/j.chemosphere.2021.131187
15. Shimizu, G. K. H.; Taylor, J. M.; Kim, S. *Science* **2013,** *341,* 354–355. doi:10.1126/science.1239872
16. Ramaswamy, P.; Wong, N. E.; Shimizu, G. K. H. *Chem. Soc. Rev.* **2014,** *43,* 5913–5932. doi:10.1039/c4cs00093e
17. Bao, S.-S.; Shimizu, G. K. H.; Zheng, L.-M. *Coord. Chem. Rev.* **2019,** *378,* 577–594. doi:10.1016/j.ccr.2017.11.029
18. Bhanja, P.; Bhaumik, A. *ChemCatChem* **2016,** *8,* 1607–1616. doi:10.1002/cctc.201501303
19. Clearfield, A.; Demadis, K., Eds. *Metal Phosphonate Chemistry: From Synthesis to Applications;* Royal Society of Chemistry: Cambridge, United Kingdom, 2011. doi:10.1039/9781849733571
20. Shearan, S. J. I.; Stock, N.; Emmerling, F.; Demel, J.; Wright, P. A.; Demadis, K. D.; Vassaki, M.; Costantino, F.; Vivani, R.; Sallard, S.; Ruiz Salcedo, I.; Cabeza, A.; Taddei, M. *Crystals* **2019,** *9,* 270. doi:10.3390/cryst9050270
21. Sevrain, C. M.; Berchel, M.; Couthon, H.; Jaffrès, P.-A. *Beilstein J. Org. Chem.* **2017,** *13,* 2186–2213. doi:10.3762/bjoc.13.219
22. Bhattacharya, A. K.; Thyagarajan, G. *Chem. Rev.* **1981,** *81,* 415–430. doi:10.1021/cr00044a004
23. Zon, J.; Garczarek, P.; BiaLek, M. Synthesis of Phosphonic Acids and Their Esters as Possible Substrates for Reticular Chemistry. *Metal Phosphonate Chemistry;* Royal Society of Chemistry: Cambridge, United Kingdom, 2011; pp 170–191. doi:10.1039/9781849733571-00170
24. Tavs, P.; Korte, F. *Tetrahedron* **1967,** *23,* 4677–4679. doi:10.1016/s0040-4020(01)92565-7
25. Tavs, P.; Weitkamp, H. *Tetrahedron* **1970,** *26,* 5529–5534. doi:10.1016/s0040-4020(01)98763-0
26. Heinicke, J.; Aluri, B. R.; Adam, M. S. S.; Jones, P. G. *Phosphorus, Sulfur Silicon Relat. Elem.* **2008,** *183,* 779–782. doi:10.1080/10426500701807905
27. Adam, M. S. S.; Kindermann, M. K.; Köckerling, M.; Heinicke, J. W. *Eur. J. Org. Chem.* **2009,** 4655–4665. doi:10.1002/ejoc.200900698
28. Beyer, O.; Homburg, T.; Albat, M.; Stock, N.; Lüning, U. *New J. Chem.* **2017,** *41,* 8870–8876. doi:10.1039/c7nj01697b
29. Hirao, T.; Masunaga, T.; Ohshiro, Y.; Agawa, T. *Tetrahedron Lett.* **1980,** *21,* 3595–3598. doi:10.1016/0040-4039(80)80245-0
30. Hirao, T.; Masunaga, T.; Ohshiro, Y.; Agawa, T. *Synthesis* **1981,** 56–57. doi:10.1055/s-1981-29335
31. Hirao, T.; Masunaga, T.; Yamada, N.; Ohshiro, Y.; Agawa, T. *Bull. Chem. Soc. Jpn.* **1982,** *55,* 909–913. doi:10.1246/bcsj.55.909
32. Balthazor, T. M.; Grabiak, R. C. *J. Org. Chem.* **1980,** *45,* 5425–5426. doi:10.1021/jo01314a059
33. Mah, R. K.; Lui, M. W.; Shimizu, G. K. H. *Inorg. Chem.* **2013,** *52,* 7311–7313. doi:10.1021/ic400274e
34. Hermer, N.; Stock, N. *Dalton Trans.* **2015,** *44,* 3720–3723. doi:10.1039/c4dt03698k
35. Zaręba, J. K.; Białek, M. J.; Janczak, J.; Zoń, J.; Dobosz, A. *Cryst. Growth Des.* **2014,** *14,* 6143–6153. doi:10.1021/cg501348g
36. Wang, Z.; Heising, J. M.; Clearfield, A. *J. Am. Chem. Soc.* **2003,** *125,* 10375–10383. doi:10.1021/ja030226c
37. Zheng, T.; Gao, Y.; Chen, L.; Liu, Z.; Diwu, J.; Chai, Z.; Albrecht-Schmitt, T. E.; Wang, S. *Dalton Trans.* **2015,** *44,* 18158–18166. doi:10.1039/c5dt02667a
38. Rueff, J.-M.; Perez, O.; Pautrat, A.; Barrier, N.; Hix, G. B.; Hernot, S.; Couthon-Gourvès, H.; Jaffrès, P.-A. *Inorg. Chem.* **2012,** *51,* 10251–10261. doi:10.1021/ic301187y
39. Rueff, J.-M.; Caignaert, V.; Chausson, S.; Leclaire, A.; Simon, C.; Perez, O.; Le Pluart, L.; Jaffrès, P.-A. *Eur. J. Inorg. Chem.* **2008,** 4117–4125. doi:10.1002/ejic.200800483
40. Taddei, M.; Costantino, F.; Vivani, R.; Sabatini, S.; Lim, S.-H.; Cohen, S. M. *Chem. Commun.* **2014,** *50,* 5737–5740. doi:10.1039/c4cc01253d
41. McKenna, C. E.; Higa, M. T.; Cheung, N. H.; McKenna, M.-C. *Tetrahedron Lett.* **1977,** *18,* 155–158. doi:10.1016/s0040-4039(01)92575-4
42. Marma, M. S.; Khawli, L. A.; Harutunian, V.; Kashemirov, B. A.; McKenna, C. E. *J. Fluorine Chem.* **2005,** *126,* 1467–1475. doi:10.1016/j.jfluchem.2005.04.002

License and Terms

This is an open access article licensed under the terms of the Beilstein-Institut Open Access License Agreement (https://www.beilstein-journals.org/bjoc/terms), which is identical to the Creative Commons Attribution 4.0 International License (https://creativecommons.org/licenses/by/4.0). The reuse of material under this license requires that the author(s), source and license are credited. Third-party material in this article could be subject to other licenses (typically indicated in the credit line), and in this case, users are required to obtain permission from the license holder to reuse the material.

The definitive version of this article is the electronic one which can be found at:
https://doi.org/10.3762/bjoc.18.160

BEILSTEIN JOURNAL OF ORGANIC CHEMISTRY

Improving the accuracy of ^{31}P NMR chemical shift calculations by use of scaling methods

William H. Hersh*[1,2] and Tsz-Yeung Chan[1,2]

Full Research Paper

Open Access

Address:
[1]Department of Chemistry and Biochemistry, Queens College, Queens, NY 11367-1597, USA and [2]Ph.D. Program in Chemistry, The Graduate Center of the City University of New York, New York, NY 10016, USA

Email:
William H. Hersh* - william.hersh@qc.cuny.edu

* Corresponding author

Keywords:
calculations; DFT; phosphorus NMR; scaling methods; stereoisomers

Beilstein J. Org. Chem. **2023,** *19,* 36–56.
https://doi.org/10.3762/bjoc.19.4

Received: 07 October 2022
Accepted: 14 December 2022
Published: 10 January 2023

This article is part of the thematic issue "Organophosphorus chemistry: from model to application".

Guest Editor: G. Keglevich

© 2023 Hersh and Chan; licensee Beilstein-Institut.
License and terms: see end of document.

Abstract

Calculation of ^{31}P NMR chemical shifts for a series of tri- and tetracoordinate phosphorus compounds using several basis sets and density functional theory (DFT) functionals gave a modest fit to experimental chemical shifts, but an excellent linear fit when plotted against the experimental values. The resultant scaling methods were then applied to a variety of "large" compounds previously selected by Latypov et al. and a set of stereoisomeric and unusual compounds selected here. No one method was best for all structural types. For compounds that contain P–P bonds and P–C multiple bonds, the Latypov et al. method using the PBE0 functional was best (mean absolute deviation/root mean square deviation (MAD/RMSD) = 6.9/8.5 ppm and 6.6/8.2 ppm, respectively), but for the full set of compounds gave higher deviations (MAD/RMSD = 8.2/12.3 ppm), and failed by over 60 ppm for a three-membered phosphorus heterocycle. Use of the M06-2X functional for both the structural optimization and NMR chemical shift calculation was best overall for the compounds without P–C multiple bonds (MAD/RMSD = 5.4/7.1 ppm), but failed by 30–49 ppm for compounds having any P–C multiple-bond character. Failures of these magnitudes have not been reported previously for these widely used functionals. These failures were then used to screen a variety of recommended functionals, leading to better overall methods for calculation of these chemical shifts: optimization with the M06-2X functional and NMR calculation with the PBE0 or ωB97x-D functionals gave values for MAD/RMSD = 6.9/8.5 ppm and 6.8/9.1 ppm, respectively, over an experimental chemical shift range of −181 to 356 ppm. Due to the unexplained failures observed, we recommend use of more than one method when looking at novel structures.

Introduction

Calculation of ^{1}H and ^{13}C NMR chemical shifts and coupling constants using density functional theory (DFT) has increasingly become an adjunct to structure determination [1-8]. In particular for complex organic compounds, determination of relative stereochemistry using such calculations is a powerful technique [9-13]. A set of recommendations for best practices

has been proposed [1-3,14] and made available online [15] describing basis set choices, geometry optimization, incorporation of solvation, and use of scaling factors derived from linear regressions between computed and experimental chemical shifts. In contrast, reports of calculation of ^{31}P NMR chemical shifts – which span a range of roughly 500 ppm – have, even recently, used empirical methods [16], and theoretical methods have focused more on the choice of basis set to better match experimental chemical shifts of relatively small molecules [17-24]. For instance, while calculations for ^{1}H NMR are considered to be sufficiently reliable using DFT methods with the 6-311+G(2d,p) basis set [15], work on ^{31}P NMR chemical shifts has favored [18,21,24] the use of larger basis sets such as the IGLO-III [25,26] and pcS-n [27,28] basis sets with a focus on improved calculation of NMR shielding constants. Some theoretical work has been carried out on specialized phosphorus compounds that cover only a small range of chemical shifts, including nucleic acids [29-32] and polyoxometalates [33]. More recently, DFT methods have been applied to transition metal phosphorus complexes that cover a wide range of chemical shifts [34,35] using methods related to what we will describe here, but such studies are beyond the scope of this paper and typically focus on one metal at a time.

In the same way that improved results are obtainable for both ^{1}H and ^{13}C NMR chemical shifts using scaling methods, calculation of ^{31}P NMR chemical shifts benefit as well from scaling. Chesnut first showed that scaling of the paramagnetic term of chemical shieldings calculated using the B3LYP functional and the 6-311+G(2d,p) basis set gave improved fits to experimental results, and further noted that while scaling is empirical, DFT methods themselves have an empirical component [36]. More recent studies have included a variety of functionals and basis sets in order to determine if there is a best combination in terms of accuracy and speed [22,23,37]. Even within the specialized studies of specific types of phosphorus compounds, scaling was found to give significant improvement [33]. A number of reports have speculated that scaling is needed to correct for rovibrational effects [21,24,36], and recent reports show that molecular dynamics methods can eliminate the need for empirical corrections [29,30,38]. However, these calculation-intensive methods are not likely to become routine soon, potentially leaving room for empirical scaling to be useful for some time.

The calculation-intensive and scaling approaches recently have been characterized by Jensen as the "purist" and "application" approaches [8], and the leading work on calculations of ^{31}P NMR chemical shifts reflect one of each, namely, the "purist" approach reported by Krivdin [24] and the "application" approach due to Latypov [37]. The Krivdin group reported a group of 53 phosphorus compounds, which were first optimized at the MP2/6-311G(d,p) level with IEF-PCM solvation; ^{31}P NMR chemical shifts were then calculated using the DFT KT2 functional [39] and a dual pcS-3/pcS-2 basis set [27,28]. In this case the use of the locally dense basis set approach, in which the larger pcS-3 basis set was used on phosphorus and the smaller pcS-2 basis set was then used on all the other atoms, allowed the computation of chemical shifts for a variety of benchmark compounds up to 35-atom triphenylphosphine oxide. Comparison of the calculated chemical shifts with the experimental values gave a mean absolute deviation and root mean square deviation (MAD/RMSD) [3,40] of 9.4/12.0 ppm over a roughly 550 ppm range. The Latypov group reported a training set of 22 phosphorus compounds, which were first optimized at a significantly lower but more easily implemented level of theory (PBE0 functional [41], 6-31+G(d) basis set, gas phase), followed by calculation of the ^{31}P NMR chemical shifts with the same PBE0 functional with the still-modest 6-311G(2d,2p) basis set. While the calculated fit to experimental values was significantly worse than the higher-level Krivdin method (MAD/RMSD = 18.7/21.9 ppm), the linear fit of the *calculated* chemical shifts of the 22 training set compounds to their *experimental* values gave a scaled set of corrected calculated values with a much-improved MAD/RMSD = 9.3/10.9 ppm over a roughly 500 ppm range. That is, scaling of the theoretical results to experimental values gave values with deviations comparable to the unscaled results obtained at much higher levels of theory. In addition, the Latypov results provide a prescription that could be applied readily to larger and more interesting novel compounds. A collection of 10 such compounds actually gave a somewhat better scaled MAD/RMSD of 6.9/9.0 ppm, using the scaling factors derived from the benchmark set of 22 compounds.

In addition to the above review of ^{31}P chemical shift calculations, a recent review by Krivdin covered an additional range of factors for higher-level calculations, scaling, and a variety of specialized compounds [42]. In this paper we describe work that had been in progress when the Latypov group's report was published. It is similar in style, in that we describe the use of significantly lower levels of DFT calculations than the Krivdin group, but the motivation was to develop a high-accuracy method that would allow identification of both unusual phosphorus compounds and of stereochemistry, and still be accessible to organic chemists without specialized software. In addition, we were concerned by some of the choices made by the Latypov group for their training set of compounds, and so sought to use a much simpler set of phosphorus compounds for scaling purposes. We report here (1) a comparison of basis sets for calculation of a range of ^{31}P NMR chemical shifts of well-known tri- and tetracoordinate phosphorus compounds, (2) de-

velopment of scaling factors for calculation of ^{31}P NMR chemical shifts, and (3) application of this method to determination of stereochemistry at phosphorus in heterocycles and to corroboration of some unusual compounds that have been reported previously. At that point we were left with two or possibly three structural types for which some of these methods failed to provide accurate chemical shifts, and so we report here (4) a search of 23 more recent combinations of DFT functionals that have been recommended for theoretical reasons, expedited by focusing on these failures.

Results and Discussion

1. Experimental chemical shifts. A number of compilations of ^{31}P NMR chemical shifts were published early in the development of NMR [43-45], followed by book-length compilations [46-48]. These chemical shifts were referenced to external 85% H_3PO_4 at 0 ppm (with positive values reported here downfield of H_3PO_4). The early work of necessity included mostly pure liquid samples, that is, without any deuterated solvents, and one of the compilations noted that chemical shift changes upon dilution with CS_2, CCl_4, $CHCl_3$, and ethanol were all small (<2 ppm) [43]. As much as possible, we have tried to use chemical shifts in $CDCl_3$ solution, and for the cases where we have literature data or have measured the chemical shifts ourselves, have found the solution values are very close to the reported liquid values (liquid/$CDCl_3$ in ppm: PCl_3 220 [44]/219.79; $P(OMe)_3$ 141 [44]/141.41; $(iPrO)_2P(O)CH_3$ 27.4 [49]/28.61; $(iPrO)_2P(O)H$ 4.2 [43]/4.54; PMe_3 −62 [44]/−61.58 [50]). We have also included chemical shifts in more polar solvents (i.e., DMSO and methanol) when those were the only reported values.

The chemical shifts of two commonly used reference standards for ^{31}P NMR calculations require comment, since a reference is needed to convert the calculated absolute magnetic shielding (σ) to the chemical shift (δ). The calculated chemical shift $\delta(^{31}P)_{calcd}$ is given by the difference between the absolute magnetic shielding values of the reference and the desired phosphorus compound calculated at the same level of theory, plus the experimental chemical shift of the reference compound (Equation 1) [18,21,26].

$$\delta\left(^{31}\mathrm{P}\right)_{\mathrm{calcd}} = \sigma\left(\mathrm{reference}\right)_{\mathrm{calcd}} - \sigma\left(^{31}\mathrm{P}\right)_{\mathrm{calcd}} + \delta\left(\mathrm{reference}\right)_{\mathrm{exp}} \quad (1)$$

Since the 85% H_3PO_4 reference standard is a roughly 1:1 molar solution of phosphoric acid in water [51], calculation of its absolute magnetic shielding might be expected to be complicated by water solvation, as well as ionization or aggregation of the phosphoric acid in water, and calculation as a gas-phase chemical shift is also unreasonable [51]. Because of these issues, other studies have used PH_3 as an alternative theoretical reference standard [18,19], despite the fact that actual use of this compound requires a fairly extraordinary experimental setup [52,53]. An additional issue with PH_3 involves the choice of using the gas-phase or liquid-phase experimental chemical shifts, which differ dramatically: the universally used value for the gas-phase chemical shift is −266.1 ppm (referenced to external 85% H_3PO_4) [54], while the liquid-phase chemical shift is −238 ppm at −90 °C [44] and is also −238 ppm at 23 °C in CCl_4 [52]. In the two ^{31}P NMR studies described in the Introduction, Latypov used the gas-phase value [37] and Krivdin the liquid-phase value [24]. As noted above, the $CDCl_3$ solution values are close to the liquid values, and so we will use the −238 ppm chemical shift for PH_3, and would argue this value is the correct one for comparisons to other solution spectra. We would further argue that the simplest solution to the reference problem when scaling is used would be the calculation of all chemical shifts referenced to H_3PO_4 with water solvation since this provides values that can be compared immediately to experimental chemical shifts; further, as will be explained below, scaling eliminates the need for the calculated absolute shielding of the reference.

2. Calculation of chemical shifts. A small number of trivalent phosphorus compounds spanning a roughly 460 ppm chemical shift range was chosen initially to examine basis set effects, namely, PH_3, $PMeH_2$, PMe_2H, PMe_3, PPh_3, $P(OMe)_3$, methoxyphospholane (i.e., $MeOP(OCH_2CH_2O)$), and PCl_3, each of which has been used in recent reports of phosphorus chemical shift calculations [18,20,21,24,37] except for the phospholane, and more surprisingly with one exception [24], PPh_3 (Figure 1; see Computational and NMR Details section). For each of these, optimization (Gaussian 09 [55], DFT with 6-31+G(d,p) basis set) included solvation using the default polarizable continuum model (IEF-PCM using $CHCl_3$), and except for trimethylphosphite resulted in one energy minimum. We found three local minima for trimethylphosphite, so NMR spectra were calculated for each and the energy-weighted average was used for the calculated chemical shift; methoxyphospholane was added as an alternative to trimethylphosphite simply because it seemed likely that it would exhibit only one local minimum, and so could provide a check on the calculated chemical shift. The choice of basis set for the optimizations was guided by recommendations by Tantillo and co-workers [3] for cases involving multiple conformations, and in addition here the presence of lone pairs on third-row atoms provides additional reason to use a higher level basis set than the usual 6-31G(d) [3]. As pointed out by van Wüllen [18], the energy-optimized structure for PCl_3 is not a good fit to the experimental geome-

try [56], and the chemical shift changes significantly with geometry. Chemical shift values for both the optimized structure and the experimental geometry were therefore calculated, and the latter was much closer to the experimental chemical shift. For each compound, GIAO calculation of the chemical shift was carried out first using the widely used 6-311+G(2d,p) basis set with the B3LYP and PBE0 functionals, both used for ^{1}H NMR calculations [3,15]. One lower-level basis set was used (6-311G(d,p)) [21], as well as two higher-level basis sets used by others [18,21,24] (IGLO-III [25,26] and pcS-2 [27,28]) specifically optimized for ^{31}P, each with the B3LYP functional. Another widely used functional, M06-2X [57,58], was also used for the optimization (again using the 6-31+G(d,p) basis set) with the NMR chemical shifts calculated using both the B3LYP and M06-2X functionals with the 6-311+G(2d,p) basis set and IEF-PCM ($CHCl_3$) solvation. Last, two versions of the Latypov method were calculated. In one, the structures were both optimized (PBE0/6-31+G(d,p), IEF-PCM using $CHCl_3$) and the NMR calculated (PBE0/6-311+G(2d,p), IEF-PCM using $CHCl_3$) in the same manner as the calculation methods described above. In the other, the same method as used by Latypov (PBE0 gas phase 6-31+G(d) optimization followed by PBE0 gas phase 6-311G(2d,2p) NMR) was carried out in order to allow a direct comparison [37]. Results may be found in Tables S1–S3 in Supporting Information File 1 for both the absolute chemical shifts and the chemical shifts referenced to that calculated for 85% H_3PO_4 at 0 ppm according to Equation 1. As described above, the same functionals and basis sets were used for H_3PO_4 but with water solvation, except when using the gas-phase Latypov method.

As expected, on the basis of the results reported by Krivdin and Latypov, the agreement between experimental and calculated chemical shifts, regardless of the basis set, for these simple compounds is poor. The MAD/RMSD values averaged 21/25 ppm and were remarkably similar for the nine combinations of DFT functionals, optimizations, and basis sets chosen. This was true both for the two larger basis sets optimized for phosphorus (IGLO-III and pcS-2) and the smaller basis set (due to the absence of diffuse orbitals) that gave significantly shortened computational times (6-311G(d,p)) [21].

A second set of tetracoordinate phosphorus compounds was then added to the trivalent set for scaling (Figure 1). In contrast to common trivalent phosphorus compounds, the chemical shifts of typical tetracoordinate analogues do not span such a large range, nor have calculations been routinely reported. A set of 13 compounds (with 14 different phosphorus atoms) was chosen, including PY_4^+ (Y = H, Me, Ph, OMe, OPh), $Y_3P{=}O$ (Y = Me, Ph), $O{=}P(OCH_2)_3P{=}O$, $Y_2P(O)H$ (Y = MeO, iOPr), $Y_2P(O)Me$ (Y = MeO, iOPr), and $EtOP(O)Me_2$. Despite spanning a chemical shift range of only about 150 ppm, this set exhibited a wider range of structural types than the trivalent compounds. A number of the compounds required inclusion of

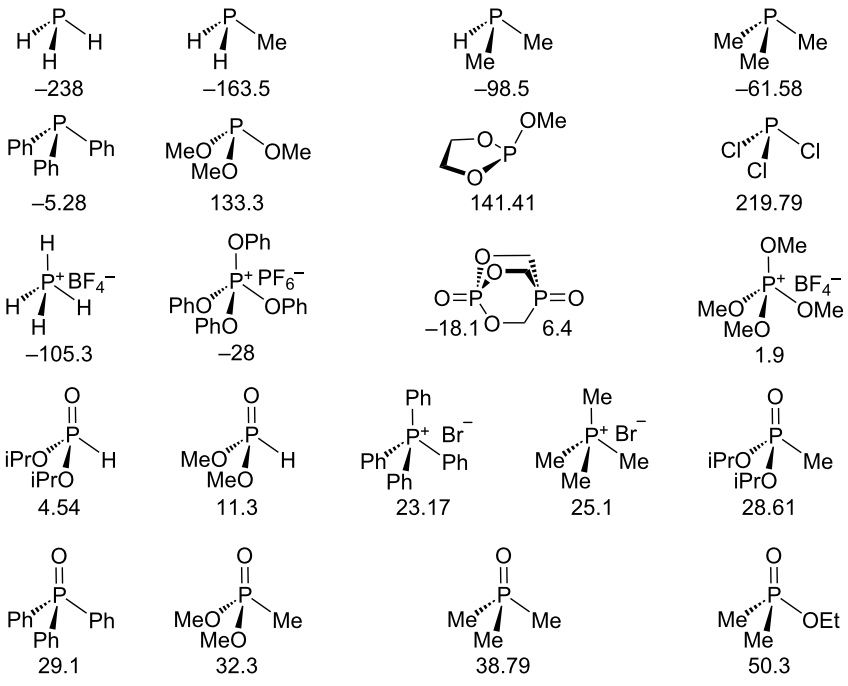


Figure 1: Training set of tri- and tetracoordinate phosphorus compounds; chemical shifts are in ppm, referenced to external 85% H_3PO_4 at 0 ppm (positive values downfield of H_3PO_4).

several conformational isomers, and for the cationic compounds, the counterions were included, and the experimental chemical shifts included compounds as pure liquids and as $CDCl_3$, CH_2Cl_2, CH_3CN, DMSO, and CH_3OH solutions (see Computational and NMR Details section). Minimizations and NMR chemical shift calculations were carried out as before, albeit all with $CHCl_3$ solvation, and once again as expected, the average MAD/RMSD values of 9/12 ppm were high (albeit lower than the trivalent compounds) and together the MAD/RMSD values averaged 13.5/18.1 ppm.

3. Scaling of chemical shifts. Each of the sets of calculated chemical shifts was next plotted against the experimental chemical shifts according to Equation 2 to give an empirical scaling relationship [36] with a unique slope and intercept for both the training set compounds and the calculation methods used (Table S4 in Supporting Information File 1).

$$\delta\left(^{31}\mathrm{P}\right)_{\text{experimental}} = m\left[\delta\left(^{31}\mathrm{P}\right)_{\text{calcd}}\right] + b \qquad (2)$$

This resulted in extraordinarily linear fits for the trivalent phosphorus compounds spanning the full chemical shift range, and a bit more scatter of the tetracoordinate compounds over their smaller range. The slope and intercept were then used to convert the DFT-calculated values to the empirically more accurate scaled values according to Equation 3, allowing the scaled MAD/RMSD values to be determined (Table 1 and Table S5 (Supporting Information File 1), and Figure 2).

$$\delta\left(^{31}\mathrm{P}\right)_{\text{scaled}} = m\left[\delta\left(^{31}\mathrm{P}\right)_{\text{calcd}}\right] + b \qquad (3)$$

The average MAD/RMSD values dropped from 13.5/18.1 ppm to an average of 6.0/7.4 ppm for most of the optimization/NMR combinations; the B3LYP method using a smaller basis set and the Latypov method using the phosphorus compounds described above both exhibited higher deviations. The higher deviations for the Latypov method (7.8/9.7 ppm), using gas-phase calculations and smaller basis sets with this set of phosphorus compounds, compared to our method (5.9/7.1 ppm) with $CHCl_3$ solvation and the larger basis sets, is notable. The greater scatter is clearly visible by comparing the scaling plot for the Latypov method in Figure 2b to the best fit method using the M06-2X functional for both optimization and the NMR calculation (Figure 2a, MAD/RMSD = 4.1/5.7 ppm). For both scaling plots, the fit shown occurs using the experimental rather than the calculated geometry for PCl_3, consistent with van Wüllen's observation [18] noted above. Also consistent with our observation on the use of the liquid chemical shift value for PH_3, the fit for both scaling plots shown occurs with the liquid rather than the gas chemical shift. That is, as seen in Figure 2a, the values for the liquid PH_3 and the experimental geometry for PCl_3 are both clearly in line with the other chemical shifts, and while the fit is not quite as good in Figure 2b, it is close. Use of the −266.1 ppm gas-phase value for PH_3 (as was done by Latypov [37]) for Figure 2b does not shift the scaling line significantly (giving a calculated scaled shift of −240.5 ppm) and a worse fit (MAD/RMSD = 8.5/11.6 ppm vs the 7.8/9.7 ppm shown for the −238 ppm liquid-phase value shown).

Since the absolute shielding of the reference (here $\sigma(H_3PO_4)_{calcd}$) is a constant, one can equally well create a scaling equation using just the experimental vs the calculated absolute shieldings by rearrangement of Equation 1 and Equa-

Table 1: MAD[a] and RMSD[a] (ppm) for scaled ^{31}P NMR chemical shifts.[b]

Optimization functional[c]	NMR functional[c]	NMR basis set[c]	MAD/RMSD all data[d]
B3LYP	B3LYP	6-311G(d,p)	8.9/10.6
B3LYP	B3LYP	6-311+G(2d,p)	7.0/8.4
M06-2X	B3LYP	6-311+G(2d,p)	6.5/8.0
M06-2X	M06-2X	6-311+G(2d,p)	**4.1/5.7**
B3LYP	B3LYP	IGLO-III	6.0/7.1
B3LYP	B3LYP	pcS-2	6.5/8.0
B3LYP	PBE0	6-311+G(2d,p)	6.2/7.6
PBE0	PBE0	6-311+G(2d,p)	5.9/7.1
PBE0[e]	PBE0[e]	6-311G(2d,2p)[e]	7.8/9.7

[a]MAD/RMSD: mean absolute deviation (MAD = $\Sigma_n|\delta_{calc} - \delta_{exp}|/n$) and root mean square deviation (RMSD = $[\Sigma_n(\delta_{calc} - \delta_{exp})^2/n]^{1/2}$) [3,40]. [b]In all tables, notable results (i.e., best and among the worst) are in bold, and the very best in bold italics. [c]Optimization basis set/solvent and NMR solvent, except as noted: 6-31+G(d,p)/$CHCl_3$. [d]Deviations calculated for the training set of tri- and tetracoordinate phosphorus compounds (Supporting Information File 1, Table S5, 22 points). [e]Optimization (6-31+G(d)/gas phase) and NMR (gas phase) for the same training set of tri- and tetracoordinate phosphorus compounds, but following Latypov's method [37].

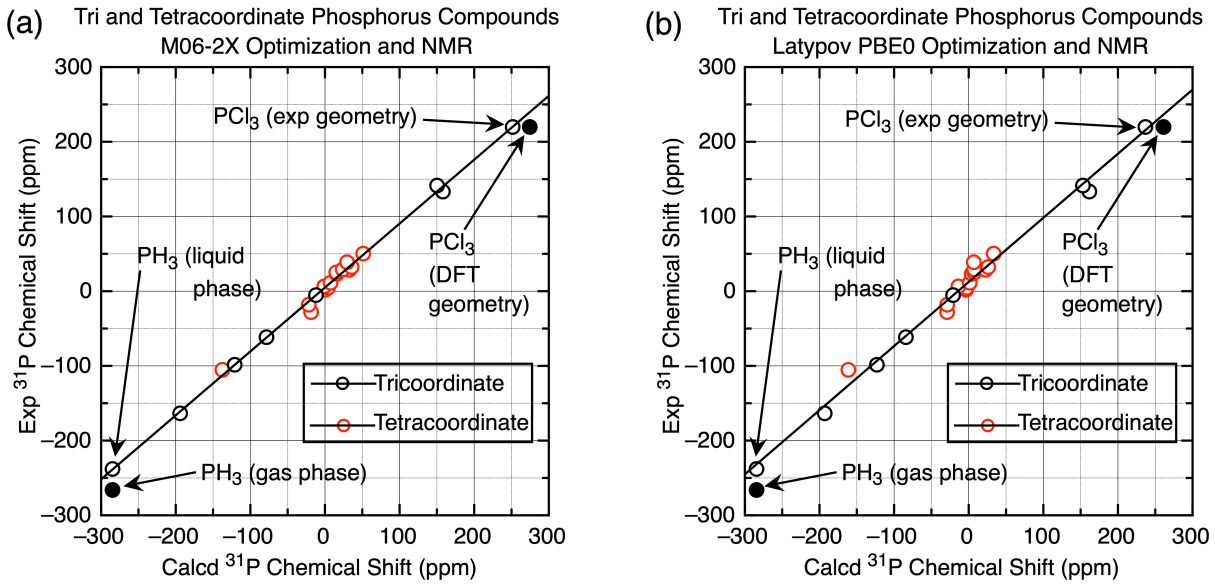


Figure 2: (a) Plot of experimental vs calculated chemical shifts of tri- and tetracoordinate phosphorus compounds (M06-2X optimization and NMR (6-311+G(2d,p) basis set) referenced to H_3PO_4, IEF-PCM $CHCl_3$ solvation). Equation 2 m = 0.855 ± 0.011, b = 4.91 ± 1.27, giving scaled MAD/RMSD = 4.1/5.7 ppm (Equation 3). (b) Plot of experimental vs calculated chemical shifts of tri- and tetracoordinate phosphorus compounds (Latypov PBE0 optimization and NMR (6-311G(2d,2p) basis set) referenced to H_3PO_4, gas phase). Equtation 2: m = 0.858 ± 0.019, b = 12.36 ± 2.19, giving MAD/RMSD = 7.8/9.7 ppm. For both (a) and (b), see Table S3 in Supporting Information File 1; the points for PCl_3 (DFT calculated geometry) and PH_3 (gas phase) were not included in the linear fits.

tion 2 to give Equation 4, where the intercept b_1 in Equation 4 simply incorporates the calculated shielding and chemical shift of the reference as shown.

$$\delta\left(^{31}\mathrm{P}\right)_{\mathrm{exp}} = -m\left[\sigma\left(^{31}\mathrm{P}\right)_{\mathrm{calcd}}\right] + b_1 \qquad \left(b_1 = m\left[\sigma\left(\mathrm{H_3PO_4}\right)_{\mathrm{calcd}} + \delta\left(\mathrm{H_3PO_4}\right)_{\mathrm{exp}}\right] + b\right) \tag{4}$$

Calculation of the absolute shielding of the reference is therefore irrelevant if one is using a scaling method, and Equation 4 gives the identical scaled chemical shifts without the need to calculate the reference shielding. In the study reported by Latypov [37], gas-phase values for the H_3PO_4 calculation were used for this purpose, so only the scaled chemical shifts would be expected to be valid. In the study reported by Krivdin [24], a partially experimental absolute shielding for 85% H_3PO_4 in water was used (σ(85% H_3PO_4) = 351.6 ppm), derived from the experimental chemical shift of PH_3 referenced to 85% H_3PO_4 [53]. The use of this value has the virtue of eliminating all theoretical complications of conformations and hydrogen bonding in phosphoric acid [51], since it is not based on a DFT-optimized structure. However, the goal of Krivdin's work was the direct calculation of chemical shifts without scaling, so that a plot of experimental vs calculated chemical shifts as in Figure 2 would give a slope of 1 and (for the H_3PO_4 reference) an intercept of 0; actual values were 0.977(16) and 1.2(1.7) [24]. Nevertheless, for the present work we will use Equations 1–3 as they are intuitively straightforward and provide an approximate check via the unscaled chemical shifts, and will expect to derive a scaling relationship since the level of calculation is considerably lower than that of Krivdin's work.

4. Calculated ^{31}P NMR chemical shifts for the Latypov test compounds. The next step, then, requires application to a variety of compounds not yet included in the training set. One such set is the set of tri- and tetracoordinate phosphorus compounds that we have already calculated chemical shifts for using the Latypov method, so if our training set is comparable to the Latypov training set, then we should obtain a similar scaling equation and similar MAD/RMSD values. In fact we do not, even though both training sets cover a similar chemical shift range with a similar number of data points. The slope of the Latypov scaling equation is 0.925, which is significantly higher than the slopes for all of the scaling equations using the tri- and tetracoordinate phosphorus compounds (i.e. that for the Latypov PBE0/PBE0 method using our training set gave a slope of 0.858, Figure 2b). The Latypov scaling equation gave a MAD/RMSD = 9.3/12.3 ppm for the tri- and tetracoordinate phosphorus compounds, so the question arose as to why the two training sets would be so different.

As described above, one difference is the choice of the PH_3 chemical shift for the training set; by using the lower gas-phase

value, the slope of the scaling equation will increase, as seen from 0.858 to 0.925, and the effect is amplified since this is the lowest chemical shift as seen in Figure 2. However, there are also other discrepancies. For instance, two of the highest field experimental chemical shifts are listed in the Latypov report [37] as −162.6 ppm for $(H_2P)_2PH$ and −203.6 ppm for $(H_2P)_2$ [59]. Problems include (a) the Latypov group did not specify whether the PH or PH_2 moiety is the one exhibiting the peak at −162.6 ppm in $(H_2P)_2PH$, (b) there is no reason both moieties should not be included, (c) the chemical shift values were determined using a complex INDOR spectrum of a mixture of compounds, exhibiting 47 lines, and so certainly subject to interpretation (and uncertainty), and (d) both $(H_2P)_2PH$ and $(H_2P)_2$ exhibited multiple conformations in our hands that especially for $(H_2P)_2PH$ affected the calculated chemical shifts, and (e) while we did not check all chemical shifts, the citation in reference [37] for CH_2=C(H)PF_2, the furthest downfield point (and hence a critical value) is wrong, although the value of 219.5 ppm is correct [60]. While these uncertainties in both the experimental and calculated chemical shifts suggest this training set may be unreliable, as seen in Figure 3 where we have plotted the Latypov data and our limited changes, these data points almost exactly cancel out in their effect on the best-fit scaling line. The MAD/RMSD of 9.5/12.4 ppm for our tri- and tetracoordinate phosphorus compounds was virtually the same as that using the original training set data reported by the Latypov group – that is, both gave an equally poor fit to the simplest phosphorus compounds.

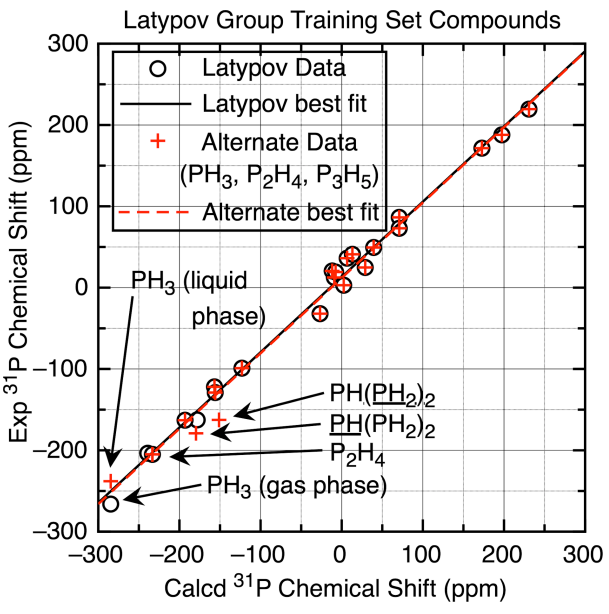


Figure 3: Plot of experimental vs calculated chemical shifts of training set compounds reported by Latypov et al. [37] (open circles, PBE0/6-31+G(d) gas-phase optimization, PBE0/6-311G(2d,2p) gas phase NMR referenced to gas phase H_3PO_4), and the best fit line to give scaling Equation 2 m = 0.925 ± 0.017, b = 13.2 ± 2.5, MAD/RMSD = 9.1/10.9 ppm. Alternate data includes PH_3, $(H_2P)_2$ (virtually unchanged), and both P atoms in $(H_2P)_2PH$ instead (red + symbols) and best fit line to give scaling Equation 2 m = 0.926 ± 0.021, b = 11.9 ± 3.1, MAD/RMSD = 10.7/13.7 ppm.

The next step requires use of the scaling equations to calculate chemical shifts for a set of 10 "large" compounds chosen by Latypov (Figure 4; there are a number of errors in the drawings and references in the Latypov paper so they are all redrawn and referenced here) [37]. Compound **1** chosen by Latypov had many different minima upon optimization in our hands, in some cases giving widely divergent chemical shifts for the two chemically equivalent phosphorus atoms, which could potentially exacerbate any deviations from the experimental chemical shifts. Since derivatives with methyl (**1a**) and butyl substitution on P_A were reported and had comparable chemical shifts [61], we substituted compound **1a** for **1**. Going forward, we used the optimization and NMR functional combinations from Table 1 that gave the lower set of MAD/RMSD values with some

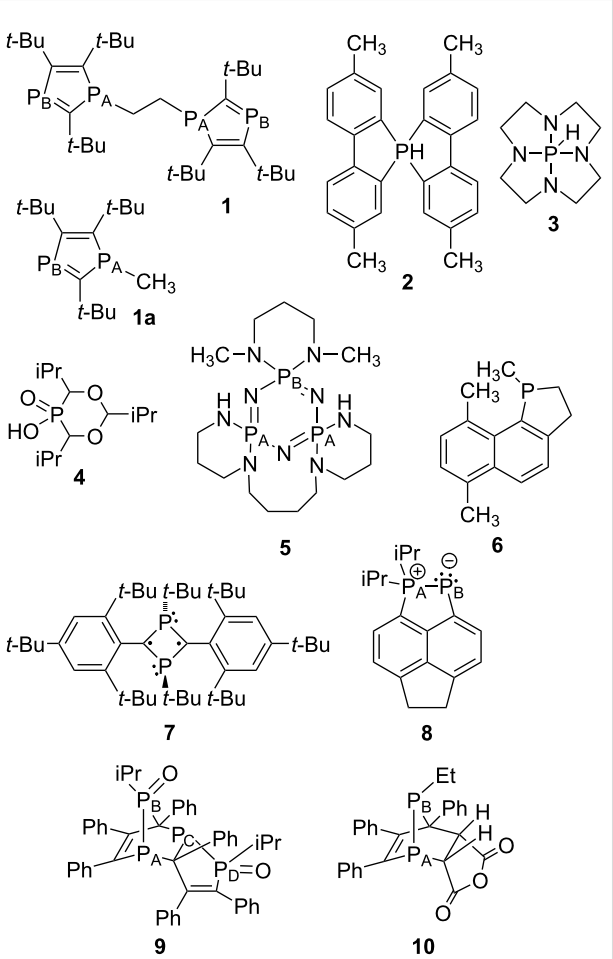


Figure 4: "Large" compounds selected for ^{31}P NMR calculation by Latypov [37].

exceptions. First, the large IGLO-III and pcS-2 basis sets failed to overcome any deficiencies in the functional used, at least for the B3LYP case, and due to the significantly higher calculation time, these basis sets were not evaluated with other functionals. Since the IGLO-III basis set was better than the pcS-2 basis set, we kept this into the next round. In order to minimize the number of different optimization calculations, we dropped the PBE0 optimization with $CHCl_3$ solvation and just included the Latypov gas-phase method, scaled both to our tri- and tetracoordinate phosphorus compound training set and to the original Latypov training set.

On the basis of the MAD/RMSD criterion (Table 2), the Latypov method using the Latypov training set is superior for

Table 2: Experimental[a] and scaled[b] ^{31}P NMR chemical shifts[c] for Figure 4 compounds.

Optimization functional:		B3LYP	B3LYP	M06-2X	M06-2X	PBE0	PBE0
NMR functional:		B3LYP	B3LYP	B3LYP	M06-2X	PBE0[d]	PBE0[d,e]
Basis set for NMR:		6-311+G(2d,p)	IGLO-III	6-311+G(2d,p)	6-311+G(2d,p)	6-311G(2d,2p)	6-311G(2d,2p)
Compound	Exp.[f]						
1a P(A)	39.6 [61]	46.8	45.2	48.4	56.1	37.2	40.3
1a P(B)	297.6	286.3	280.0	288.1	**338.9**	279.1	303.0
2	−110 [62]	−109.1	−103.4	−108.8	−106.2	−98.6	−107.2
3	−54.5 [63]	−50.7	−47.8	−50.1	−47.1	−46.5	−50.5
4	24 [37]	23.8	25.4	22.4	26.1	31.7	34.3
5 P(A)	18.3 [64]	10.2	11.4	13.0	20.3	17.3	18.8
5 P(B)	27.6	17.9	19.2	22.2	28.2	25.2	27.4
6	−10.2 [65]	3.0	4.5	0.1	−5.7	−7.5	−8.1
7	38.7 [66]	45.0	42.7	39.3	44.8	43.9	47.7
8 P(A)	76.7 [67]	74.9	77.7	74.9	75.3	67.2	72.9
8 P(B)	−157.7	**−110.6**	**−112.4**	−121.8	**−115.5**	−135.6	−147.3
9 P(A)	−29.7 [68]	−4.8	−3.9	−19.6	−24.4	−23.6	−25.7
9 P(B)	100.5	90.7	91.7	85.5	94.5	84.5	91.7
9 P(C)	−10.6	15.4	14.5	15.1	13.4	6.3	6.7
9 P(D)	75.7	64.3	66.1	65.4	72.5	62.7	68.1
10 P(A)	−22.6 [69]	1.0	2.6	−5.9	−9.8	−19.0	−20.6
10 P(B)	84.1	105.8	104.5	93.3	99.1	76.1	82.6
MAD[g]		13.3	13.7	10.1	11.4	**9.1**	***5.3***
RMSD[g]		17.7	17.7	13.5	17.0	**11.0**	***7.0***
9, **10** (P–P)[h]							
MAD		19.6	19.2	14.5	11.1	10.6	6.9
RMSD		20.6	20.5	15.6	13.2	11.7	8.7
1a, **8** (P=C))[i]							
MAD		16.8	17.3	14.0	**25.3**	13.1	***5.1***
RMSD		24.5	24.4	19.1	**30.7**	15.2	***6.2***
2–**7**, **9**, **10**[j]							
MAD		12.3	12.6	**8.9**	**7.1**	**7.8**	***5.4***
RMSD		15.0	15.1	**11.2**	**9.5**	**9.3**	***7.2***

[a]Experimental chemical shifts referenced to external 85% H_3PO_4 at 0.00 ppm, positive values downfield. [b]NMR calculations were carried out using GIAO with IEF-PCM solvation on optimized structures (DFT/6-31G+(d,p)/IEF-PCM) except as noted for the last two columns; the IGLO-III basis set was taken from the Basis Set Exchange [70], and all other basis sets were taken from Gaussian. Except as noted for the final column, all calculations scaled using the tri- and tetracoordinate training set. [c]Chemical shifts calculated from the absolute isotropic chemical shieldings according to Equation 1 (Tables S6–S8 in Supporting Information File 1), where H_3PO_4 was optimized and its NMR was calculated using the same basis sets and functionals, and except for the final two columns, IEF-PCM using water, and scaled using parameters in S4 (Equation 2) giving scaled shifts (Supporting Information File 1, Table S9, Equation 3). [d]Optimized (PBE0/6-31+G(d)/gas phase), NMR (PBE0/6-311G(2d,2p)/gas phase), and H_3PO_4 reference (gas phase) following Latypov [37]. [e]Scaled using the Latypov training set, and values for **2**–**10** taken from Latypov [37]. [f]Compounds **1a**–**4** were measured and calculated in benzene, and **5**–**10** in chloroform. [g]See note a in Table 1. [h]MAD/RMSD (ppm) for compounds that contain a P–P bond with no P–C multiple bonding. [i]MAD/RMSD for compounds with P–C multiple bonding. [j]MAD/RMSD (ppm) for compounds that contain no P–C multiple bonding.

this collection of compounds; the substitution of **1a** – which still exhibited two conformations – for **1** actually gave better results for the Latypov method than for the others, and gave a much better fit than had **1**. Inspection of the deviations showed that (1) use of the large IGLO-III basis set did not provide any advantage, and (2) the B3LYP and M06-2X methods using the M06-2X optimization were mostly comparable to the Latypov PBE0 method when scaled to our collection of compounds (i.e., MAD ranging from 9.1–11.4 ppm), but not to the Latypov training set. These B3LYP and M06-2X methods initially appeared to fare worst for compounds having P–P bonds (i.e., **8–10**), while the M06-2X NMR calculation for compound **1a** gave a large downfield chemical shift deviation for the phosphorus atom with a multiple bond to carbon. However, the largest deviation for the P–P-bonded compounds was that of P_B in **8** of up to roughly 40 ppm. An alternative hypothesis for this deviation might be that it could be due to multiple P–C bond character rather than the P–P bond itself, due to π overlap of dicoordinate P_B with the naphthalene ring. The MAD/RMSD values for the limited number of data points for compounds **9** and **10** support this in that the MAD values for the M06-2X and PBE0 NMR calculations (using the tri- and tetracoordinate phosphorus scaling equation) were similar (10.6–11.1 ppm). However, the MAD value for the M06-2X NMR calculation for P_B in **1a** and P_B in **8**, that is the atoms that we propose have multiple P–C bonding, were double (25.3 ppm) the P–P MAD value.

At least part of the cause for the P–P chemical shift deviations might be that the Latypov method gives better agreement of the P–P bond lengths with those observed by X-ray, but simply using the X-ray structure geometries with the other functionals (or even with the PBE0 functional) does not give better agreement of the calculated to the experimental chemical shifts. That is, the P–P bond length in compound **8** is 2.147(6) Å by X-ray [67] and is 2.143 Å using the Latypov PBE0/6-31+G(d)/gas-phase optimization method. This optimized geometry gave a scaled NMR (PBE0/6-311G(2d,2p)/gas phase) of −147.3 ppm compared to the experimental chemical shift of −157.7 ppm. The P–P bond length was 2.175 Å and 2.156 Å using the B3LYP and M06-2X optimizations, respectively, giving scaled chemical shifts of −115 to −120 ppm for the former and −116 and −128 ppm for the latter optimization. Calculation of the scaled chemical shifts using the X-ray geometry gave −133.5 and −121.8 ppm for the B3LYP and M06-2X functionals, so clearly the more accurate M06-2X bond length did not give better agreement with the experimental chemical shift. A similar bond length comparison was seen for compounds **9** and **10**, where the PBE0 functional gave P–P bond lengths that were closest to the X-ray geometries, but using the X-ray geometry for the B3LYP and M06-2X NMR functionals gave some improved and some far worse calculated NMR chemical shifts. Clearly the problems with both the B3LYP and M06-2X NMR calculations are with the functionals themselves, not the geometries.

In order to test if the P–C multiple bond effect was reproducible, we optimized 3,4-dimethylphosphabenzene (a training set compound chosen by Latypov, with experimental and scaled chemical shifts of 187.9 [71] and 197.4 [37] ppm) and found the scaled chemical shift was 175.1 ppm for the M06-2X (optimization) and B3LYP (6-311+G(2d,p) NMR) combination, but was 225.2 ppm when the M06-2X functional was used for both the optimization and NMR. As will be seen below, this chemical shift calculation failure was seen in all the subsequent cases we examined that have P–C multiple bonding when the M06-2X functional was used for the NMR calculation.

The results in Table 2 show that the Latypov functionals, used without any solvation and with the Latypov training set for scaling, gave the best fit for these 10 compounds (MAD/RMSD = 5.3/7.0 ppm). Use only of our different training set gave a significantly worse fit (MAD/RMSD = 9.1/11.0 ppm), showing that Jensen's point that choice of functional resembles data fitting [8] can also be applied to choice of training set. Following removal of the multiple bonded P–C chemical shifts, the Latypov scaling was still best (and essentially unchanged) but the M06-2X NMR method was closer (MAD/RMSD = 7.1/9.5 ppm) and was better than the Latypov method scaled with the alternate training set (MAD/RMSD = 7.8/9.3 ppm).

5. Calculated ^{31}P NMR chemical shifts for stereoisomers and unusual structures. We next chose our own set of phosphorus compounds (Figure 5, **11**–**29**; for simplicity compounds **30**–**34[O]** discussed later are included in the MAD/RMSD values here). This was done to to determine if the calculation and scaling would be accurate enough to distinguish stereoisomers via chemical shifts rather than coupling constants [72,73] and provide confirmation of unusual structures and chemical shifts, and with the further stipulation that multiple P–C bonding would likely give inaccurate M06-2X NMR calculations (Table 3; results with the IGLO-III basis set are included in Supporting Information File 1, Tables S6–S9, and as expected gave higher MAD/RMSD values). The M06-2X (optimization) and B3LYP (NMR) functional combination gave the best MAD/RMSD, and the relatively low RMSD is consistent with the fact that there were no glaring discrepancies in experimental and calculated chemical shifts, both for the initial group of **1a**–**10** (Table 2) and the new group of **11**–**34[O]**. As expected the M06-2X functional gave the highest values when it was used for the NMR calculation due to the presence of compounds with P–C multiple bonds. In all cases for the sets of

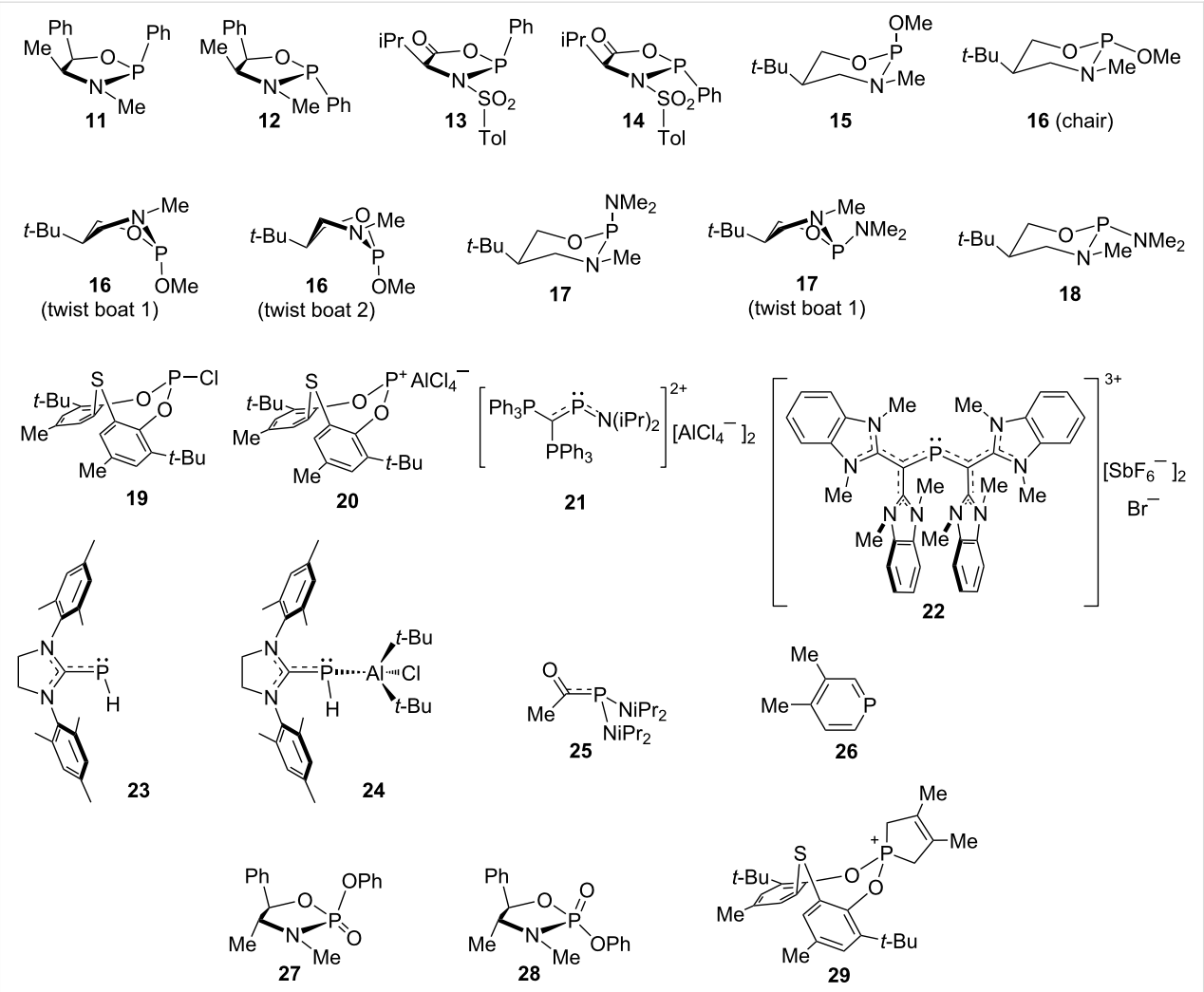


Figure 5: Stereoisomers and unusual phosphorus compounds used for chemical shift calculations.

stereoisomers (i.e., **11**/**12**, **13**/**14**, **15**/**16**, **17**/**18**, and **27**/**28**), the correct order of calculated upfield and downfield shifts was observed, although the calculated difference between the *cis* and *trans* isomers tended to be larger than the experimental difference for the trivalent compounds. Conformational differences play a role here, particularly for the six-membered rings in compounds **15**–**18**, where the twist boat conformations can be the major isomers in solution [74] (see Table 3 footnotes and Supporting Information File 1 for details), although care was taken to find all important conformations to be included in the NMR calculations.

Unusual structures such as phosphenium cation **20**, having a chemical shift upfield of the trivalent chloride **19**, contrary to expectation where the cation is typically 100 ppm downfield of the corresponding chloride [77,84-86], were confirmed by each of the calculation methods, as were the remarkably downfield shifts for the novel di- and trications **21** and **22**, for which even drawing suitable resonance structures is a challenge. Two phosphinidenes (**23**, **24**), i.e., carbene analogues with potentially anionic phosphorus atoms, have remarkably upfield chemical shifts that are once again confirmed by the calculated values. Both of the P–C bond lengths are indicative of single bond character albeit relatively short (both the X-ray [80] and DFT structures), although the large downfield deviations for the M06-2X NMR calculation suggest multiple P–C bonding – perhaps a novel use of this DFT failure.

The acylphosphonodiamidite **25** is another novel structure confirmed by the chemical shift calculation, although the largest deviation was seen for the M06-2X NMR calculation, again perhaps suggesting multiple P–C bonding. The case for multiple P–C bonding in compound **25** is supported by the amide-like CO infrared stretching frequency of 1654 cm^{-1}. This compound further warrants mention since one might suppose that the carbonyl carbon atom would be found near 170 ppm in the

Table 3: Experimental[a] and scaled[b] ^{31}P NMR chemical shifts[c] for the compounds shown in Figure 5, Figure 6, and Figure 7.

Optimization functional:		B3LYP	M06-2X	M06-2X	PBE0
NMR functional:		B3LYP	B3LYP	M06-2X	PBE0[d]
Compound	Exp.[e]				
11[f]	152.9 [75]	156.9	153.3	152.1	166.5
12[f]	139.3 [75]	142.0	138.5	139.3	150.6
13	133.0 [76]	133.8	125.4	125.0	128.8
14[f]	136.7 [76]	144.8	128.8	132.0	138.8
15[f]	132.2[74]	129.3	126.4	124.7	137.5
16[f]	138.5 [74]	142.1	137.2	134.8	150.3
17[f]	125.8 [74]	128.6	126.2	124.9	133.7
18[f]	145.3 [74]	146.7	144.5	142.3	152.8
19[g]	169 [77]	181.3	178.9	172.3	186.0
20[g]	153 [77]	147.8	146.4	148.7	169.2
21[h]	355.7 [78]	350.9	355.2	**398.1**	372.4
21 (Ph_3P)	26.2	20.7	19.2	23.8	20.9
22[i]	302 [79]	310.4	299.7	**350.9**	306.4[j]
23	–127.2 [80]	–125.7	–124.8	**–107.0**	–130.0
24	–151.0 [80]	–129.0	–131.2	**–120.6**	–140.3
25	63.5 [81]	64.7	68.7	**73.6**	63.6
26	187.9 [71]	181.7	182.1	**224.9**	197.3
27[f]	13.9 [82]	11.0	12.3	17.7	19.6
28	16.0 [82]	14.2	15.4	20.6	22.7
29[g]	93 [77]	80.8	97.1	104.6	94.1
anti-**30**	24.2 [83]	34.8	25.2	17.9	18.8
syn-**30**[f]	11.3 [83]	23.5	15.6	9.1	7.8
anti-**30[O]**	54.1 [83]	44.8	42.1	45.4	44.7
syn-**30[O]**[f]	61.8 [83]	49.7	46.3	49.3	50.1
anti-**31**	–24.4	–12.1	–29.2	–27.9	–31.2
syn-**31**	–21.8	–0.9	–21.4	–19.6	–22.2
32[f]	–181	**–59.2**	–169.3	–180.1	**–119.8**
33	–79	–78.8	–74.7	–72.1	–90.3
34	–14	–3.6	–11.2	–10.0	–20.4
33[O]	38	27.2	30.3	36.3	24.6
34[O]	26	12.6	13.7	20.8	11.0
11–**34[O]**					
MAD/RMSD[k]		11.1/23.7	***5.4/7.3***	9.7/15.8	9.8/14.4
1a–**34[O]**					
MAD/RMSD		11.9/21.8	***7.1/9.9***	10.3/16.3	8.2/12.3
2–**7**, **9**–**20**, **27**–**34[O]**[l]					
MAD/RMSD		12.0/22.8	6.4/8.5	***5.4/7.1***	8.7/13.1

[a,b,c,d]See notes a–d for Table 2; NMR basis sets and solvation were 6-311+G(2d,p) and $CHCl_3$ except for PBE0 (6-311G(2d,2p) and gas phase). [e]Compounds **11**, **12**, and **30**–**31** were optimized and the NMR spectra calculated in toluene, **13**, **14**, **19**, **20**, **25**, **26**, **29**, and **32**–**34[O]** in chloroform, **15**–**18**, **23**, **24**, **27**, and **28** in benzene, **21** in dichloromethane, and **22** in acetonitrile. [f]Major conformations shown in Figures 5–7 but compounds **11**, **12**, **14**, **16**–**18**, **27**, *syn*-**30**, *syn*-**30[O]**, and **32** exhibit multiple conformations; for **16** twist-boat 1 and twist-boat 2 are significant, and for **17** the chair and twist boat 1 are significant; for **15** only the chair was significant (Table S7, Supporting Information File 1). [g]Optimizations and NMR calculations were carried out on the compounds without the methyl groups *para* to the oxygen atoms due to problems with convergence because of methyl rotation; no significant chemical shift differences were seen. [h]BF_4^- rather than the actual $AlCl_4^-$ ions were used in the calculations to minimize the size of the calculation. [i]PF_6^- and Cl^- ions rather than the actual SbF_6^- and Br^- ions were used in the calculations to minimize the size of the calculation. [j]In the absence of solvation the trication structure could not be optimized in the presence of anions so this calculation is for the trication alone. [k]See note a in Table 1. [l]Combined MAD/RMSD for all compounds in Table 2 and Table 3 with no multiple P–C bonds.

^{13}C NMR spectrum by analogy to amides, but was instead observed at 228 ppm and confirmed by a calculated (unscaled) value of 242 ppm [81]! Such a result demonstrates the value of DFT calculations for structures not having any experimental NMR precedent.

We include here phosphabenzene **26** [71], which as noted above was used as part of the Latypov training set, for these four methods. As expected the calculations confirm the failure of only the M06-2X NMR method for compounds with multiple P–C bond character.

We finish with two challenging examples, one a relatively recent report by the Radosevich group of a novel catalytic oxygen transfer reaction involving four-membered ring phosphorus compounds [83], and one involving a 57-year old report by the Katz group of the first characterized three-membered ring phosphorus heterocycle [87]. The four-membered ring phosphetanes and proposed intermediate structures (**30**, **30[O]**, **31**, Figure 6) provide examples of novel structures [83] where stereochemistry is also confirmed by calculations, even for the challenging intermediates *anti* and *syn*-**31**. The authors of that study chose to optimize the structures using the M06-2X functional with the 6-311++G(d,p) basis set, but we found that the smaller 6-31+G(d,p) basis set that we had been using was adequate. Each of the methods allowed the stereoisomers to be distinguished, although the optimization and NMR with the B3LYP functional was much worse (MAD/RMSD = 12.9/13.4 ppm) while the M06-2X optimization and NMR was the best (MAD/RMSD = 5.9/7.0 ppm). We also note that the calculated chemical shifts reported in the phosphetane study [83] were referenced to *anti*-**30** rather than H_3PO_4, while here all the values were calculated with reference to H_3PO_4, before being scaled.

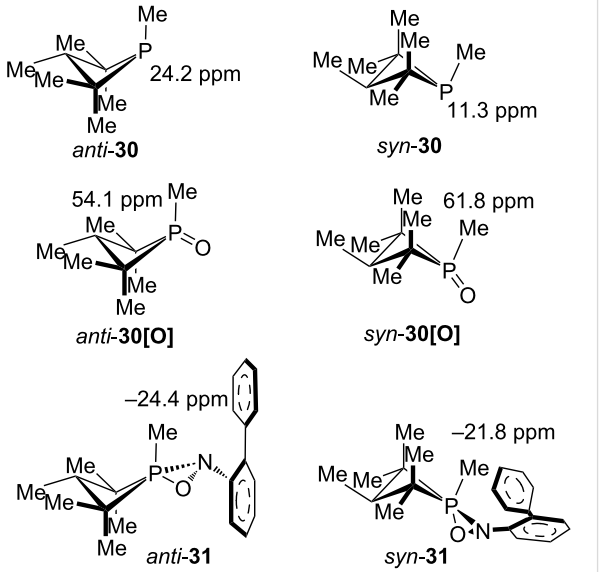


Figure 6: Phosphorus-catalyzed oxygen transfer reaction intermediates.

As the final example, Katz reported in 1966 [87] the reaction of cyclooctatetraene dianion with $PhPCl_2$ to give a single phosphine product **32** having an unusually high field ^{31}P NMR chemical shift of −181 ppm. Compound **32** underwent a stereospecific thermal [1,5]-sigmatropic rearrangement to bicyclic **33** exhibiting a ^{31}P NMR chemical shift of −79 ppm. Pyrolysis of **33** at 480 °C gave isomeric **34** having a ^{31}P NMR chemical shift of −14 ppm, while H_2O_2 oxidation of compounds **33** and **34** gave the corresponding phosphine oxides **33[O]** and **34[O]** with chemical shifts of 38 and 26 ppm, respectively (Figure 7). Identification of the isomers by ^{31}P NMR would represent a nice example of the utility of the calculations described here. Results for **33**, **34**, **33[O]**, and **34[O]** all confirmed the 1966 identifications (although the deviations are smallest for the two M06-2X optimization methods), but the ^{31}P NMR of the compound of primary interest, **32**, differed by 61 ppm from the calculated value using the Latypov method and 122 ppm using the B3LYP optimization, but gave excellent agreement using the M06-2X optimization, especially with the M06-2X NMR calculation (Table 3)! The X-ray structure of **32** was reported in 2004 [88,89] so the identification is correct, and provides a surprisingly extreme example of how these DFT functionals can differ. Comparison of bond lengths showed that this might be due to sensitivity of the DFT chemical shift to bond lengths. The three-membered phosphorus ring in the X-ray structure exhibited C–C and average C–P bond lengths of 1.495(2) and 1.869(5) Å, while the values for the M06-2X, Latypov, and B3LYP optimizations were 1.495/1.869, 1.488/1.882, and 1.489/1.908 Å, respectively. This suggested that the virtually exact match of the M06-2X optimization with the X-ray structure contributed to the agreement of the NMR calculation with

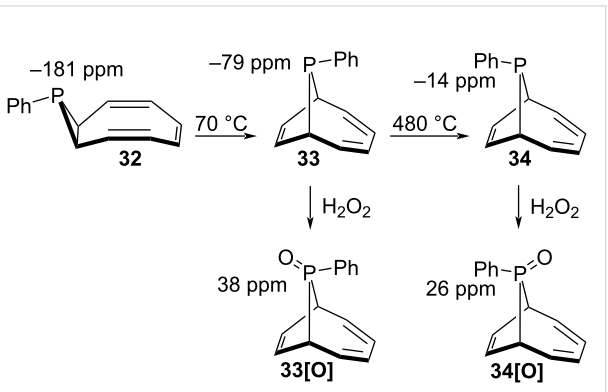


Figure 7: Phosphirane reactions.

the experimental chemical shift. Consistent with this, calculation of the NMR chemical shifts using the X-ray structure geometry also gave near perfect fits to the experimental for the B3LYP and PBE0 functionals. However as noted above use of the X-ray geometries of **8**–**10** with the B3LYP and M06-2X NMR functionals showed that the poor agreement of the NMR chemical shift calculations was due to the NMR functionals, not the geometries used.

6. The search for a failure-free functional. Looking at the complete collection of compounds evaluated (Table 2 and Table 3), the best MAD/RMSD (7.1/9.9 ppm) for **1a**–**34[O]** was seen for the M06-2X optimization and B3LYP NMR. As seen in the last row of Table 3, elimination of the failures due to compounds with P–C multiple bonding character gave the best MAD/RMSD = 5.4/7.1 ppm for optimization and NMR calculations both with the M06-2X functional. Clearly we are looking at a better "fitting" functional as described by Jensen [8], but what truly distinguishes these ^{31}P NMR results from the better-studied ^{1}H and ^{13}C results is the existence of the ^{31}P NMR failures.

The failures that we encountered included (1) the P–C multiple bonds for the M06-2X NMR calculations (i.e., **1a**), (2) *possibly* P–P bonding for both the M06-2X and B3LYP NMR calculations (i.e., **8** and to a lesser extent **9** and **10**), and (3) the phosphirane **32** for the B3LYP/B3LYP method and the PBE0 method of Latypov. We therefore set out to look at these outliers with recently recommended functionals rather than the widely-used functionals [15,90] that we have already tried (i.e., B3LYP, PBE0, M06-2X). In this way we might hope to see if this could provide a short-cut to find the best NMR functional, that is, one that might give the best fit with the least scatter (i.e., the lowest MAD), but also with none of the failures.

A recent review assessed 200 density functionals [91] and assigned them to the five rungs of "Jacob's ladder" [92-95]. In principle these 200 functionals could be evaluated for our ^{31}P NMR chemical shift problem, but in that same review Mardirossian and Head-Gordon noted that while DFT methods have been successfully used for chemical shift calculations, magnetic properties are not included in conventional functional development nor in the energy benchmarks that are used. Instead, we looked at recent work, mostly on ^{13}C NMR spectroscopy, for recommendations [7,90,91,96-98].

Results are collected in Table 4 for the chemical shifts for compounds **1a**, **8**, and **32**, scaled using only the first and last points for the trivalent series, PCl_3 and PH_3 (see Computational and NMR Details below). Comparison of the two-point scaling values for entries 1–4 in Table 4 with the full linear regression for scaling in Table 2 and Table 3 validates this short-cut. The GIAO NMR method was used for all of the calculations described to this point, as well as for the commonly recommended methods for ^{1}H and ^{13}C calculations [15]. However, the first method to be tried for this group of three compounds utilized the alternative CSGT NMR method recommended by Iron [7] with the TPSSTPSS [92,99,100] functional for the NMR calculation (albeit we used the computationally less intensive basis sets and the M06-2X optimization method already employed). As seen in entry 5 (Table 4) the GIAO method gave no improvement over entries 3 and 4, but use of the recommended CSGT method did give a reduction in the MAD (Table 4, entry 6). Optimization with the TPSSTPSS functional followed by the TPSSTPSS/CSGT NMR (Table 4, entry 7) failed, especially for compound **32**. Iron further found that long-range corrected (LC) functionals all out-performed the non-corrected functionals, so this was tested as seen by entries 8 and 9 (Table 4) for both the GIAO and CSGT calculation. The GIAO entry was only slightly better while the CSGT entry was worse, but more interestingly, both failed for the P–C multiple-bonded case, giving chemical shifts over 80 ppm downfield from the non-long-range corrected calculations for P_B in **1a** (Table 4, entries 5 and 6). The related PBETPSS functionals recommended by Modrzejewski et al. [98] exhibited the identical downfield failure for P–C multiple bonding (Table 4, entries 10–13) upon adding in the LC calculation. An obvious hypothesis for the M06-2X P-C multiple bonding NMR failure therefore was that this functional employs too much long-range correction, and Truhlar has described it as a medium-range method [57,101]. We therefore tried the local version of the M06-2X functional, namely the M06-L functional [102], for the NMR calculation (Table 4, entries 14–16), and were rewarded with the best MAD for these three compounds when using the M06-2X optimization and the M06-L/GIAO NMR calculation (Table 4, entry 14). Interestingly, this functional was *not* recommended in a recent study on calculation of solid-state chemical shifts for ^{31}P NMR [103]. Use of the CSGT NMR method gave a higher MAD (Table 4, entry 15) and M06-L optimization gave a very poor result (entry 16). Use of the newer local M11-L functional [104] for the NMR however was much worse (Table 4, entries 17 and 18) due entirely to the poor fit of **1a** when using M06-2X optimization but all four chemical shifts were poor (even P_A in **1a**, used essentially as a control) using M11-L optimization. Two fourth rung [90] functionals, M11 and MN12-SX [105,106], also failed to give any improvement (Table 4, entries 19 and 20), and these were also worse than the older fourth rung [90] functional M06-2X. Grimme's D3 dispersion correction has been recommended for general use as it increases the accuracy of many calculations [97,98], particularly with the BLYP functional (Table 4, entry 21) [97], but for the cases we tried no improvement was seen (Table 4, entries

Table 4: Scaled (using PH_3 and PCl_3) chemical shifts for the "failures" **1a**, **8**, and **32** for various optimization and NMR functionals.

Entry	Optimization	NMR[a]	**1a** P_A	**1a** P_B	**8** P_B	**32**	MAD[b]
	experimental		**39.6**	**297.6**	**–157.7**	**–181**	
1	PBE0 (Latypov)	PBE0 (Latypov)	37.2	282.5	–139.6	–112.7	33.9
2	B3LYP	B3LYP	42.1	278.4	–114.2	–59.2	61.5
3	M06-2X	B3LYP	40.3	272.2	–125.7	–167.9	23.5
4	M06-2X	M06-2X	56.2	336.0	–115.1	–175.2	28.9
5	M06-2X	TPSSTPSS	36.9	256.4	–135.8	–164.1	26.7
6	**M06-2X**	**TPSSTPSS***	**34.3**	**260.3**	**–148.1**	**–173.3**	**18.2**
7	TPSSTPSS	TPSSTPSS*	31.8	259.0	–132.9	–20.9	74.5
8	M06-2X	LC-TPSSTPSS	38.1	339.4	–132.4	–184.8	23.6
9	M06-2X	LC-TPSSTPSS*	33.4	345.0	–149.8	–199.0	24.4
10	M06-2X	PBETPSS	44.1	260.1	–124.5	–152.2	33.1
11	M06-2X	PBETPSS*	41.4	264.4	–139.0	–162.3	23.5
12	M06-2X	LC-PBETPSS	40.9	342.1	–127.4	–178.4	25.8
13	M06-2X	LC-PBETPSS*	35.0	348.7	–147.5	–195.4	25.3
14	**M06-2X**	**M06-L**	**36.5**	**274.4**	**–156.7**	**–180.9**	**8.1**
15	M06-2X	M06-L*	32.1	278.1	–171.5	–190.8	14.4
16	M06-L	M06-L	27.4	257.4	–161.4	–61.5	54.5
17	M06-2X	M11-L	23.6	231.5	–156.5	–181.8	22.7
18	M11-L	M11-L	7.8	212.3	–172.6	–70.1	70.4
19	M11	M11	43.8	339.8	–124.9	–194.4	29.5
20	MN12-SX	MN12-SX	27.2	274.6	–154.9	–145.6	20.4
21	BLYP-D3	BLYP-D3	34.4	242.3	–100.1	–7.6	95.4
22	M06-2X-D3	M06-2X-D3	56.1	336.0	–115.0	–175.2	29.0
23	M06-L-D3	M06-L-D3	27.3	257.4	–161.3	–61.5	54.4
24	TPSSTPSS-D3	TPSSTPSS-D3*	31.8	259.6	–140.5	–23.1	71.0
25	**M06-2X**	**ωB97X-D**	**39.3**	**293.1**	**–132.8**	**–177.7**	**10.9**
26	**ωB97X-D**	**ωB97X-D**	**38.0**	**292.8**	**–136.9**	**–174.2**	**10.8**
27	**M06-2X**	**PBE0**	**43.3**	**285.1**	**–133.2**	**–169.0**	**16.3**

[a]CSGT method indicated by *; all others are GIAO. [b]MAD for **1a** isomer A P_B, **8** P_B, and **32** isomer A; scaled chemical shifts for **1a** isomer A P_A (which has a P–C single bond) are shown for comparison but are not included in the MAD calculation, and scaled chemical shifts for **8** P_A are not included because these are correctly calculated by all methods previously (Table 2).

21–24). Last, Modrzejewski et al. [98] noted that Head-Gordon's ωB97X-D, a long-range corrected range-separated functional with dispersion correction [96], was also found to be highly accurate, and it was the most recently developed of the five representative functionals chosen by Jensen for evaluation [8]. Somewhat surprisingly, given the long-range correction that we previously found had resulted in the failure of P–C multiple bonding calculation, this functional (Table 4, entries 25 and 26) gave two of the best MAD values, with optimization either by the M06-2X or ωB97X-D functionals. Last, given the success of many of the M06-2X optimizations here and the Latypov PBE0 method, it seemed appropriate to test that (Table 4, entry 27). Here the PBE0 NMR calculation was carried out in the same way as entries 2–26, with $CHCl_3$ solvation and the 6-311+G(2d,p) basis set, and as seen it gave one of the best results.

The optimization/NMR methods that gave the lowest MAD values in Table 4 (entries 6, 14, 25–27, apart from entry 15 which was worse than the related entry 14) were then used for the full set of tri- and tetracoordinate compounds for scaling, and then the full set of test compounds **1a**–**34[O]**; MAD/RMSD results are listed in Table 5 (see Supporting Information File 1, Tables S7 and S10–S17 for all data) along with comparisons to the four best prior methods in Table 4 (entries 1, 3, and 4). As can be seen by examination of the results for the training set of tri- and tetracoordinate compounds in the first column, two of the new combinations, namely the M06-2X/PBE0 and the M06-2X/ωB97x-D functionals for optimization and NMR calculations, were among the best for the MAD/RMSD values in Table 1 and Table 5. These two also exhibited the lowest MAD/RMSD values of 6.9/8.5 and 6.8/9.1 ppm, respectively, for the full set of test compounds **1a**–**34[O]**. The higher RMSD for the

Table 5: Comparison of the best[a] functionals for **1a–34[O]**.

	MAD/RMSD (ppm)					
Opt/NMR[b]	P3 and P4 training set	**1a–34[O]**	P–P: **8–10**	**1a–7**, **11–34[O]**	P=C: **1a**, **8**P_B, **21–26**	**2–8**P_A, **9–20**, **27–34[O]**
M06-2X/B3LYP	**6.5/8.0**	**7.1/9.9**	15.6/18.5	**5.4/7.1**	9.7/14.0	6.4/8.5
M06-2X/ M06-2X	**4.1/5.7**	10.3/16.3	13.7/18.8	9.7/15.7	29.1/32.8	**5.4/7.1**
PBE0/PBE0[c]	7.8/9.7	**8.2/12.3**[d]	**6.9/8.5**	8.5/12.9	**6.6/8.2**	8.7/13.1
M06-2X/M06-L	7.2/8.8	7.5/9.3	9.3/10.7	7.2/9.0	8.2/9.6	7.4/9.2
M06-2X/TPSSTPSS*[e]	6.7/8.2	8.7/12.1	11.8/13.1	8.0/11.8	17.2/20.7	6.4/8.4
M06-2X/ωB97x-D	**5.9/7.3**	**6.8/9.1**	11.6/13.8	**5.8/7.9**	10.4/13.9	**5.9/7.4**
ωB97x-D/ωB97x-D	6.1/7.5	7.4/9.4	11.0/13.3	6.6/8.4	9.8/12.6	6.7/8.3
M06-2X/PBE0	**5.8/7.1**	**6.9/8.5**	10.8/13.0	**6.1/7.2**	8.4/10.7	6.5/7.7

[a]Best results are in bold. [b]Functionals for optimization (6-31+G(d,p) basis set) and NMR (6-311+G(2d,p) basis set), both with $CHCl_3$ solvation (IEF-PCM) except as noted. [c]Optimization and NMR following Latypov, gas phase and 6-31+G(d) and 6-311G(2d,2p) basis sets, respectively. [d]Without **32**, MAD/RMSD = **7.1**/**8.6** ppm. [e]CSGT NMR method; all others are GIAO.

M06-2X/ωB97x-D combination is due to the relatively large number of scaled chemical shifts that differ by 18–26 ppm from the experimental chemical shifts, while the M06-2X/PBE0 combination exhibits only one of those large chemical shift deviations. The next best M06-2X/M06-L combination (MSD/RMSD = 7.5/9.3 ppm) exhibits four such large deviations, although it was the best for the troublesome P_B of **8**. In fact, the only other combination that has only one large deviation is Latypov's gas-phase PBE0/PBE0 calculation, and as described above that is the phosphirane **32**, with a scaled chemical shift calculation of −120 ppm compared to the experimental value of −181 ppm. Without that one data point, the MAD/RMSD drops from 8.2/12.3 ppm to 7.1/8.6 ppm, which is one of the best results. As seen in Figure 8, plotting the experimental chemical shifts against the scaled calculated values for **1a–34[O]** for the M06-2X/PBE0 and the Latypov PBE0/PBE0 combinations each gives a set of values very close to the desired straight line with a slope of 1 and an intercept of 0, except for the one failure for compound **32** as shown; by inspection it can be seen that the Latypov plot does exhibit more scatter about the perfect fit line, so the higher MAD/RMSD for the points other than that for **32** makes sense.

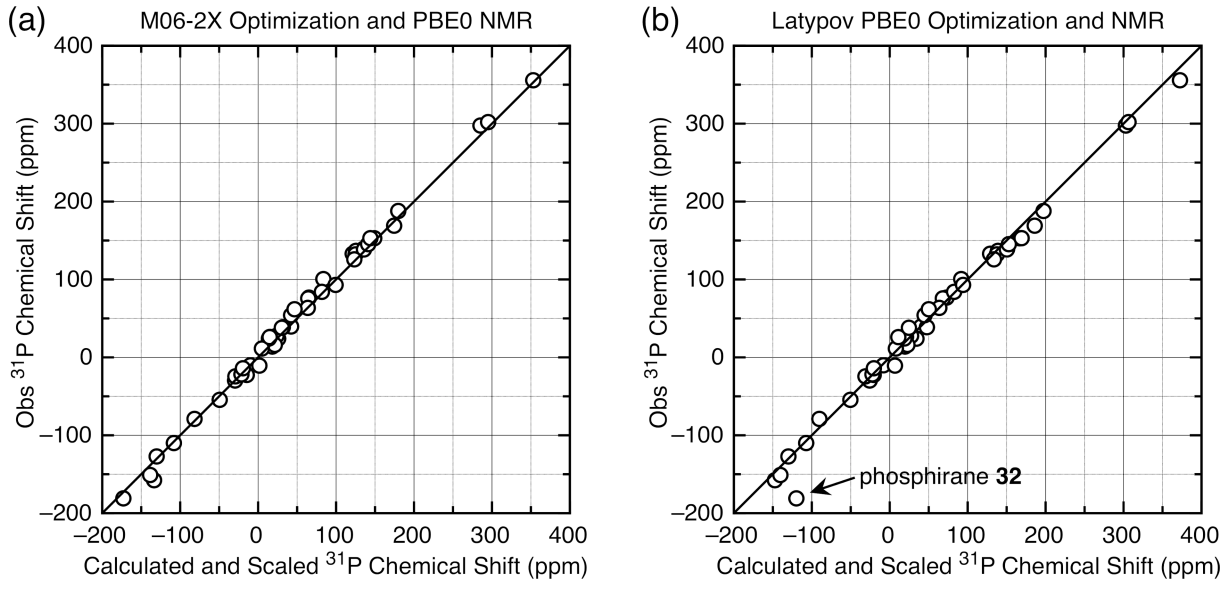


Figure 8: (a) Plot of experimental vs scaled chemical shifts derived from the tri- and tetracoordinate phosphorus training set compounds (M06-2X optimization and PBE0 NMR (6-311+G(2d,p) basis set) referenced to H_3PO_4, IEF-PCM $CHCl_3$ solvation; see Supporting Information File 1, Table S17 for values). The line drawn (slope = 1, intercept = 0) is the perfect fit line. (b) Plot of experimental vs scaled chemical shifts derived from the Latypov training set compounds (PBE0 optimization and PBE0 NMR (6-311G(2d,2p) basis set) referenced to H_3PO_4, no solvation; see Supporting Information File 1, Table S9 for values). The line drawn is the perfect fit line.

We conclude this section by examining separation of the P–P-bonded compounds or the P–C multiple-bonded compounds. Separating out first the P–P-bonded compounds **8**–**10** showed that the Latypov PBE0/PBE0 method was by far the best for those compounds, with the M06-2X/M06-L method that gave the best calculated chemical shift for P_B in **8** (−148.0 vs −157.7 ppm for the experimental value) the only other method that was close; the M06-2X/B3LYP method was the worst. When compiling the MAD/RMSD values for the remaining non-P–P-bonded compounds **1a**–**7** and **11**–**34[O]**, the overall results were somewhat better and the M06-2X/B3LYP method was the best. On the other hand, when the P–C multiple-bonded compounds **1a**, **8**(P_B), and **21**–**26** were separated out, the failure of the M06-2X/M06-2X was confirmed (MAD/RMSD = 29.1/32.8 ppm), and surprisingly the M06-2X/TPSSTPSS* method also failed (MAD/RMSD = 17.2/20.7 ppm) – surprising since this had been selected in the screening method. The Latypov PBE0/PBE0 method was once again the best for this subset, with the M06-2X/M06-L and M06-2X/PBE0 methods the only others that were close. When these multiple-bonded compounds were eliminated from the test set and the MAD/RMSD values compiled for **2**–**8**(P_A), **9**–**20**, and **27**–**34[O]**, however, the M06-2X/M06-2X was best (MAD/RMSD = 5.4/7.1 ppm).

Conclusion

We have developed a method for accurate calculation of ^{31}P NMR chemical shifts using a training set of well-known tri- and tetracoordinate phosphorus compounds that allows scaling of the readily accessible DFT chemical shifts. The present method follows established norms [15] of optimization of compound geometries in solution and weighting of the calculated chemical shifts on the basis of calculated equilibrium ratios in solutions of the different conformers. We compare this to the previously reported method described by Latypov [37], which uses a somewhat eclectic mix of unusual phosphorus compounds, some of which have questionable chemical shifts, and that are optimized using gas-phase calculations. The Latypov method, using the PBE0 functional for both optimization of compound geometry and chemical shift calculation, was found to be superior for compounds that contain P–P bonds and P–C multiple bonds. Optimization with the M06-2X functional was found to be superior for all compound types *except* the P–P-bonded compounds when the B3LYP functional was used for the chemical shift calculation, and the M06-2X functional was also found to be superior for all compound types *except* the P–C multiple-bonded compounds when the M06-2X functional was used for the chemical shift calculation.

One of the goals of this work was that the calculated chemical shifts should be sufficiently accurate to distinguish stereoisomers and confirm structures of unusual compounds. In fact, the methods were able to correctly reproduce the relative chemical shifts of stereoisomers that differed by as little as 3 ppm. However, for the unusual compounds, some combinations of functionals failed for confirmation of structures that contained multiple P–C bonding, P–P bonding, and for a 3-membered phosphirane ring. For instance, use of the M06-2X functional for both optimization and NMR calculations gave large downfield shifts of 30–49 ppm from the experimental values if there was any P–C multiple-bonding character, and B3LYP and PBE0 optimization led to downfield shifts of 61–124 ppm from the experimental value for the phosphirane ring. The P–P bonding failure is less clear, with downfield shift failures of 20–47 ppm for P_B in **8** for all pairs of functionals *except* the Latypov PBE0/PBE0 method and the M06-2X/M06-L combination, both of which gave downfield shifts of 10 ppm. A screening method was used to allow rapid calculations of scaled values to detect methods that would avoid these three failures, in hopes that this might lead to better overall methods. The results show that the strategy of screening methods using the "failures" did in fact lead to improvements in calculations, including a potential method using a localized version (M06-L) of the M06-2X functional for the NMR, and the two best methods for general use: the best combination involved optimization using the M06-2X functional with NMR calculations using the PBE0 functional, and use of the ωB97x-D functional for the NMR calculations was a close second. For compounds without P–P bonds, the M06-2X/B3LYP combination, on the basis of fairly limited data, can be used, and for compounds without P–C multiple bonds, the M06-2X/M06-2X combination is a good choice. For compounds with those functionalities, the Latypov method is best. Given the unexpected failures noted, for compounds with novel structures not covered here, more than one method should be used.

On the interesting question posed by Jensen [8] on whether the search for the "best" functionals and basis sets for chemical shift scaling is an exercise in data fitting, we note that unlike the case for ^{1}H and ^{13}C chemical shifts, ^{31}P chemical shifts must depend on a far more variable collection of phosphorus bond lengths and geometries. The functionals that give the most accurate bond lengths to phosphorus might give the best calculated chemical shifts, but changing the bond lengths to the correct lengths using the X-ray geometries does not necessarily then yield the correct chemical shifts as described in detail for **8** and in brief for **9** and **10**, and of course this is not a viable strategy to confirm novel and unknown structures. In the failure of the M06-2X functional with multiple bonding, the cause is clearly not due to failure to give proper bond lengths, as chemical shifts using the B3LYP functional are reliable using the identical

M06-2X optimized structures. The decrease in scatter using the M06-2X optimization, however, can be considered as improved data fitting as described by Jensen [8], but the failures, including P–P bonding, P–C multiple bonding, and, for the Latypov optimization, the three-membered phosphirane ring, are examples of functionals that clearly do not give a fit to experimental chemical shifts due to serendipitous cancelling of errors, but rather must have some fundamental flaw for those structural types. Reports of comparisons of functionals do not describe such failures [7,8,107], so the observation here of a closer fit of calculated to experimental chemical shifts for most compounds using the M06-2X functional for the NMR calculation, but with major significant failures for some structural types, is unique and so must be taken into account when looking at novel structures.

Overall these scaling methods were shown to provide excellent support for confirmation of stereochemistry and of solution structures of unusual phosphorus compounds, and should be considered part of standard practice for DFT calculation of ^{31}P NMR chemical shifts of novel compounds and those with unknown stereochemistry. Future work, however, should focus on the outlier compounds described here, whose unusual bonding gives rise to increased sensitivity to chemical shift calculations, and may help to more rapidly uncover which functionals are best for both geometry optimization and NMR chemical shift calculation.

Computational and NMR Details

For the trivalent phosphorus compounds, NMR chemical shifts (referenced to external 85% H_3PO_4 at 0.00 ppm, positive values downfield) were measured in $CDCl_3$ on a 400 MHz Bruker spectrometer for PPh_3 (−5.28 ppm), $P(OMe)_3$ (141.41 ppm), and PCl_3 (219.79 ppm) or were taken from the literature: PH_3 (−238 ppm, liquid sample at −90 °C [44] and at room temperature in CCl_4 [52]), $PMeH_2$ (−163.5 ppm, liquid sample [44]), PMe_2H (−98.5 ppm, liquid sample [44]), PMe_3 (−61.58 ppm in $CDCl_3$ [50]), $MeOP(OCH_2CH_2O)$ (133.3 ppm, in $CDCl_3$ [108]). For PCl_3 the experimental geometry was used for the NMR calculations (P–Cl = 2.043 Å, ∠(ClPCl) = 100.1°) [56] rather than the DFT optimized geometries (B3LYP: P–Cl = 2.096 Å, ∠(ClPCl) = 100.9°; M06-2X: P–Cl = 2.069 Å, ∠(ClPCl) = 100.0°; PBE0: P–Cl = 2.070 Å, ∠(ClPCl) = 100.7°; PBE0/6-31+G(d)/gas phase: P–Cl = 2.066 Å, ∠(ClPCl) = 101.0°).

For the tetracoordinate phosphorus compounds, NMR chemical shifts (referenced to external 85% H_3PO_4 at 0.00 ppm, positive values downfield) were measured in $CDCl_3$ on a 400 MHz Bruker spectrometer for $(iPrO)_2P(O)H$ (4.54 ppm), Ph_4P^+ Br^- (23.17 ppm), and $(iPrO)_2P(O)Me$ (28.61 ppm) or were taken from the literature: PH_4^+ BF_4^- (−105.3 ppm in CH_3OH/CH_3OD solution [109,110]), $(PhO)_4P^+$ PF_6^- (−28.0 ppm in CH_3CN solution [111]), $O=\boldsymbol{P}(OCH_2)_3P=O$ (−18.1 ppm in DMSO solution [112]), $O=P(OCH_2)_3\boldsymbol{P}=O$ (6.4 ppm in DMSO solution [112]), $(MeO)_4P^+$ BF_4^- (1.9 ppm in CH_2Cl_2 solution [113]), $(MeO)_2P(O)H$ (11.3 ppm, liquid sample [45]), Me_4P^+ Br^- (25.1 ppm in DMSO solution [114]), $Ph_3P=O$ (29.10 ppm in $CDCl_3$ solution [115]), $(MeO)_2P(O)Me$ (32.3 ppm, liquid sample [116]), $Me_3P=O$ (38.79 ppm in $CDCl_3$ solution [115]), $EtOP(O)Me_2$ (50.3 ppm, liquid sample [43]).

Chemical shifts for the phosphonium salts R_4P^+ (R = MeO, Me, Ph) require comment. In the case of $(MeO)_4P^+$ BF_4^-, initial reports gave the ^{31}P NMR chemical shift as 51.5 ppm [117,118], while all of our initial calculations placed it near −3 ppm. Subsequent work found the chemical shift to be 1.9 ppm [113], in agreement with our calculated shift, and no explanation for the original report has been offered [113]. For both of the R_4P^+ (R = Me, Ph) salts, chemical shift data were readily available for the Br^- but not the Cl^- salts. Bromine is not included in the IGLO-III and pcS-2 basis sets, however, so in those cases the calculated chloride salt chemical shifts were substituted. For Me_4P^+, the other basis sets gave identical chemical shifts for the Cl^- and Br^- salts, but for the Ph_4P^+ salts the Br^- salts were on average 2.7(0.2) ppm upfield of the Cl^- salts; if this correction were made, the deviations for the IGLO-III and pcS-2 basis sets would have been further reduced. Given the small difference and the absence of a strong justification for the correction, the chloride calculations were used without change.

Calculations were carried out using Gaussian 09, Revision D.01 [55]. The IGLO-III and pcS-2 basis sets were taken from the Basis Set Exchange [70], and all other basis sets were taken from Gaussian. X-ray structure coordinates were used as a starting point for optimizations when available. Energy optimizations were all accompanied by vibrational frequency calculations to ensure that stationary points were minima (all vibrations positive), and to ensure that true stationary points were confirmed in the vibrational frequency calculation. For the relatively large molecules, it was often found that the best results (in particular convergence to a minimum) were obtained using the "nosymm" instruction, and an initial calculation of all force constants ("calcfc"), rather than using the tight convergence criterion. All optimizations for the tri- and tetracoordinate phosphorus compounds utilized the 6-31G+(d,p) basis set with the polarizable continuum model, IEF-PCM/$CHCl_3$, except for the Latypov calculations, which used the 6-31+G(d) basis set and no solvation [37]. NMR calculations (GIAO) were then carried out on these optimized structures using the same solvation method (IEF-PCM/$CHCl_3$) or for the Latypov calculations, with

no solvation. The reference calculations on H_3PO_4 were carried out the same way, using water solvation, again except for the Latypov calculations where no solvation was included. For compounds **1a**–**34[O]** the same solvent used for the experimental NMR spectrum was used for each optimization and NMR calculation, again except for the Latypov calculation where no solvent was used. Keywords to run M06-2X calculations were m062x and integral=ultrafine, and for PBE0 pbe1pbe. For compounds where multiple optimized minima were found, energies were taken from the vibrational calculation (sum of electronic and thermal free energies) and used to calculate the relative amount of each conformation present at 298.15 K or at the temperature of the literature NMR when available [59], and the energy-weighted NMR chemical shifts were then computed. Coordinates and GaussView 6 images for all optimized structures including conformational minima may be found in Tables S18–S26 in Supporting Information File 1.

For Table 4, isotropic absolute magnetic shielding values were calculated for isomer A of **1a** and **32** (both of which were about 90% of the total, and isomer B did not differ significantly for both) and for **8** for each method. In order to scale these isotropic values, the absolute shieldings were calculated in each case for the two most distant points in the trivalent scaling plots corresponding to Figure 2, namely, PH_3 (liquid phase) and PCl_3 (experimental geometry), and these two points were then used (Equation 4, which does not require the reference H_3PO_4) to scale the test compound values. Comparison of the values for the first four entries in Table 4 to those in Table 2 and Table 3 shows the agreement is acceptable. In order to compare each method, the MAD for each was determined using only the problematical chemical shifts for **1a** (that is, C=P_B) and **8** (dicoordinate P_B) as well as that for **32**, but P_A for **1a** was also listed for each.

Supporting Information

Supporting Information File 1

Tables of calculated absolute isotropic chemical shifts, isomer ratios, unscaled chemical shifts, linear regressions, scaled chemical shifts and deviations, and coordinates of DFT optimized structures used for NMR calculations.
[https://www.beilstein-journals.org/bjoc/content/supplementary/1860-5397-19-4-S1.pdf]

Supporting Information File 2

Tables S1–S17 in editable format.
[https://www.beilstein-journals.org/bjoc/content/supplementary/1860-5397-19-4-S2.xlsx]

Funding

This work was supported by the City University of New York PSC-CUNY Research Award Program. Calculations were carried out at the Center for Computational Infrastructure for the Sciences (CCiS) at Queens College.

ORCID® iDs

William H. Hersh - https://orcid.org/0000-0002-9129-3464

References

1. Jain, R.; Bally, T.; Rablen, P. R. *J. Org. Chem.* **2009,** *74,* 4017–4023. doi:10.1021/jo900482q
2. Bally, T.; Rablen, P. R. *J. Org. Chem.* **2011,** *76,* 4818–4830. doi:10.1021/jo200513q
3. Lodewyk, M. W.; Siebert, M. R.; Tantillo, D. J. *Chem. Rev.* **2012,** *112,* 1839–1862. doi:10.1021/cr200106v
4. Grimblat, N.; Sarotti, A. M. *Chem. – Eur. J.* **2016,** *22,* 12246–12261. doi:10.1002/chem.201601150
5. Navarro-Vázquez, A. *Magn. Reson. Chem.* **2017,** *55,* 29–32. doi:10.1002/mrc.4502
6. Xin, D.; Sader, C. A.; Chaudhary, O.; Jones, P.-J.; Wagner, K.; Tautermann, C. S.; Yang, Z.; Busacca, C. A.; Saraceno, R. A.; Fandrick, K. R.; Gonnella, N. C.; Horspool, K.; Hansen, G.; Senanayake, C. H. *J. Org. Chem.* **2017,** *82,* 5135–5145. doi:10.1021/acs.joc.7b00321
7. Iron, M. A. *J. Chem. Theory Comput.* **2017,** *13,* 5798–5819. doi:10.1021/acs.jctc.7b00772
8. Jensen, F. *J. Chem. Theory Comput.* **2018,** *14,* 4651–4661. doi:10.1021/acs.jctc.8b00477
9. Bifulco, G.; Dambruoso, P.; Gomez-Paloma, L.; Riccio, R. *Chem. Rev.* **2007,** *107,* 3744–3779. doi:10.1021/cr030733c
10. Saielli, G.; Nicolaou, K. C.; Ortiz, A.; Zhang, H.; Bagno, A. *J. Am. Chem. Soc.* **2011,** *133,* 6072–6077. doi:10.1021/ja201108a
11. Tantillo, D. J. *Nat. Prod. Rep.* **2013,** *30,* 1079–1086. doi:10.1039/c3np70028c
12. Marell, D. J.; Emond, S. J.; Kulshrestha, A.; Hoye, T. R. *J. Org. Chem.* **2014,** *79,* 752–758. doi:10.1021/jo402627s
13. Brown, S. G.; Jansma, M. J.; Hoye, T. R. *J. Nat. Prod.* **2012,** *75,* 1326–1331. doi:10.1021/np300248w
14. Rablen, P. R.; Pearlman, S. A.; Finkbiner, J. *J. Phys. Chem. A* **1999,** *103,* 7357–7363. doi:10.1021/jp9916889
15. Lodewyk, M. W.; Siebert, M. R.; Tantillo, D. J.; Rablen, P. R.; Bally, T. CHESHIRE CCAT- CHEmical SHIft REpository with Coupling Constants Added To. http://cheshirenmr.info (accessed Sept 27, 2022).
16. Tong, J.; Liu, S.; Zhang, S.; Li, S. Z. *Spectrochim. Acta, Part A* **2007,** *67A,* 837–846. doi:10.1016/j.saa.2006.08.041
17. Dransfeld, A.; Ragué Schleyer, P. v. *Magn. Reson. Chem.* **1998,** *36* (Suppl. 1), S29–S43. doi:10.1002/(sici)1097-458x(199806)36:13<s29::aid-omr288>3.0.co;2-t
18. van Wüllen, C. *Phys. Chem. Chem. Phys.* **2000,** *2,* 2137–2144. doi:10.1039/b000461h
19. Patchkovskii, S.; Ziegler, T. *J. Phys. Chem. A* **2002,** *106,* 1088–1099. doi:10.1021/jp014184v
20. Rezaei-Sameti, M. *J. Mol. Struct.: THEOCHEM* **2008,** *867,* 122–124. doi:10.1016/j.theochem.2008.07.016

21. Chernyshev, K. A.; Krivdin, L. B. *Russ. J. Org. Chem.* **2010,** *46,* 785–790. doi:10.1134/s1070428010060023
22. Tafazzoli, M.; Ebrahimi, H. P. *Phosphorus, Sulfur Silicon Relat. Elem.* **2011,** *186,* 1491–1500. doi:10.1080/10426507.2010.520141
23. Maryasin, B.; Zipse, H. *Phys. Chem. Chem. Phys.* **2011,** *13,* 5150–5158. doi:10.1039/c0cp02653k
24. Fedorov, S. V.; Rusakov, Y. Y.; Krivdin, L. B. *Magn. Reson. Chem.* **2014,** *52,* 699–710. doi:10.1002/mrc.4122
25. Fleischer, U.; Schindler, M.; Kutzelnigg, W. *J. Chem. Phys.* **1987,** *86,* 6337–6347. doi:10.1063/1.452419
26. Kutzelnigg, W.; Fleischer, U.; Schindler, M. The IGLO-Method: Ab-initio Calculation and Interpretation of NMR Chemical Shifts and Magnetic Susceptibilities. In *NMR Basic Principles and Progress;* Diehl, P.; Fluck, E.; Günther, H.; Cosfeld, R.; Seelig, J., Eds.; Springer-Verlag: Berlin, 1990; Vol. 23, pp 165–262. doi:10.1007/978-3-642-75932-1_3
27. Jensen, F. *J. Chem. Theory Comput.* **2008,** *4,* 719–727. doi:10.1021/ct800013z
28. Jensen, F. *J. Chem. Theory Comput.* **2014,** *10,* 1074–1085. doi:10.1021/ct401026a
29. Přecechtělová, J.; Novák, P.; Munzarová, M. L.; Kaupp, M.; Sklenář, V. *J. Am. Chem. Soc.* **2010,** *132,* 17139–17148. doi:10.1021/ja104564g
30. Přecechtělová, J.; Munzarová, M. L.; Vaara, J.; Novotný, J.; Dračínský, M.; Sklenář, V. *J. Chem. Theory Comput.* **2013,** *9,* 1641–1656. doi:10.1021/ct300488y
31. Fukal, J.; Páv, O.; Buděšínský, M.; Šebera, J.; Sychrovský, V. *Phys. Chem. Chem. Phys.* **2017,** *19,* 31830–31841. doi:10.1039/c7cp06969c
32. Fukal, J.; Páv, O.; Buděšínský, M.; Rosenberg, I.; Šebera, J.; Sychrovský, V. *Phys. Chem. Chem. Phys.* **2019,** *21,* 9924–9934. doi:10.1039/c9cp01460h
33. Pascual-Borràs, M.; López, X.; Poblet, J. M. *Phys. Chem. Chem. Phys.* **2015,** *17,* 8723–8731. doi:10.1039/c4cp05016a
34. Payard, P.-A.; Perego, L. A.; Grimaud, L.; Ciofini, I. *Organometallics* **2020,** *39,* 3121–3130. doi:10.1021/acs.organomet.0c00309
35. Kondrashova, S. A.; Polyancev, F. M.; Latypov, S. K. *Molecules* **2022,** *27,* 2668. doi:10.3390/molecules27092668
36. Chesnut, D. B. *Chem. Phys. Lett.* **2003,** *380,* 251–257. doi:10.1016/j.cplett.2003.08.104
37. Latypov, S. K.; Polyancev, F. M.; Yakhvarov, D. G.; Sinyashin, O. G. *Phys. Chem. Chem. Phys.* **2015,** *17,* 6976–6987. doi:10.1039/c5cp00240k
38. Kwan, E. E.; Liu, R. Y. *J. Chem. Theory Comput.* **2015,** *11,* 5083–5089. doi:10.1021/acs.jctc.5b00856
39. Keal, T. W.; Tozer, D. J. *J. Chem. Phys.* **2003,** *119,* 3015–3024. doi:10.1063/1.1590634
40. Sarotti, A. M.; Pellegrinet, S. C. *J. Org. Chem.* **2009,** *74,* 7254–7260. doi:10.1021/jo901234h
41. Adamo, C.; Barone, V. *J. Chem. Phys.* **1999,** *110,* 6158–6170. doi:10.1063/1.478522
42. Krivdin, L. B. *Magn. Reson. Chem.* **2020,** *58,* 478–499. doi:10.1002/mrc.4965
43. Muller, N.; Lauterbur, P. C.; Goldenson, J. *J. Am. Chem. Soc.* **1956,** *78,* 3557–3561. doi:10.1021/ja01596a002
44. Van Wazer, J. R.; Callis, C. F.; Shoolery, J. N.; Jones, R. C. *J. Am. Chem. Soc.* **1956,** *78,* 5715–5726. doi:10.1021/ja01603a002
45. Jones, R. A. Y.; Katritzky, A. R. *Angew. Chem., Int. Ed. Engl.* **1962,** *1,* 32–41. doi:10.1002/anie.196200321
46. Mark, V.; Dungan, C. H.; Crutchfield, M. M.; van Wazer, J. R. *Top. Phosphorus Chem.* **1967,** *5,* 227–457.
47. Tebby, J. C. *CRC Handbook of Phosphorus-31 Nuclear Magnetic Resonance Data;* CRC Press: Boca Raton, FL, 1991.
48. Quin, L. D.; Verkade, J. G., Eds. *Phosphorus-31 NMR Spectral Properties in Compound Characterization and Structural Analysis;* Wiley: New York, NY, USA, 1994.
49. Nielsen, M. L.; Pustinger, J. V.; Strobel, J. *J. Chem. Eng. Data* **1964,** *9,* 167–170. doi:10.1021/je60021a003
50. Alajarín, M.; Molina, P.; Vidal, A.; Tovar, F. *Tetrahedron* **1997,** *53,* 13449–13472. doi:10.1016/s0040-4020(97)00855-7
51. Chesnut, D. B. *J. Phys. Chem. A* **2005,** *109,* 11962–11966. doi:10.1021/jp0555910
52. Zumbulyadis, N.; Dailey, B. P. *Mol. Phys.* **1974,** *27,* 633–640. doi:10.1080/00268977400100551
53. Lantto, P.; Jackowski, K.; Makulski, W.; Olejniczak, M.; Jaszuński, M. *J. Phys. Chem. A* **2011,** *115,* 10617–10623. doi:10.1021/jp2052739
54. Jameson, C. J.; De Dios, A.; Keith Jameson, A. *Chem. Phys. Lett.* **1990,** *167,* 575–582. doi:10.1016/0009-2614(90)85472-o
55. *Gaussian 09,* Revision D.01; Gaussian, Inc.: Wallingford, CT, 2013.
56. Harmony, M. D.; Laurie, V. W.; Kuczkowski, R. L.; Schwendeman, R. H.; Ramsay, D. A.; Lovas, F. J.; Lafferty, W. J.; Maki, A. G. *J. Phys. Chem. Ref. Data* **1979,** *8,* 619–721. doi:10.1063/1.555605
57. Zhao, Y.; Truhlar, D. G. *Acc. Chem. Res.* **2008,** *41,* 157–167. doi:10.1021/ar700111a
58. Alipour, M. *Theor. Chem. Acc.* **2018,** *137,* No. 8. doi:10.1007/s00214-017-2182-z
59. Junkes, P.; Baudler, M.; Dobbers, J.; Rackwitz, D. *Z. Naturforsch., B: Anorg. Chem., Org. Chem., Biochem., Biophys., Biol.* **1972,** *27,* 1451–1456. doi:10.1515/znb-1972-1204
60. Althoff, W.; Fild, M.; Rieck, H.-P.; Schmutzler, R. *Chem. Ber.* **1978,** *111,* 1845–1856. doi:10.1002/cber.19781110519
61. Steinbach, J.; Binger, P.; Regitz, M. *Synthesis* **2003,** 2720–2724. doi:10.1055/s-2003-42452
62. Hellwinkel, D.; Wilfinger, H. J. *Phosphorus Relat. Group V Elem.* **1976,** *6,* 151–159.
63. Richman, J. E.; Atkins, T. J. *Tetrahedron Lett.* **1978,** *19,* 4333–4336. doi:10.1016/s0040-4039(01)95217-7
64. Çiftçi, G. Y.; Eçik, E. T.; Yıldırım, T.; Bilgin, K.; Şenkuytu, E.; Yuksel, F.; Uludağ, Y.; Kılıç, A. *Tetrahedron* **2013,** *69,* 1454–1461. doi:10.1016/j.tet.2012.12.027
65. Quin, L. D.; Mesch, K. A.; Orton, W. L. *Phosphorus Sulfur Relat. Elem.* **1982,** *12,* 161–177. doi:10.1080/03086648208077444
66. Yoshifuji, M.; Hirano, Y.; Schnakenburg, G.; Streubel, R.; Niecke, E.; Ito, S. *Helv. Chim. Acta* **2012,** *95,* 1723–1729. doi:10.1002/hlca.201200442
67. Surgenor, B. A.; Bühl, M.; Slawin, A. M. Z.; Woollins, J. D.; Kilian, P. *Angew. Chem., Int. Ed.* **2012,** *51,* 10150–10153. doi:10.1002/anie.201204998
68. Zagidullin, A.; Ganushevich, Y.; Miluykov, V.; Krivolapov, D.; Kataeva, O.; Sinyashin, O.; Hey-Hawkins, E. *Org. Biomol. Chem.* **2012,** *10,* 5298–5306. doi:10.1039/c2ob25532d
69. Miluykov, V.; Bezkishko, I.; Zagidullin, A.; Sinyashin, O.; Lönnecke, P.; Hey-Hawkins, E. *Eur. J. Org. Chem.* **2009,** 1269–1274. doi:10.1002/ejoc.200801181
70. Pritchard, B. P.; Altarawy, D.; Didier, B.; Gibson, T. D.; Windus, T. L. *J. Chem. Inf. Model.* **2019,** *59,* 4814–4820. doi:10.1021/acs.jcim.9b00725

71. Alcaraz, J.-M.; Mathey, F. *Tetrahedron Lett.* **1984,** *25,* 4659–4662. doi:10.1016/s0040-4039(01)91226-2
72. Hersh, W. H.; Lam, S. T.; Moskovic, D. J.; Panagiotakis, A. J. *J. Org. Chem.* **2012,** *77,* 4968–4979. doi:10.1021/jo3003776
73. Tichotová, M.; Ešnerová, A.; Tučková, L.; Bednárová, L.; Císařová, I.; Baszczyňski, O.; Procházková, E. *J. Magn. Reson.* **2022,** *336,* 107149. doi:10.1016/j.jmr.2022.107149
74. Huang, Y.; Yu, J.; Bentrude, W. G. *J. Org. Chem.* **1995,** *60,* 4767–4773. doi:10.1021/jo00120a020
75. Brown, J. M.; Carey, J. V.; Russell, M. J. H. *Tetrahedron* **1990,** *46,* 4877–4886. doi:10.1016/s0040-4020(01)85600-3
76. Hersh, W. H.; Xu, P.; Simpson, C. K.; Grob, J.; Bickford, B.; Hamdani, M. S.; Wood, T.; Rheingold, A. L. *J. Org. Chem.* **2004,** *69,* 2153–2163. doi:10.1021/jo035508+
77. Solovieva, S. E.; Gruner, M.; Antipin, I. S.; Habicher, W. D.; Konovalov, A. I. *Org. Lett.* **2001,** *3,* 1299–1301. doi:10.1021/ol015658b
78. Tay, M. Q. Y.; Lu, Y.; Ganguly, R.; Vidović, D. *Angew. Chem., Int. Ed.* **2013,** *52,* 3132–3135. doi:10.1002/anie.201209223
79. Đorđević, N.; Ganguly, R.; Petković, M.; Vidović, D. *Chem. Commun.* **2016,** *52,* 9789–9792. doi:10.1039/c6cc04161b
80. Lemp, O.; Balmer, M.; Reiter, K.; Weigend, F.; von Hänisch, C. *Chem. Commun.* **2017,** *53,* 7620–7623. doi:10.1039/c7cc04422d
81. Hersh, W. H. *Beilstein J. Org. Chem.* **2015,** *11,* 184–191. doi:10.3762/bjoc.11.19
82. Setzer, W. N.; Black, B. G.; Hovanes, B. A.; Hubbard, J. L. *J. Org. Chem.* **1989,** *54,* 1709–1713. doi:10.1021/jo00268a038
83. Nykaza, T. V.; Ramirez, A.; Harrison, T. S.; Luzung, M. R.; Radosevich, A. T. *J. Am. Chem. Soc.* **2018,** *140,* 3103–3113. doi:10.1021/jacs.7b13803
84. Cowley, A. H.; Kemp, R. A. *Chem. Rev.* **1985,** *85,* 367–382. doi:10.1021/cr00069a002
85. Spinney, H. A.; Yap, G. P. A.; Korobkov, I.; DiLabio, G.; Richeson, D. S. *Organometallics* **2006,** *25,* 3541–3543. doi:10.1021/om060466b
86. Reiß, F.; Schulz, A.; Villinger, A. *Eur. J. Inorg. Chem.* **2012,** 261–271. doi:10.1002/ejic.201100978
87. Katz, T. J.; Nicholson, C. R.; Reilly, C. A. *J. Am. Chem. Soc.* **1966,** *88,* 3832–3842. doi:10.1021/ja00968a029
88. Bulo, R. E.; Jansen, H.; Ehlers, A. W.; de Kanter, F. J. J.; Schakel, M.; Lutz, M.; Spek, A. L.; Lammertsma, K. *Angew. Chem., Int. Ed.* **2004,** *43,* 714–717. doi:10.1002/anie.200351855
89. Bulo, R. E.; Jansen, H.; Ehlers, A. W.; de Kanter, F. J. J.; Schakel, M.; Lutz, M.; Spek, A. L.; Lammertsma, K. *Angew. Chem., Int. Ed.* **2004,** *43,* 3748a–3748. doi:10.1002/anie.200490098
90. Mardirossian, N.; Head-Gordon, M. *J. Chem. Theory Comput.* **2016,** *12,* 4303–4325. doi:10.1021/acs.jctc.6b00637
91. Mardirossian, N.; Head-Gordon, M. *Mol. Phys.* **2017,** *115,* 2315–2372. doi:10.1080/00268976.2017.1333644
92. Tao, J.; Perdew, J. P.; Staroverov, V. N.; Scuseria, G. E. *Phys. Rev. Lett.* **2003,** *91,* 146401. doi:10.1103/physrevlett.91.146401
93. Perdew, J. P.; Ruzsinszky, A.; Tao, J.; Staroverov, V. N.; Scuseria, G. E.; Csonka, G. I. *J. Chem. Phys.* **2005,** *123,* 062201. doi:10.1063/1.1904565
94. Su, N. Q.; Zhu, Z.; Xu, X. *Proc. Natl. Acad. Sci. U. S. A.* **2018,** *115,* 2287–2292. doi:10.1073/pnas.1713047115
95. Zhang, I. Y.; Xu, X. *Wiley Interdiscip. Rev.: Comput. Mol. Sci.* **2021,** *11,* e1490. doi:10.1002/wcms.1490
96. Chai, J.-D.; Head-Gordon, M. *Phys. Chem. Chem. Phys.* **2008,** *10,* 6615–6620. doi:10.1039/b810189b
97. Grimme, S.; Antony, J.; Ehrlich, S.; Krieg, H. *J. Chem. Phys.* **2010,** *132,* 154104. doi:10.1063/1.3382344
98. Modrzejewski, M.; Hapka, M.; Chalasinski, G.; Szczesniak, M. M. *J. Chem. Theory Comput.* **2016,** *12,* 3662–3673. doi:10.1021/acs.jctc.6b00406
99. Staroverov, V. N.; Scuseria, G. E.; Tao, J.; Perdew, J. P. *J. Chem. Phys.* **2003,** *119,* 12129–12137. doi:10.1063/1.1626543
100. Staroverov, V. N.; Scuseria, G. E.; Tao, J.; Perdew, J. P. *J. Chem. Phys.* **2004,** *121,* 11507. doi:10.1063/1.1795692
101. Hohenstein, E. G.; Chill, S. T.; Sherrill, C. D. *J. Chem. Theory Comput.* **2008,** *4,* 1996–2000. doi:10.1021/ct800308k
102. Zhao, Y.; Truhlar, D. G. *J. Chem. Phys.* **2006,** *125,* 194101. doi:10.1063/1.2370993
103. Shenderovich, I. G. *Chem.: Methods* **2021,** *1,* 61–70. doi:10.1002/cmtd.202000033
104. Peverati, R.; Truhlar, D. G. *J. Phys. Chem. Lett.* **2012,** *3,* 117–124. doi:10.1021/jz201525m
105. Peverati, R.; Truhlar, D. G. *J. Phys. Chem. Lett.* **2011,** *2,* 2810–2817. doi:10.1021/jz201170d
106. Peverati, R.; Truhlar, D. G. *Phys. Chem. Chem. Phys.* **2012,** *14,* 16187–16191. doi:10.1039/c2cp42576a
107. Laskowski, R.; Blaha, P.; Tran, F. *Phys. Rev. B* **2013,** *87,* 195130. doi:10.1103/physrevb.87.195130
108. Besserre, D.; Coffi-Nketsia, S. *Org. Magn. Reson.* **1980,** *13,* 313–318. doi:10.1002/mrc.1270130502
109. Sheldrick, G. M. *Trans. Faraday Soc.* **1967,** *63,* 1077–1082. doi:10.1039/tf9676301077
110. Wasylishen, R. E.; Burford, N. *Can. J. Chem.* **1987,** *65,* 2707–2712. doi:10.1139/v87-449
111. Peake, S. C.; Fild, M.; Hewson, M. J. C.; Schmutzler, R. *Inorg. Chem.* **1971,** *10,* 2723–2727. doi:10.1021/ic50106a020
112. Coskran, K. J.; Verkade, J. G. *Inorg. Chem.* **1965,** *4,* 1655–1657. doi:10.1021/ic50033a026
113. Finley, J. H.; Denney, D. Z.; Denney, D. B. *J. Am. Chem. Soc.* **1969,** *91,* 5826–5831. doi:10.1021/ja01049a021
114. Grim, S. O.; McFarlane, W.; Davidoff, E. F.; Marks, T. J. *J. Phys. Chem.* **1966,** *70,* 581–584. doi:10.1021/j100874a502
115. Hilliard, C. R.; Bhuvanesh, N.; Gladysz, J. A.; Blümel, J. *Dalton Trans.* **2012,** *41,* 1742–1754. doi:10.1039/c1dt11863c
116. Moedritzer, K.; Maier, L.; Groenweghe, L. C. D. *J. Chem. Eng. Data* **1962,** *7,* 307–310. doi:10.1021/je60013a043
117. Cohen, J. S. *Tetrahedron Lett.* **1965,** *6,* 3491–3496. doi:10.1016/s0040-4039(01)89332-1
118. Cohen, J. S. *J. Am. Chem. Soc.* **1967,** *89,* 2543–2547. doi:10.1021/ja00987a008

License and Terms

This is an open access article licensed under the terms of the Beilstein-Institut Open Access License Agreement (https://www.beilstein-journals.org/bjoc/terms), which is identical to the Creative Commons Attribution 4.0 International License (https://creativecommons.org/licenses/by/4.0). The reuse of material under this license requires that the author(s), source and license are credited. Third-party material in this article could be subject to other licenses (typically indicated in the credit line), and in this case, users are required to obtain permission from the license holder to reuse the material.

The definitive version of this article is the electronic one which can be found at:
https://doi.org/10.3762/bjoc.19.4

BEILSTEIN JOURNAL OF ORGANIC CHEMISTRY

Dipeptide analogues of fluorinated aminophosphonic acid sodium salts as moderate competitive inhibitors of cathepsin C

Karolina Wątroba[1], Małgorzata Pawełczak[2] and Marcin Kaźmierczak[*1,3]

Full Research Paper

Open Access

Address:
[1]Faculty of Chemistry, Adam Mickiewicz University in Poznań, Uniwersytetu Poznańskiego 8, 61-614 Poznań, Poland, [2]Institute of Chemistry, Opole University, 45-052 Opole, Poland and [3]Centre for Advanced Technologies, Adam Mickiewicz University in Poznań, Uniwersytetu Poznańskiego 10, 61-614 Poznań, Poland

Email:
Marcin Kaźmierczak[*] - marcin.kazmierczak@amu.edu.pl

* Corresponding author

Keywords:
aminophosphonates; cathepsin C; dipeptide; fluorine; solvolysis

Beilstein J. Org. Chem. **2023,** *19,* 434–439.
https://doi.org/10.3762/bjoc.19.33

Received: 22 February 2023
Accepted: 05 April 2023
Published: 12 April 2023

This article is part of the thematic issue "Organophosphorus chemistry: from model to application".

Guest Editor: G. Keglevich

© 2023 Wątroba et al.; licensee Beilstein-Institut.
License and terms: see end of document.

Abstract

In this paper, we present the solvolysis reaction of dipeptide analogues of fluorinated aminophosphonates with simultaneous quantitative deprotection of the amino group. To the best of our knowledge, this work is the first reported example of the application of fluorinated aminophosphonates in cathepsin C inhibition studies. The new molecules show moderate inhibition of the cathepsin C enzyme, which opens the door to consider them as potential therapeutic agents. Overall, our findings provide a new avenue for the development of fluorinated aminophosphonate-based inhibitors.

Introduction

Cathepsin C, also known as dipeptidyl peptidase I (DPPI) belongs to the family of lysosomal cysteine proteases encompassing 11 human enzymes (cathepsins B, C, F, H, K, L, O, S, V, W, and X) [1]. Cathepsin C is considered a good target for designing new anticancer agents with broad substrate specificity [2].

Cathepsin C, which affects the processing of keratin, is of great importance in maintaining the structural organization of the epidermis, primarily the extremities, and the integrity of the teeth' tissues. Genetic studies have shown that a mutation in the gene encoding DPPI leads to early periodontitis, premature tooth loss, and keratosis of the palms and soles [3,4]. These conditions occur in Papillon–Lefevre syndrome and Haim–Munk syndrome [1]. Cathepsin C is an emerging pharmacological target due to its involvement in inflammatory and autoimmune diseases. Cathepsin C is upregulated in immune-related cells. DPPI also plays a role in the development of cancer – particularly in the liver and breast, hence the potential contribution of its inhibitors in chemotherapies to support tradi-

tional anticancer drugs. Moreover, there is a growing interest in the topic of cathepsin C inhibition, which directly affects serine protease activity [5,6]. Inhibitors of cathepsin C can be cystatins that show activity against a large group of cysteine proteases [7]. Other inhibitors are dipeptide derivatives showing substrate-like sequences. One of the most effective inhibitors is the dipeptide Gly-Phe-CHN_2 (glycylphenylalanine-diazomethane), which, however, has not been used as a therapeutic substance due to the instability of the diazomethylketone group [8,9]. Based on its structure, many other inhibitors have been developed, such as vinyl sulfones, fluoromethyl ketones, and semicarbazides [8,9]. These inhibitors covalently bind to the nucleophilic thiol group of Cys234 in the active site of cathepsin C via a thioether bond.

Phosphonates have been identified as potential inhibitors of cathepsins. The phosphorus atom by default should mimic the tetrahedral intermediate, but this role may also be played by the hydroxy group present in hydroxyphosphonates, which mimic the carbonyl carbon in the peptide bond by forming a hydrogen bond with the amino group of the catalytic cysteine Cys234 [10]. Phosphonates, as well as their analogues phosphonic acids, can be modified in a number of ways, one of which is the introduction of a fluorine atom into their molecules by fluorination or alkylfluorination [11-14]. However, the reaction of β-aminoalcohols with nucleophilic deoxyfluorinating reagents often does not lead to the expected products with a fluorine atom in place of the –OH group. They usually undergo rearrangement, and intramolecular cyclization leading to products that are constitutional isomers [15].

The solvolysis reaction of phosphonates to the corresponding phosphonic acids or their salts is often a necessary step to measure activity in enzyme inhibition bioassays [16-22]. Therefore, our goal was to determine the best conditions for carrying out the solvolysis reaction of synthesized dipeptide analogues of fluorinated aminophosphonates [23,24] with the simultaneous deprotection of the amino group. The free amines were subjected to kinetic studies to investigate their interaction with cathepsin C. The required steps should be simple and fast, and the conditions of the reactions should be as mild as possible. The reactions should proceed with high yields, and any byproducts should be easily removeable.

Results and Discussion

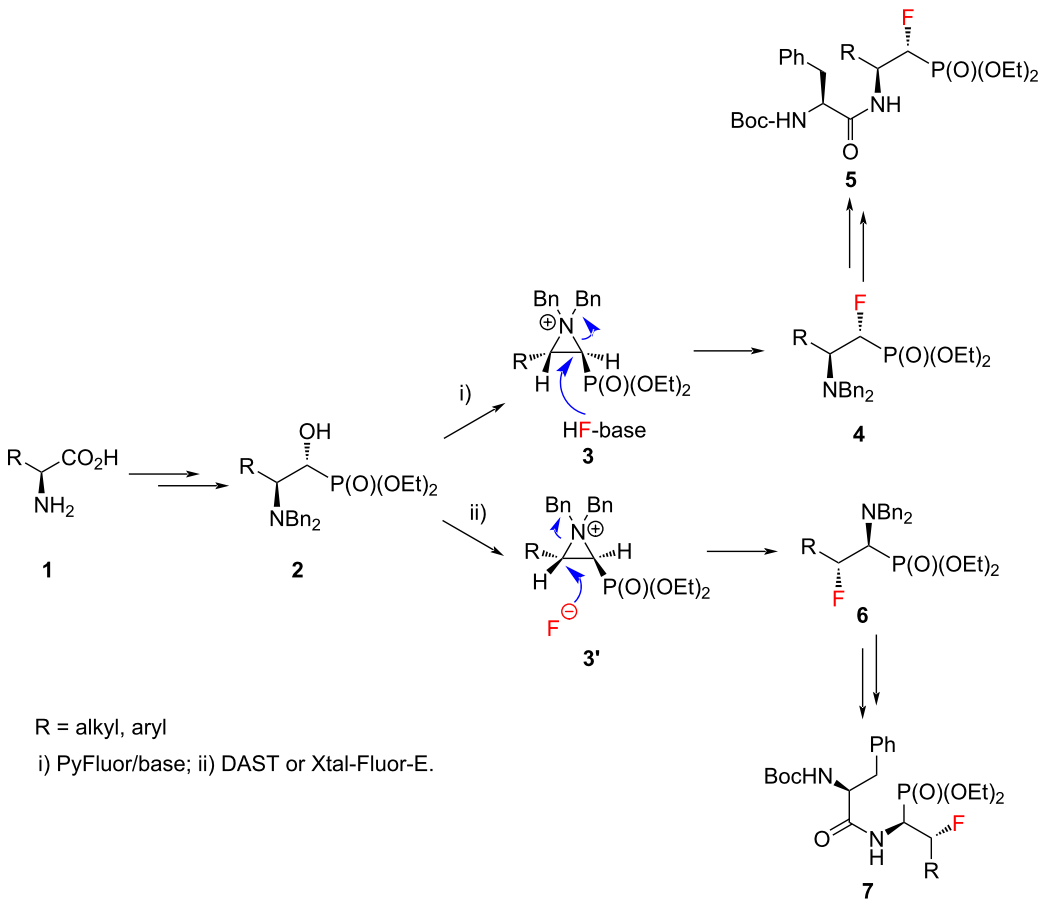
Dipeptide analogues of α- and β-fluorinated aminophosphonates **5** and **7** were obtained from the corresponding L-amino acids [23,24] **1**. In the key step of the synthesis fluorine was introduced to the corresponding α- and β-fluorinated aminophosphonates **4**, **6** (Scheme 1) by regioselective deoxyfluorination reactions of α-hydroxy-β-aminophosphonates **2** [24-26].

Next, the conditions for the solvolysis were carefully assembled (Scheme 2). The optimized reaction conditions included 8 equiv of trimethylsilyl bromide (TMSBr) and freshly distilled methylene chloride as a solvent. In each case the reactions were carried out at room temperature overnight under an argon atmosphere. The next day, the solvent, volatile byproducts, and TMSBr residues were thoroughly evaporated. Time of solvolysis reactions varies in the literature, ranging from 10 minutes to several hours [27-29]. In our case the alcoholysis was carried out for 30 minutes. During this process, disappearance of the brownish or yellowish color of the compounds was observed. According to the literature, addition of diethyl ether in the next step should make precipitation more efficient [10]. This was done for compound **8a**, but no improvement was observed. Much better results were obtained with additional double wash of the precipitate with methanol combined with evaporation of the solvent under reduced pressure. As a result of the reactions carried out, the dipeptide analogues of α- and β-fluorinated aminophosphonic acids **8** and **10** were obtained. All the samples were solids, with very poor solubility in water and organic solvents such as DMSO and MeOH.

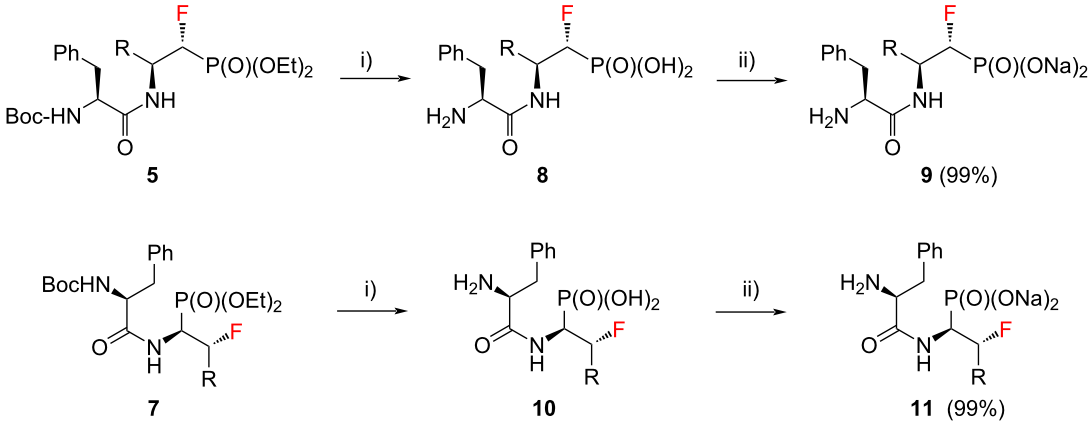
The final step of the synthesis was the reaction of the resulting phosphonic acids **8** and **10** with a 1 M aqueous NaOH solution. Based on the literature data, alternatively to this method [30-32], phosphonic acids can be passed through an ion exchange column [33]. The reactions of compounds **8** and **10** with 1 M NaOH were carried out at room temperature (Scheme 2). When a clear solutions were obtained, the reaction was carried out for another 15 minutes. The solutions were then concentrated under reduced pressure. The precipitated salts were washed with methanol [31] and the solvent evaporation procedure was repeated. Sublimation drying (lyophilization) was carried out, obtaining white powders with a yield of 99% in each case. The resulting sodium salts of phosphonic acids **9** and **11** were subjected to ^{1}H, ^{13}C, ^{19}F, and ^{31}P NMR spectroscopic analysis as well as mass spectrometry (MS) confirming their purity. The spectroscopic data of **9** and **11** are in agreement with the literature data of the starting esters **5** and **7** literature data [23,24]. A very good correlation of chemical shifts was also observed in the ^{13}C NMR spectra for the key signals from the C1 and C2 atoms (Table 1). Each sample was pure; no byproducts were present.

Kinetic studies

Due to the homology and similar structural requirements, bovine cathepsin C is often used in research as a model for human cathepsin C as it was well documented by Poręba et al. [34] in the study of the substrate specificity of these two mammalian cathepsins. They showed the best fit of amino acids with larger side to the S1 pocket of the enzyme. In contrast, the



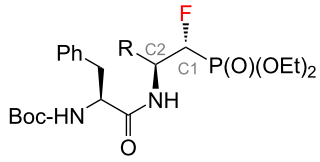
Scheme 1: Synthetic strategy towards **5** and **7**.



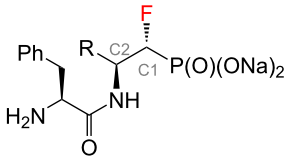
Scheme 2: Synthesis of **9** and **11**. (**a**) R = -CH_3; (**b**) R = -$CH(CH_3)_2$; (**c**) R = -$CH_2CH(CH_3)_2$; (**d**) R = -$CH(CH_3)CH_2CH_3$, (**e**) R = -CH_2Ph; i) (a) **5** or **7** (1 equiv), TMSBr (8 equiv), CH_2Cl_2, rt, 20 h, (b) MeOH, 30 min.; ii) 8 or 10 (1 equiv), 1 M NaOH (2 equiv), H_2O, 15 min.

S2 pocket preferably accommodates amino acids having short aliphatic side-chains, but also recognizes aromatic amino acids, preferably phenylalanine. To study the structural requirements of the S1 binding site of the enzyme, we synthesized a series of ten dipeptide analogues of fluorinated aminophosphonic acid sodium salts **9**, **11** with phenylalanine at the *N*-terminus and evaluated their inhibitory activity against bovine cathepsin C. Inhibition kinetics were carried out at 37 °C for 10 minutes in

Table 1: The ^{13}C NMR chemical shifts of C1 and C2 carbon atoms.

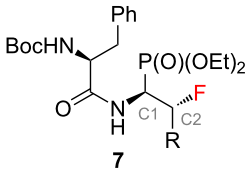


5

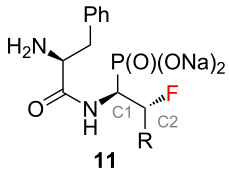


9

R =	**5** C1 [ppm]	**9** C1 [ppm]	**5** C2 [ppm]	**9** C2 [ppm]
(**a**) -CH_3	89.56	94.72	45.66	47.77
(**b**) -$CH(CH_3)_2$	88.97	93.30	54.77	57.29
(**c**) -$CH_2CH(CH_3)_2$	91.33	95.36	48.62	50.22
(**d**) -$CH(CH_3)CH_2CH_3$	88.89	92.17	54.45	56.33
(**e**) -CH_2Ph	88.05	94.79	51.39	52.93



7

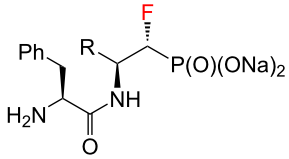
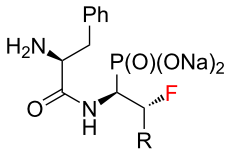


11

R =	**7** C1 [ppm]	**11** C1 [ppm]	**7** C2 [ppm]	**11** C2 [ppm]
(**a**) -CH_3	49.51	54.13	89.00	92.58
(**b**) -$CH(CH_3)_2$	47.55	50.45	98.03	99.23
(**c**) -$CH_2CH(CH_3)_2$	50.00	54.09	92.21	94.76
(**d**) -$CH(CH_3)CH_2CH_3$	47.16	49.91	95.16	96.08
(**e**) -CH_2Ph	48.69	53.55	93.24	96.21

acetate buffer at pH 5. Changes in product concentration versus time were monitored spectrophotometrically at λ = 405 nm. Seven of the tested compounds were moderate competitive inhibitors with millimolar inhibitory activity (Table 2). Three of them at higher concentrations precipitated from 0.1 M acetate buffer at pH 5.0. Dipeptide analogues of α-fluorinated amino-

Table 2: Inhibitory constants of the studied of α- and β-fluorinated aminophosphonic acid sodium salts towards bovine cathepsin C.

Dipeptide	 **9** K_I ± SD [mM]	 **11** K_I ± SD [mM]
Phe-Ala (**a**) -CH_3	0.603 ± 0.1	0.733 ± 0.087
Phe-Val (**b**) -$CH(CH_3)_2$	0.0951 ± 0.05	1.869 ± 0.171
Phe-Leu (**c**) -$CH_2CH(CH_3)_2$	0.309 ± 0.066	0.847 ± 0.38
Phe-Ile (**d**) -$CH(CH_3)CH_2CH_3$	0.273 ± 0.15	up to a concentration of 0.37 mM, it does not inhibit activity; at a higher concentration, it precipitates
Phe-Phe (**e**) -CH_2Ph	precipitates in a buffer	precipitates in buffer

phosphonic acid sodium salts **9** were more active against cathepsin C than β-fluorinated analogues **11**.

The dipeptide analogue of α-fluorinated aminophosphonic acid sodium salt bearing the valine residue as a second amino acid in the chain (**9b**) showed the greatest inhibitory power (Figure 1). The type of inhibition and the inhibition constant were determined from the Dixon-type linearization of Equation 1 [35]. For each of the simple data, Equation 1 determines the slope factor a, whereby a weighted fit was used. The statistical weight for each point in the above-mentioned transformation $1/V_{0,i} = f(I)$ is equal to $w_i = V^4_{(0,i)}$.

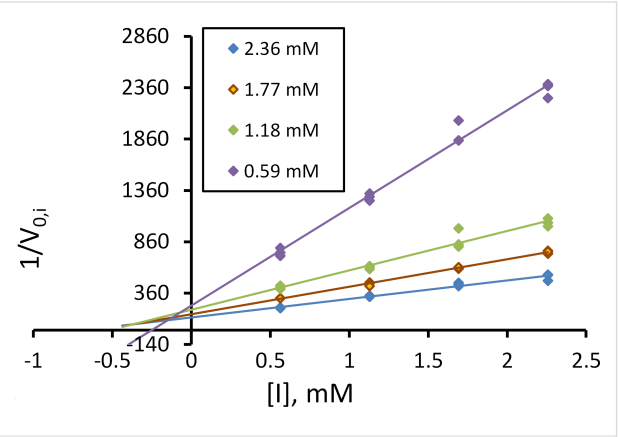


Figure 1: Dixon plot for the hydrolysis of Gly-Phe-*p*NA substrate catalyzed by bovine cathepsin C in the presence of **9b** (T = 37 °C, pH 5.0).

$$V_{0,i} = \frac{V_{max} \cdot [S]}{K_M \cdot \left(1 + \frac{[I]}{K_{ic}}\right) + [S] \cdot \left(1 + \frac{[I]}{K_{iu}}\right)} \quad (1)$$

where:

V_{max} = maximum reaction velocity, K_M = Michaelis constant, K_{ic} = competitive inhibitory constant, K_{iu} = uncompetitive inhibitory constant, [S] = concentration of the substrate, [I] = concentration of the inhibitor.

Conclusion

In conclusion, we demonstrated the solvolysis reaction of dipeptide analogues of fluorinated aminophosphonates with the simultaneous deprotection of the amino group. The resulting acids were converted into the corresponding salts. All the reactions proceeded quantitatively. Obtained compounds were subjected to kinetic studies against cathepsin C, and the results indicated that they are moderate competitive inhibitors of this enzyme. This study presented the first kinetic investigation of fluorinated dipeptide derivatives of aminophosphonic acid salts against cathepsin C, thus contributing to the development of the novel cathepsin C inhibitors. We are currently working on the development of more effective fluorinated inhibitors of cathepsin C in our laboratory.

Supporting Information

Supporting Information File 1

Experimental procedures, biological protocol, NMR data.
[https://www.beilstein-journals.org/bjoc/content/supplementary/1860-5397-19-33-S1.pdf]

Acknowledgements

The authors would like to thank Prof. Donata Pluskota-Karwatka for providing access to the apparatus and for her assistance in the performance of the lyophilization process.

Funding

We thank the National Science Centre (grant no. HARMONIA 2017/26/M/ST5/00437) for the financial support.

ORCID® iDs

Małgorzata Pawełczak - https://orcid.org/0000-0002-3382-9697
Marcin Kaźmierczak - https://orcid.org/0000-0003-0199-9197

References

1. Turk, D.; Janjić, V.; Štern, I.; Podobnik, M.; Lamba, D.; Dahl, S. W.; Lauritzen, C.; Pedersen, J.; Turk, V.; Turk, B. *EMBO J.* **2001,** *20,* 6570–6582. doi:10.1093/emboj/20.23.6570
2. Korkmaz, B.; Caughey, G. H.; Chapple, I.; Gauthier, F.; Hirschfeld, J.; Jenne, D. E.; Kettritz, R.; Lalmanach, G.; Lamort, A.-S.; Lauritzen, C.; Łgowska, M.; Lesner, A.; Marchand-Adam, S.; McKaig, S. J.; Moss, C.; Pedersen, J.; Roberts, H.; Schreiber, A.; Seren, S.; Thakker, N. S. *Pharmacol. Ther.* **2018,** *190,* 202–236. doi:10.1016/j.pharmthera.2018.05.011
3. Rai, R.; Thiagarajan, S.; Mohandas, S.; Natarajan, K.; Shanmuga Sekar, C.; Ramalingam, S. *Int. J. Dermatol.* **2010,** *49,* 541–543. doi:10.1111/j.1365-4632.2010.04300.x
4. Pham, C. T. N.; Ivanovich, J. L.; Raptis, S. Z.; Zehnbauer, B.; Ley, T. J. *J. Immunol.* **2004,** *173,* 7277–7281. doi:10.4049/jimmunol.173.12.7277
5. Shen, X. B.; Chen, X.; Zhang, Z. Y.; Wu, F. F.; Liu, X. H. *Eur. J. Med. Chem.* **2021,** *225,* 113818. doi:10.1016/j.ejmech.2021.113818
6. Xiao, Y.; Cong, M.; Li, J.; He, D.; Wu, Q.; Tian, P.; Wang, Y.; Yang, S.; Liang, C.; Liang, Y.; Wen, J.; Liu, Y.; Luo, W.; Lv, X.; He, Y.; Cheng, D.-d.; Zhou, T.; Zhao, W.; Zhang, P.; Zhang, X.; Xiao, Y.; Qian, Y.; Wang, H.; Gao, Q.; Yang, Q.-c.; Yang, Q.; Hu, G. *Cancer Cell* **2021,** *39,* 423–437.e7. doi:10.1016/j.ccell.2020.12.012
7. Breznik, B.; Mitrović, A.; Lah, T. T.; Kos, J. *Biochimie* **2019,** *166,* 233–250. doi:10.1016/j.biochi.2019.05.002
8. Kam, C.-M.; Götz, M. G.; Koot, G.; McGuire, M.; Thiele, D.; Hudig, D.; Powers, J. C. *Arch. Biochem. Biophys.* **2004,** *427,* 123–134. doi:10.1016/j.abb.2004.04.011

9. Mølgaard, A.; Arnau, J.; Lauritzen, C.; Larsen, S.; Petersen, G.; Pedersen, J. *Biochem. J.* **2007,** *401,* 645–650. doi:10.1042/bj20061389
10. Drąg, M.; Wieczerzak, E.; Pawełczak, M.; Berlicki, Ł.; Grzonka, Z.; Kafarski, P. *Biochimie* **2013,** *95,* 1640–1649. doi:10.1016/j.biochi.2013.05.006
11. Turcheniuk, K. V.; Kukhar, V. P.; Röschenthaler, G.-V.; Aceña, J. L.; Soloshonok, V. A.; Sorochinsky, A. E. *RSC Adv.* **2013,** *3,* 6693–6716. doi:10.1039/c3ra22891f
12. Cytlak, T.; Kaźmierczak, M.; Skibińska, M.; Koroniak, H. *Phosphorus, Sulfur Silicon Relat. Elem.* **2017,** *192,* 602–620. doi:10.1080/10426507.2017.1287706
13. Naydenova, E. D.; Todorov, P. T.; Troev, K. D. *Amino Acids* **2010,** *38,* 23–30. doi:10.1007/s00726-009-0254-7
14. Kafarski, P. *RSC Adv.* **2020,** *10,* 25898–25910. doi:10.1039/d0ra04655h
15. Kaźmierczak, M.; Bilska-Markowska, M. *Eur. J. Org. Chem.* **2021,** 5585–5604. doi:10.1002/ejoc.202101027
16. Lejczak, B.; Kafarski, P.; Zygmunt, J. *Biochemistry* **1989,** *28,* 3549–3555. doi:10.1021/bi00434a060
17. Herczegh, P.; Buxton, T. B.; McPherson, J. C.; Kovács-Kulyassa, Á.; Brewer, P. D.; Sztaricskai, F.; Stroebel, G. G.; Plowman, K. M.; Farcasiu, D.; Hartmann, J. F. *J. Med. Chem.* **2002,** *45,* 2338–2341. doi:10.1021/jm0105326
18. Grembecka, J.; Mucha, A.; Cierpicki, T.; Kafarski, P. *J. Med. Chem.* **2003,** *46,* 2641–2655. doi:10.1021/jm030795v
19. Pfund, E.; Lequeux, T.; Masson, S.; Vazeux, M.; Cordi, A.; Pierre, A.; Serre, V.; Hervé, G. *Bioorg. Med. Chem.* **2005,** *13,* 4921–4928. doi:10.1016/j.bmc.2005.05.026
20. Drąg, M.; Grembecka, J.; Pawełczak, M.; Kafarski, P. *Eur. J. Med. Chem.* **2005,** *40,* 764–771. doi:10.1016/j.ejmech.2005.02.011
21. Amin, S. A.; Adhikari, N.; Jha, T. *J. Med. Chem.* **2018,** *61,* 6468–6490. doi:10.1021/acs.jmedchem.7b00782
22. Wanat, W.; Talma, M.; Pawełczak, M.; Kafarski, P. *Pharmaceuticals* **2019,** *12,* 139. doi:10.3390/ph12030139
23. Kaźmierczak, M.; Koroniak, H. *Beilstein J. Org. Chem.* **2020,** *16,* 756–762. doi:10.3762/bjoc.16.69
24. Kaźmierczak, M.; Dutkiewicz, G.; Cytlak, T. *Synthesis* **2020,** *52,* 2364–2372. doi:10.1055/s-0040-1707813
25. Kaźmierczak, M.; Koroniak, H. *J. Fluorine Chem.* **2012,** *139,* 23–27. doi:10.1016/j.jfluchem.2012.03.016
26. Kaźmierczak, M.; Kubicki, M.; Koroniak, H. *Eur. J. Org. Chem.* **2018,** 3844–3852. doi:10.1002/ejoc.201800631
27. Goldeman, W.; Nasulewicz-Goldeman, A. *Bioorg. Med. Chem. Lett.* **2014,** *24,* 3475–3479. doi:10.1016/j.bmcl.2014.05.071
28. Xu, Y.; Jiang, G.; Tsukahara, R.; Fujiwara, Y.; Tigyi, G.; Prestwich, G. D. *J. Med. Chem.* **2006,** *49,* 5309–5315. doi:10.1021/jm060351+
29. Chiminazzo, A.; Borsato, G.; Favero, A.; Fabbro, C.; McKenna, C. E.; Dalle Carbonare, L. G.; Valenti, M. T.; Fabris, F.; Scarso, A. *Chem. – Eur. J.* **2019,** *25,* 3617–3626. doi:10.1002/chem.201805436
30. Goetz, D. B.; Varney, M. L.; Wiemer, D. F.; Holstein, S. A. *Bioorg. Med. Chem.* **2020,** *28,* 115604. doi:10.1016/j.bmc.2020.115604
31. Grison, C.; Coutrot, P.; Comoy, C.; Balas, L.; Joliez, S.; Lavecchia, G.; Oliger, P.; Penverne, B.; Serre, V.; Hervé, G. *Eur. J. Med. Chem.* **2004,** *39,* 333–344. doi:10.1016/j.ejmech.2004.01.006
32. Liu, Y.; Wu, Y.; Sun, I.; Gu, Y.; Hu, L. *Eur. J. Med. Chem.* **2020,** *191,* 112181. doi:10.1016/j.ejmech.2020.112181
33. Voos, K.; Schönauer, E.; Alhayek, A.; Haupenthal, J.; Andreas, A.; Müller, R.; Hartmann, R. W.; Brandstetter, H.; Hirsch, A. K. H.; Ducho, C. *ChemMedChem* **2021,** *16,* 1257–1267. doi:10.1002/cmdc.202000994
34. Poreba, M.; Mihelic, M.; Krai, P.; Rajkovic, J.; Krezel, A.; Pawelczak, M.; Klemba, M.; Turk, D.; Turk, B.; Latajka, R.; Drag, M. *Amino Acids* **2014,** *46,* 931–943. doi:10.1007/s00726-013-1654-2
35. Cortés, A.; Cascante, M.; Cárdenas, M. L.; Cornish-Bowden, A. *Biochem. J.* **2001,** *357,* 263–268. doi:10.1042/bj3570263

License and Terms

This is an open access article licensed under the terms of the Beilstein-Institut Open Access License Agreement (https://www.beilstein-journals.org/bjoc/terms), which is identical to the Creative Commons Attribution 4.0 International License (https://creativecommons.org/licenses/by/4.0). The reuse of material under this license requires that the author(s), source and license are credited. Third-party material in this article could be subject to other licenses (typically indicated in the credit line), and in this case, users are required to obtain permission from the license holder to reuse the material.

The definitive version of this article is the electronic one which can be found at:
https://doi.org/10.3762/bjoc.19.33